POLITECNICO DI MILANO

Facoltá di Ingegneria Industriale

Corso di Laurea Magistrale in Ingegneria Aeronautica

Real time control of a scaled wind turbine and experimental test of a wind farm

RELATORE: Prof. Alessandro Croce
CORRELATORE: Prof. Carlo L. Bottasso

Tesi di Laurea di:

Andrea Fugazza
799239

Juan Sebastián Rojas Sandoval
798273

Anno Accademico 2014 - 2015

Abstract

This research, developed at Technische Universität München, describes the activities necessary to allow the operation of six models of wind turbines, fully instrumented and controlled, which have been used in experimental tests in the Politecnico di Milano civil wind tunnel. The wind turbine models, characterized by a small size to allow the test of a whole wind farm, have been scaled down, with a geometric scaling factor of 1:155, from an existing wind turbine, built by Samsung Heavy Industries and characterized by a rated power of 7 MW.

To allow the functioning of the six scaled wind turbines, several codes that permit the operation of the models in different modes have been written in C language and have been integrated inside the CPU, built by Bachmann Gmbh., that rules the functioning of the scaled models as well as that of real multi MegaWatt wind turbines. Low level control algorithms govern the functioning of actuators, whereas high level control algorithms allow, by acting on torque and pitch angle, the operation of the machine according to the desired regulation curves, which, for these kind of machines, correspond to certain angular speed, blade pitch angle and torque expressed as function of wind speed. The PID controllers allow the models to run both in automatic mode, deciding rotor speed, torque and pitch angle based on look-up tables and measurements, and in manual mode, achieving user defined values. The communication with the Maxon pitch motor is performed through a CAN network, whereas the communication with the generator is carried out through analog protocol.

Two other control algorithms were also integrated within the CPU. The first, developed at Kyungpook National University (KNU), is aimed at the control of a single wind turbine through PID control laws; the second, developed together by KNU and Samsung Heavy Industries, is used to control the whole wind farm with the goal of maximing the production of power.

Moreover, three graphical interfaces, based on Java language, were developed using the SolutionCenter software. The first allows, in a simple and intuitive manner, the management of the wind turbine model through a state machine, the regulation of all the necessary parameters, the visualization fo the results, both as values and plots, and the recording of data; the second interface allow the management of a whole row of wind turbines, whereas the third permits the control of the environmental parameters of the wind tunnel, such as the wind speed measured by Pitot sensors and the air density.

A Simulink model of the wind turbine, reproducing both the dynamics of the model and the same control algorithm implemented in the C codes installed in the CPU, was also developed; this allowed to check the results of the model in order to verify the written codes.

Besides the programming activities, six wind turbine models were completely assembled, cabled and instrumented; several others actions necessary to guarantee the correct functioning of the machines were performed, such as the calibration of sensors and the development of a test bench, which has been used to simulate the wind in order to test the control algorithms also outside the wind tunnel.

The six scaled wind turbine models have finally been tested in the wind tunnel in order to validate the control algorithsm, to detect the actual performance and to check the effects caused by the presence of several models close to each other. During the test,

some problems, especially related to vibrations, were encountered; therefore, after the tests, several weeks were devoted to the analysis of these problems and to the detection of possible solutions, which will allow to achieve better results in the future experimental tests.

Keywords: wind turbine, scaled model, control, C, real-time, Bachmann, Simulink, wind tunnel, test bench, state machine, wake, partialization.

Sommario

Il presente lavoro di tesi, svolto alla Technische Universität München, consiste nella descrizione delle attivitá che hanno permesso il funzionamento di sei modelli di generatori eolici pienamente strumentati e controllati, che sono stati utilizzati in test sperimentali nella galleria del vento civile del Politecnico di Milano. I modelli, di dimensioni ridotte per consentire test di un intero parco eolico, sono scalati, con coefficiente di scalatura geometrico pari a 1:155, a partire da un esemplare di aerogeneratore realmente esistente, prodotto da Samsung Heavy Industries e caratterizzato da una potenza nominale di 7 MW.

Al fine di consentire il pieno funzionamento dei modelli di aerogeneratori, sono stati scritti diversi codici in linguaggio C che garantiscono l'operativitá dei modelli in diverse condizioni d'uso e, successivamente, integrati nella CPU, prodotta da Bachmann Gmbh., che governa tanto il funzionamento dei modelli in scala quanto quello di reali generatori eolici. Tali codici si distinguono tra algoritmi di "basso livello", che governano il funzionamento degli attuatori, e di "alto livello", che implementano logiche di controllo che, agendo sul momento torcente e sul passo della pala, consentono il funzionamento in maniera automatica di ogni singolo modello di generatore al fine di produrre energia seguendo le curve di regolazione tipiche di questo tipo di macchine, in cui la velocitá angolare del rotore, il passo della pala, il momento torcente e la potenza prodotta sono espresse al variare della velocitá del vento. I controllori PID implementati permettono tanto il funzionamento automatico dell'aerogeneratore, sulla base delle misure rilevate dai sensori e di look-up tables inserite dall'utente, sia quello manuale in base ai valori di velocitá e passo della pala decisi dall'utilizzatore. La comunicazione con il motore Maxon che regola il passo della pala é realizzata mediante protocollo di comunicazione CAN, mentre quella relativa al generatore tramite protocollo di comunicazione analogica.

É stato inoltre implementato un secondo algoritmo di controllo sviluppato dalla Kyungpook National University e dedito al controllo di ogni singolo generatore eolico. Infine é stato integrato nella logica di funzionamento real-time un terzo algoritmo di controllo, sviluppato in collaborazione tra Kyungpook National University e Samsung Heavy Industries e dedicato al controllo dell'intero parco eolico al fine di massimizzare la produzione di potenza.

Sono state anche sviluppate delle interfacce grafiche, basate su linguaggio Java, che permettono, in maniera semplice ed intuitiva, la gestione della turbina tramite una macchina agli stati, la regolazione di tutti i parametri che descrivono il comportamento della macchina, la visualizzazione dei risultati e la registrazione dei dati. Altre due interfacce grafiche, infine, permettono la gestione di una intera riga di aerogeneratori e il controllo dei principali parametri che caratterizzano la galleria del vento, quali la densitá e la velocitá dell'aria.

É stato infine sviluppato un codice Simulink che riproduce la dinamica del modello di aerogeneratore e lo stesso sistema di controllo implementato nella CPU che gestisce il funzionamento real-time della turbina eolica; esso ha permesso un confronto con il comportamento reale al fine di validare i codici scritti.

Accanto alla programmazione di codici di controllo, sono stati interamente assemblati, cablati e strumentati i sei modelli di aerogeneratore e sono state svolte varie attivitá indispensabili a garantire il corretto funzionamento delle macchine, quali la calibrazione

dei sensori e lo sviluppo di un banco prova che ha permesso di simulare la presenza del vento anche all'esterno della galleria.

I modelli sono stati infine testati in galleria del vento al fine di validare il funzionamento degli algoritmi di controllo, di rilevare le effettive prestazioni e curve caratteristiche delle macchine e di verificare gli effetti della presenza contemporanea di diversi generatori eolici e la loro interazione reciproca. Al termine dei test sperimentali sono state dedicate diverse settimane di lavoro alla risoluzione di diversi problemi, specialmente di carattere vibratorio, riscontrati in questa campagna di prove; tali accorgimenti garantiranno un migliore svolgimento di tutte le prove sperimentali previste dopo la conclusione della presente tesi.

Parole chiave: aerogeneratore, modello in scala, controllo, C, real-time, Bachmann, Simulink, galleria del vento, banco prova, macchina agli stati, scia, parzializzazione.

Contents

List of Figures

List of Tables

Chapter 1

Introduction

The present thesis work is set within the context of a close collaboration between three main stakeholders: the Wind Energy Department of the Technische Universität München (TUM) on one side, the Kyungpook National University (KNU) and Samsung Heavy Industries (SHI) one the other side. The continuously growing importance of renewable energy sources on today's economy, in fact, has led Samsung to heavily invest on the wind energy market, producing, in only a few years, Multi-Megawatt wind turbines. Being wind turbines and specially wind farms a current research trend, experimental tests and collaboration between companies and universities still represents a key factor in the development of wind energy technologies. Moreover, being wind turbines the largest rotating machine in the world, often located in isolated places, wind tunnel tests on scaled models represent a fundamental element since they are much more easier and cheaper than those performed on-field on full-scale machines and in the design phase are, in most of the cases, the only choice.

This interest in wind energy technologies led these three partners into a research agreement to conduct together experimental tests on wind turbines and especially on wind farms in a closed, strictly controlled environment such as the wind tunnel facilities of Politecnico di Milano. The main, long term, goal of these activities is to develop and test wind farms control algorithms that allow to maximize the power production of a whole wind farm. Although control algorithms for the single wind turbine are well known and quite consolidated, they cause the turbine to operate in such a way as to maximize its own performance, without considering the detrimental effects on the nearby turbines within a wind farm. Several studies, however, have shown that this control logic leads to a sub-optimal behaviour of the whole wind farm, as described in [8], [26], [18], [20], [16].

In the last few years, a strong research effort was carried out towards new, innovative, control laws that involve the whole wind farm and that aim at reducing the power production of the leader turbine of a row, thus sacrificing its AEP, in order to improve the performance of the downstream turbines and therefore increasing the overall wind farm power production; this idea is based on the fact that, by de-rating the first turbine, the wind speed improvement experienced by the downstream turbines significantly increases their performance. Several studies have been conducted at a theoretical level, often applying semplified wake models, such as the Park model (see [17]) or the eddy viscosity model (see [1]), which provide a fast tool to describe the wake interactions. More advanced, high fidelity but computationally expensive, CFD models have also been extensively researched, e.g. [33], [23]. A comprehensive description and comparison of the most widely wake models is also described in [2].

The present activity is the next step in this huge research effort. Its main objective is to develop all the necessary hardware and software applications in order to test the wind farm control logics explored in a simulated environment during the past years. The extent of this test campaign entails the involvement of a fourth crucial partner, the Politecnico di Milano (POLIMI), that provides the required facilites for the experimental activities and to which belong the authors of the present work. This master thesis, therefore, focuses on the construction of six scaled wind turbine models (1:155), fully equipped and instrumented, and in the implementation of all the required software applications for its safe operation during the wind tunnel testing, i.e. communication protocols, graphic user interphase (GUI) and control algorithms. It is important to highlight that a big effort was made to create flexible applications since the experimental campaign will last at least three years and many different control strategies will be tested. Moreover, the first experimental testing has been conducted successfully during the present work in which we have demonstrated the robustness of the models and applications developed and that all the encountered issues have been corrected. Finally, during this preliminary testing, wake, performance and power partialization measurements, including the control proposed by partners Samsung and KNU, have been carried out and discussed.

1.1 Design criteria

The scaled wind turbine model has been designed before the beginning of this thesis, for instance in [3], and the criteria used to design it are here briefly summarized.

The model has been scaled from the Samsung S7.0-171 wind turbine, an offshore turbine designed with a rated power of 7 MW and a diameter of 171.2 m. In order to achieve suitable results in the wind tunnel tests, the scaled model must replicate as well as possible the aerodynamic characteristics of the real wind turbine, such as the turbolence intensity and the wake size. Moreover, the Reynolds number should also be as close as possible to the real one; this, however, is not possible due to space limitations and to the low wind speeds that can be achieved in the wind tunnel and thus a certain mismatch must be taken into account. In particular, the Reynolds number will be much lower than the real one and, to compensate for this effect, special low-Reynolds airfoils are used.

The model was scaled down by keeping constant the tip speed ratio λ

$$\lambda_M = \lambda_F \tag{1.1}$$

where the subscript M indicates the scaled model and F the full-scale turbine. The scaled model is therefore completely defined by the radius and rotor speed ratios, also called geometrical and time scale factor:

$$n = \frac{R_M}{R_F} = 1/155 \tag{1.2}$$

$$n_t = \frac{\Omega_F}{\Omega_M} = 0.012 \tag{1.3}$$

Table 1.1 summarizes the main properties of the scaled model.

1.2 The scaled wind turbine model

The scaled model is mainly composed of three parts: the rotor, the nacelle and the tower.

Quantity	Scale coefficient	7MW Turbine	Scaled Model
Rotor diameter [m]	n	171.2	1.1
Rotor speed [rpm]	n_t	10.4	850
Rated wind speed [m/s]	n/n_t	11.5	6
Rated power [W]	n^5/n_t^3	$7.7 \cdot 10^6$	45

Table 1.1: Scaled model properties

The rotor, shown in Figure 1.1, deploys three blades whose airfoils, as previously said, have been changed in order to adapt to the lower Reynolds number. The blades are provided only with a collective pitch control, which is actuated by a motor placed in the nacelle and whose movement is transferred to the blades by means of a gear wheel. The pitch motor is commanded by the EPOS 24/2 control board and communicates with the CPU through a CAN network. At least one of the blades is equipped with a hall sensor, a device that is used in the calibration of the pitch angle before the tests.

Figure 1.1: Rotor structure

The second part of the model, the nacelle, is shown in Figure 1.2; it is quite a complex element since it fulfills several purposes. First, it connects the rotating part, the rotor, to the non rotating one, the tower; the shaft runs through a metallic box, fixed to the tower, and lays on two ball-bearings that allow the relative movement. Moreover, since the cables connected to the hall sensor and the pitch motor are rotating together with the shaft, while the power supplies, the control boards and the CPU are fixed on the ground, the signal has to be transferred from the the rotating part to the non rotating. This is accomplished by means of a slip ring placed inside the metallic box. Additionally, several sensors are located in the nacelle: a digital encoder is settled right behind the slip ring and allows to read the rotational speed of the shaft, whereas a torquemeter, placed just before the generator, permits to measure the torque. Finally, the motion of the rotor has to be converted to power; this is fulfilled by locating a generator on the other side of the shaft. Two springs connect the main shaft, the torquemeter and the

generator. The generator is also equipped with its own encoder; this, however, measures the rotational speed of the motor, which differs from that of the shaft because of the planetary gearhead.

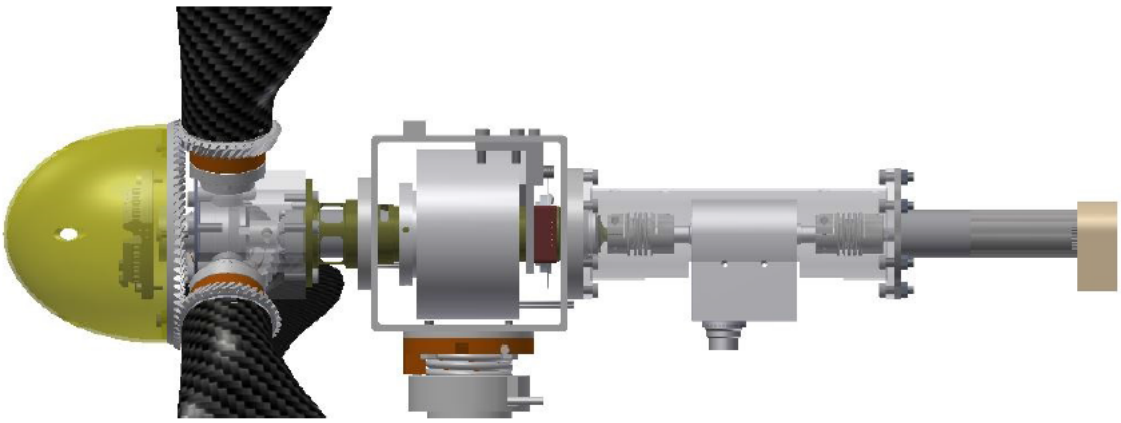

Figure 1.2: Nacelle structure

The last element of the model is the tower, shown in Figure 1.3: it was designed as a soft tubular steel tower with a particular care regarding the natural frequencies of bending modes, in order to avoid couplings with the frequency of the rotor and its multiples at the nominal rotor speed. Since the tower has to be equipped with a yaw motor, a hole was made on the side of the tower in order to have space to place the motor and perform the necessary operations. The bottom part of the tower also hosts some strain gages, which allow the measurement of bending moments, both side-side and fore-aft.

All the cables that supply power or transfer signals to the sensors and the motors are connected to a cabinet, inside of which are placed the power supply and the CPU. For a more detailed description of the connections, see [22]. The cabinet structure is shown in Figure 1.4.

The most important element inside the cabinet is the M1 Bachmann control board; it is a real time control unit produced by Bachmann Gmbh and used also for real wind turbines. The control unit is connected to the Internet by means of an ethernet cable and exchanges data with the computer using a wireless communication. A direct connection of the CPU with a PC is also possible through an ethernet cable. As shown in Figure 1.5, the Bachmann control board is made up of 6 modules, which are identified by a Card number and whose configuration parameters are defined in the MConfig.ini file.

The purpose and characteristics of each module are here briefly described:

- **NT255**: this component, identified by the Slot number 1, supplies power to the CPU.
- **MC210**: this element is the processor module. It is equipped with two ethernet ports, which allow the connection of the machine to the Internet, and with a USB port, used to store data into a 16 GB USB pen drive. It is also equipped with a memory card, where all the important information of the machine, such as the MConfig.ini file, are stored.
- **CM202**: it is identified by Card number 4 and is the module devoted to the management of the CAN network. Each module can operate up to 2 different CAN

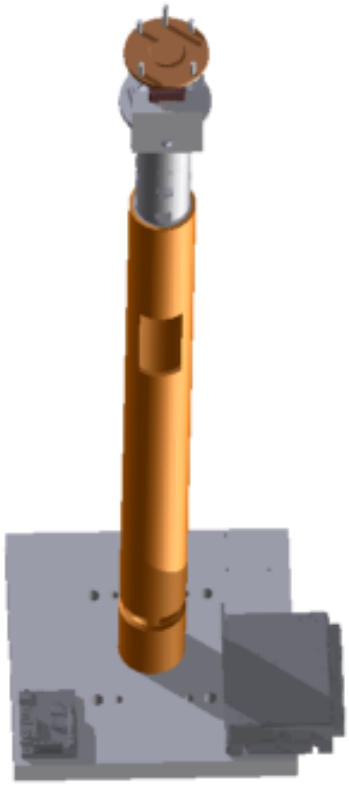

Figure 1.3: Tower structure

networks with 64 nodes; in this wind turbine model both the CAN networks are employed in order to communicate with the pitch and yaw motors.

- **CNT204/R**: identified by Card number 5, it is the counter module. Each module can contain up to 4 counters. Two of these, however, are used as inputs to the incremental encoder located on the shaft.

- **AIO288**: the analog input/output module is in charge of managing the analog signals and offers up to 8 analog input and 8 analog output channels. In this case, two AIO288 modules are employed and are identified by the Card numbers 6 and 7. Number 6 is connected to the power generator and the sensors (except the torquemeter), while number 7 is connected to the torquemeter and the motor that simulates the torque produced by the wind.

1.3 Thesis overview

The present thesis deals with the construction and development of several scaled wind turbine models and their later test in the wind tunnel facilities at the Politecnico di Milano.

At the beginning of the thesis, a first model, slightly different from the ones that were tested but characterized by the same scaling coefficient and aerodynamic performance, was already partially assembled at the Wind Energy Department of the Technische Universität München.

Figure 1.4: Cabinet structure

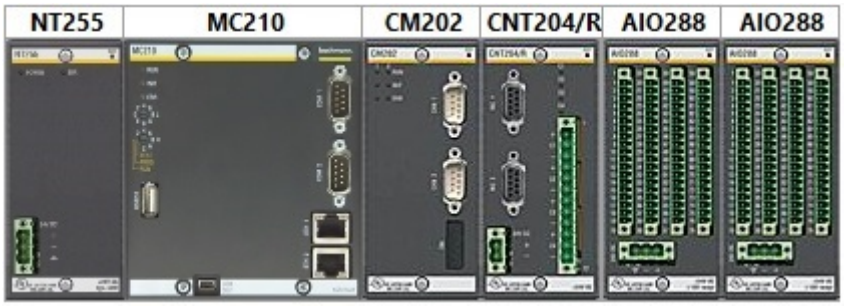

Figure 1.5: Bachmann architecture

Chapter 1 describes the structure of the models and that of the cabinet used to control them. It also summarizes the most interesting paramenters that govern the operation of the machines.

Chapter 2 deals with several tasks not strictly related to the software that controls the machine that were necessary to perform in order to guarantee the full functionality of the models. This includes the development of a test bench, in order to be able to test the wind turbines even without the wind, the characterization of the relationship between current, speed and torque that describes the behaviour of the motors, the measurement of the friction for each model and the calibration of the strain . It also describes the Simulink model that was used to compare and simulate the behaviour of the machine and it analyzes some vibration problems, caused by resonance of the tower with the external load, that occurred during the tests, offering some possible solutions to better

perform the following tests.

Chapter 3 describes the development of several codes, or applications, written in C language, that allow the real time comunication between sensors and actuators and to introduce a PID control system that, by acting on pitch and torque, regulates the rotor speed. This control system was then integrated into the state machine, the application that controls the operating mode of the wind turbine. Three graphical interfaces have also been developed in order to ease the operation of the model, the recording of data and the visualization of results. The first allows the control of the single wind turbine and the visualization of the most interesting parameters as plots; the second interface, instead, permits to set the parameters related to the wind farm control. The latter, finally, allows to manage the most important parameteres of the wind tunnel, such as the speed signal coming from the Pitot sensors and the air density.

Chapter 4 explains the experiments performed in the wind tunnel, describing the setup of each test and showing the results. The main goals of these tests were the measurement of the aerodynamic characteristics of the turbines and the wake characterization. Furthermore, the long term goal is to test several wind farm control algorithms to prove that, by partializing the power production of the upwind wind turbines, it is possible to maximize the overall power production of the wind farm. It should be noted, however, that the main goal of this thesis was not the conduction of experimental tests, rather the assembly of six scaled wind turbines and the development of control algorithms to allow the tests.

Chapter 5, finally summarizes the goal achieved with this thesis, the results of the experimental tests and offers some suggestions for future developments.

Chapter 2

Test Bench development

In the wind tunnel experiments, the rotor will be subjected to the aerodynamic forces generated by the interaction between the wind and the airfoils of the blades. It is important, however, to test the model before the scheduled experiments take place; in this way, it is possible to try different technical solutions, to test several control algorithms, to perform all the necessary preliminary tests and therefore to assure the proper functioning of the model. For these reasons, a test bench has been developed.

2.1 Wind actuation system

Outside of the wind tunnel, therefore, the aerodynamic forces caused by the wind must be replicated by other means. In this case, an electric motor was chosen to replicate the aerodynamic torque that would act on the rotor. The electric motor is the EC-4pole 22mm motor produced by Maxon, which is coupled with a planetary gear head and an encoder. The main characteristics of these three components are described in Table 2.1.

EC-4pole	
Nominal speed [rpm]	14700
Nominal current [A]	3.92
Stall torque [Nmm]	639

(a) Motor characteristics

SCH-16F	
Counts per turn	500
N of channels	3
Max speed [rpm]	12000

(b) Encoder characteristics

GP 22 HP	
Reduction	14 : 1
Recommended speed [rpm]	< 12000
Number of stages	2

(c) Gearhead characteristics

Table 2.1: Wind actuation system characteristics

The motor is connected to the shaft through a spring, shown in Figure 2.1, which has a high torsional stiffness to transmit motion and a lower bending stiffness to account for possible misalignments between the shaft of the model and the shaft of the motor.

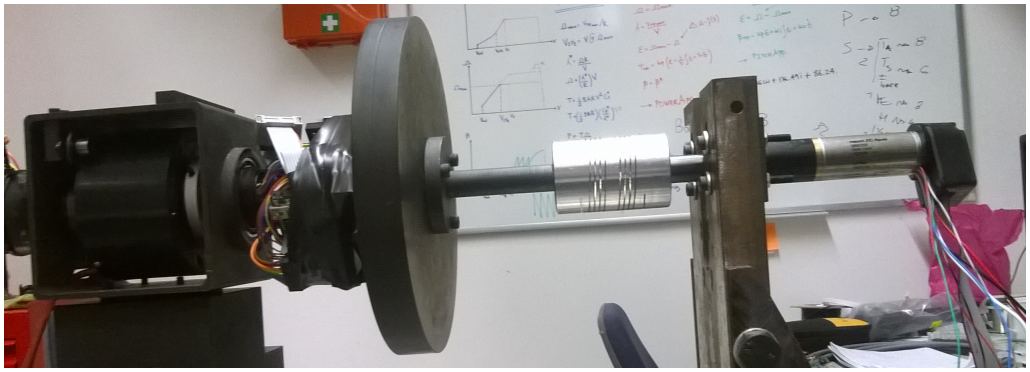

Figure 2.1: Junction between wind motor and rotor shaft

The motor is controlled by the ESCON 50/5 control board, a small sized servo controller that can handle up to 16 analog and digital inputs and outputs; in this case, the controller operates in current control mode but it could also operate in speed control mode. To command the motors, the user should provide two different inputs: the first allows to enable the power stage, the second defines the set value (current or speed, depending on the control mode).

As explained in [9], 8 cables are connected to the motor and need to be linked to the ESCON control board and to the module 7 of the Bachmann AIO288. The connections are summarized in Table 2.2.

Name	ESCON	AIO288
Winding 1	J2.1	
Winding 2	J2.2	
Winding 3	J2.3	
Hall sensor 1	J3.1	
Hall sensor 2	J3.2	
Hall sensor 3	J3.3	
V_{Hall}	J3.4	
Ground	J3.5	
Digital Input 1	J5.1	33
Ground	J5.5	34
Analog Input 1 (+)	J6.1	14
Analog Input 1 (-)	J6.2	15 (brg 16)
Analog Output 1	J6.5	21
Analog Output 2	J6.6	40
Ground	J6.7	22 (brg 23)
Ground	J6.7	41(brg 42)

Table 2.2: Motor - ESCON - AIO288 connections

2.2 Motors characterization

Both the wind motor and the power generator are current controlled, which means that, to achieve the desired speed, the the right amount of current must be provided. The user, however, usually does not know what current corresponds to a certain speed; it is thus necessary to find out the relationship between current, speed and torque, expressed in Eq. 2.1.

$$Q = \alpha\omega + \beta i + \gamma \tag{2.1}$$

where i is the current, ω the rotational speed and Q the torque. The characterization of the motors therefore is simply the computation of the three coefficients α, β and γ. The procedure to find out these three coefficients consists in controlling the power generator in speed mode and the wind motor in current mode. By trying several combinations of speed and current and measuring the torque, it is possible to build a database that, through a regression, provides the coefficients that characterize the two motors.

Figures 2.2 and 2.3 show the curves that have been obtained by controlling the power generator with speeds between 0 and 900 rpm and the wind motor with currents ranging from 0 to 3.55 A.

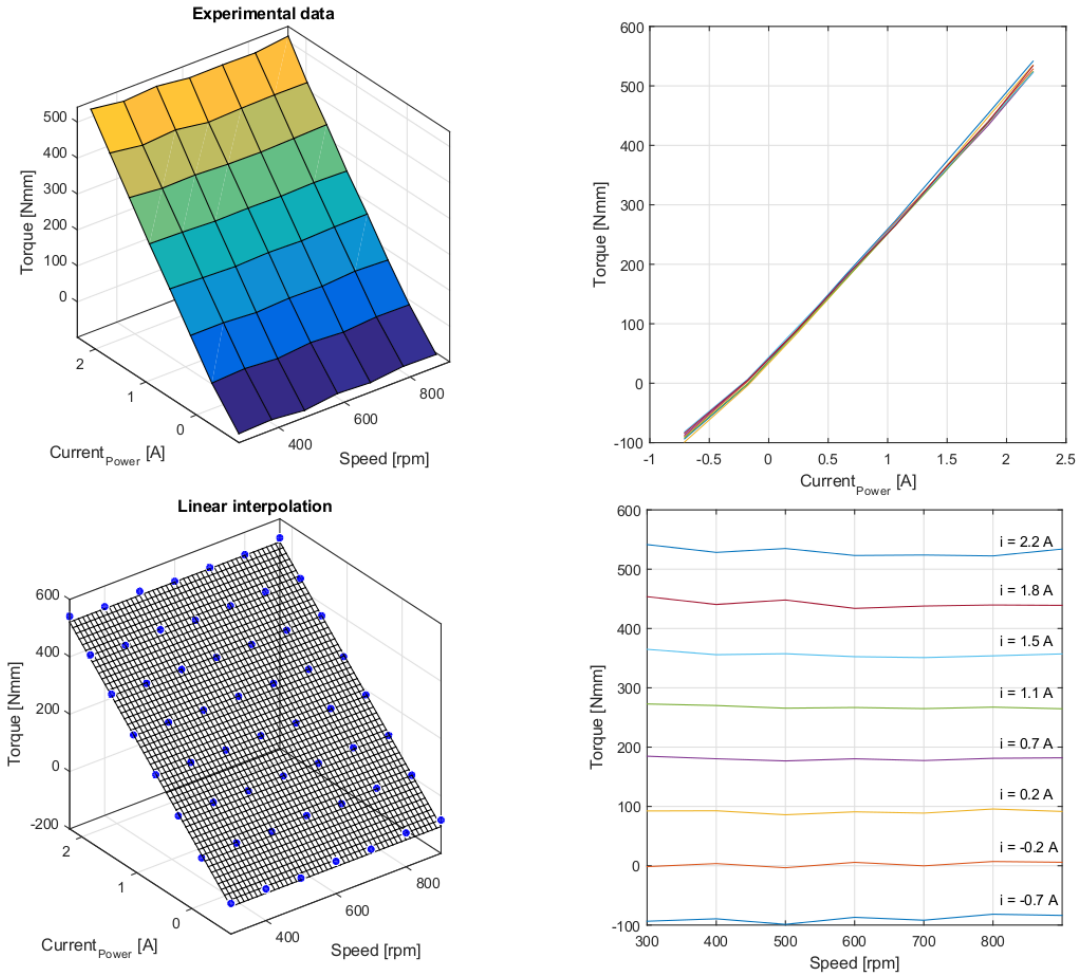

Figure 2.2: Power generator curve

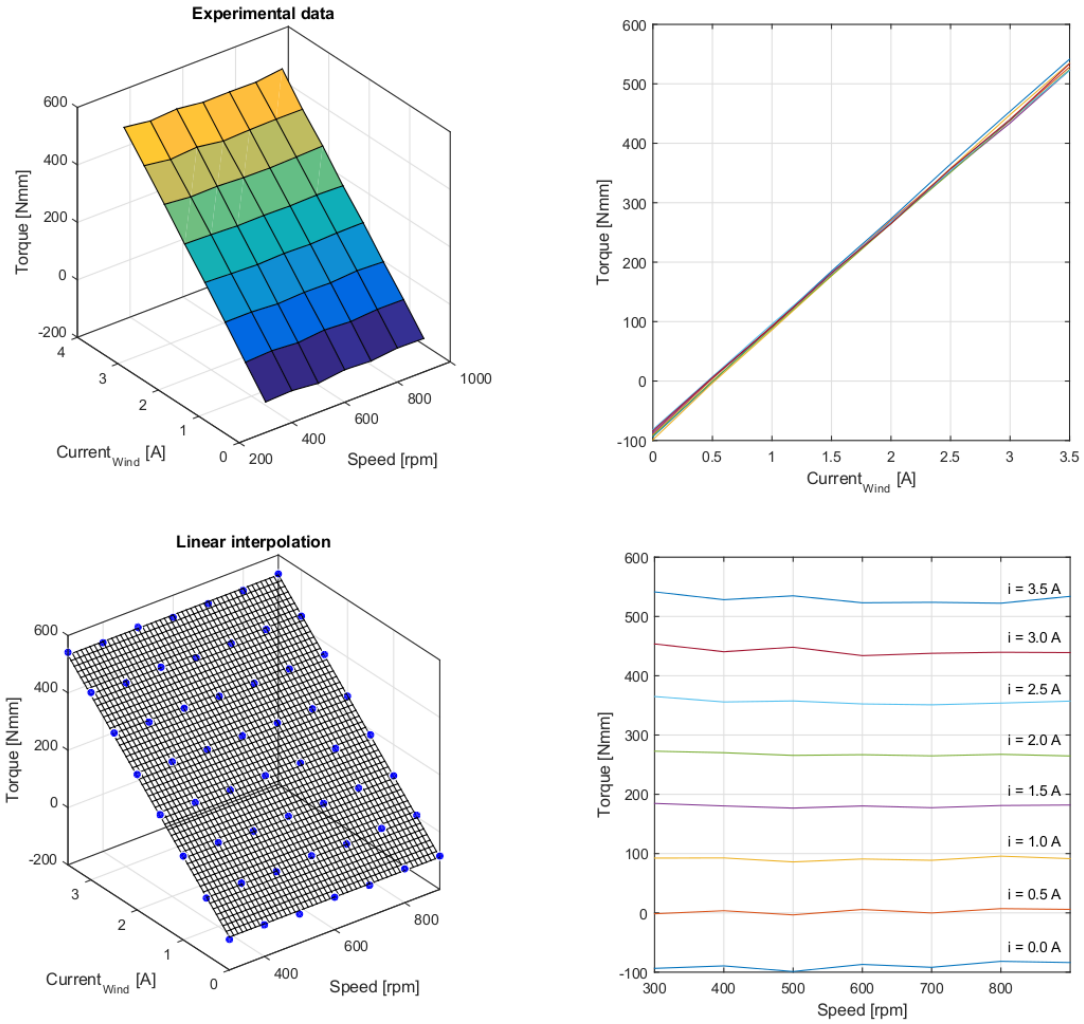

Figure 2.3: Wind motor curve

The values of α, β and γ are summerized in Table 2.3. It is clear that the speed has very little influence over the current, which is mainly determined by torque. Moreover, it is also worth noting the presence of a constant term γ: this is due to the fact that the linear approximation of Eq. (2.1) is suitable only when we consider operative conditions far from the origin. Instead, when we consider conditions close to zero current, the behaviour is nonlinear; this values of current, however, are far from the operative condition of the machine and therefore not particulary interesting.

Coefficient	Power generator	Wind motor
α [1/rpm]	-0.0036033	-0.0036033
β [1/A]	213.4411	176.49
γ [Nmm]	46.0017	-86.2395

Table 2.3: Motors characterization table

2.3 Friction measurement

In order to have reliable data, it is important to measure the friction due to the mechanical connections. By commanding the power generator in speed control, the measured torque corresponds to the friction and it is possible to find its relationship with the rotor speed; this procedure has been repeated for 7 different nacelles and the results plotted in Figure 2.4 show a substantially cubic trend. Since turbine number 1 shows a much higher friction with respect to the others and only 6 nacelles were needed, it was discarded.

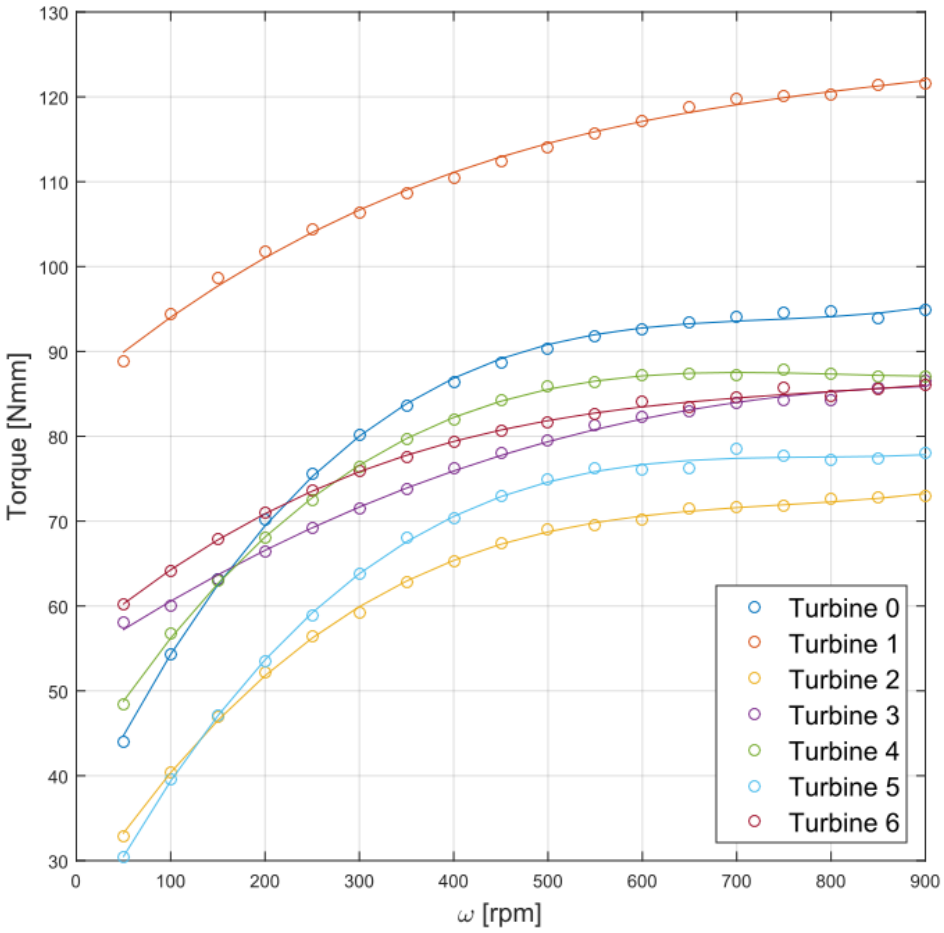

Figure 2.4: Friction

2.4 Strain gages calibration

. The tower base is equipped with four strain gages that allow the measurement of the bending moments both in the fore-aft and side-side directions. The tower base is equipped with two conditioning boards (WAT 02 R3) that permit to perform some manipulation of the signal, such as amplification, and to adjust specific settings of the strain gages. In this case, for instance, the amplifier gain was set to the maximum allowable value of 3 mV/V whenever possible; in a couple of towers, however, problems of saturation occured and the gain was therefore lowered. Moreover, by acting on the R16 trimmer illustrated

in Figure 2.5, the zero of the control boards was set; a few strain gages, however, were too unbalanced to completly delete the offset.

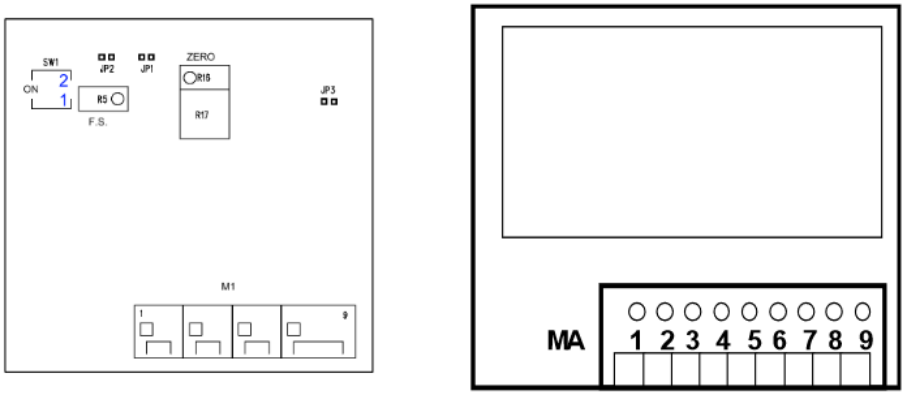

Figure 2.5: WAT 02 R3 condition board

Table 2.4 summarizes the electrical connections to the conditioning board necessary to activate the strain gages.

Control board port	Cable
BB/1	Power supply (+)
BB/2	Power supply (-)
BB/3	Strain gage signal
BB/4	Strain gage signal
BB/5	Strain gage signal
BB/6	Strain gage signal
BB/7	-
BB/8	Signal (+)
BB/9	Signal (-)

Table 2.4: WAT 02 R3 connections

Since the strain gages output is a voltage, it was necessary to calibrate the strain gages and find out the relationship between the bending moment and the voltage, as expressed by Eq. 2.2.

$$\begin{Bmatrix} M_1 \\ M_2 \end{Bmatrix} = \begin{bmatrix} S_{11} & S_{12} \\ S_{21} & S_{22} \end{bmatrix} \begin{Bmatrix} V_1 \\ V_2 \end{Bmatrix} + \begin{Bmatrix} M_{01} \\ M_{02} \end{Bmatrix} \tag{2.2}$$

In theory, of course, the two equations are decoupled and the constant terms M_{01} and M_{02} are equal to zero.

The signal has been first recorded keeping the tower in vertical position and with no loads appied; the measurement thus corresponds to the offset of the strain gages, which, as previously said, has been reduced when possible by acting on the zero regulation trimmer.

To compute the other coefficients of Eq. 2.2, the tower was attached to the wall in a horizontal position, as illustrated in Figure 2.6, and known loads were applied to the tip of the tower using a magnetic hook. It is worth noting that, since only mass forces

are applied, if the tower base was to be placed on the wall with an exact zero inclination angle, one of the strain gages would not experience any deformation. The orientation angle, therefore, is an important parameter that must be measured to ensure the quality of the measurements. The weights that have been used for this operation range from 0.5 kg to 2.5 kg of nominal mass with an interval of 0.5 kg and, before their application, they have been weighted on a scale to measure the real mass.

Figure 2.6: Setup for the strain gages calibration

The calibration procedure was repeated for 7 towers in total and Figure 2.8 shows the calibration curve obtained for one of these towers. As expected, the relationship is linear; the offset in the this curve is partially due to the real offset of the strain gages and partially to the fact that, even though no external loads are voluntarily applied, the weight of the tower is still causing a deformation of the strain gages.

Table 2.5 summarizes the coefficients of Eq. 2.2 obtained for the 7 tested towers. The coefficients S_{12} and S_{21} are equal to zero and are therefore not shown.

2.5 Vibrations

The tower of the wind turbine has been designed in order to have natural frequencies far away from the frequency of the excitation; at the same time, however, the tower was not supposed to be too stiff, in order to replicate a dynamic behaviour similar to that of a real wind turbine. Considering the nominal rated speed of 850 rpm, the main load is mainly determined by the 1/rev excitation, which corresponds to a frequency of 14.17 Hz. The tower, according to the FE model, was expected to have a fore-aft and a side-side natural frequency of respectively 18 and 17 Hz. During the wind tunnel tests, however,

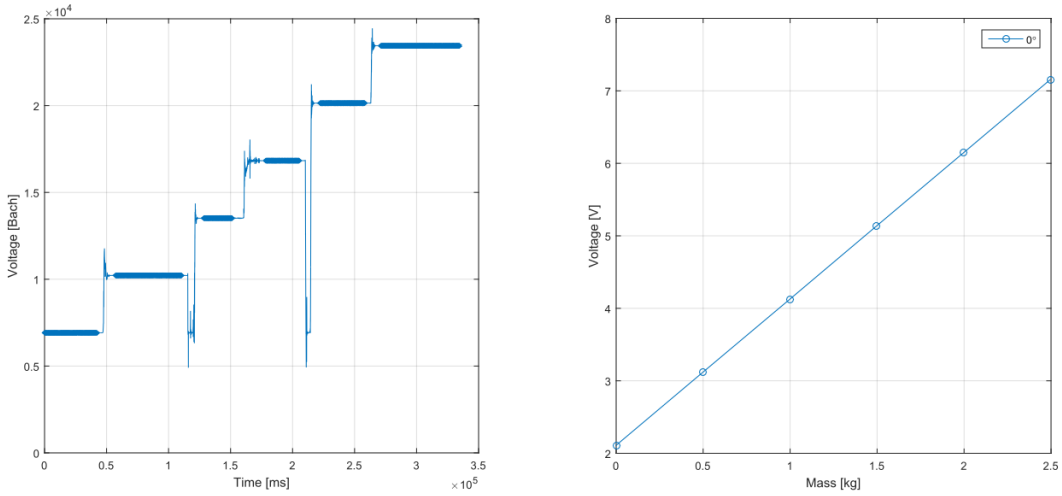

Figure 2.7: Strain gage calibration curve

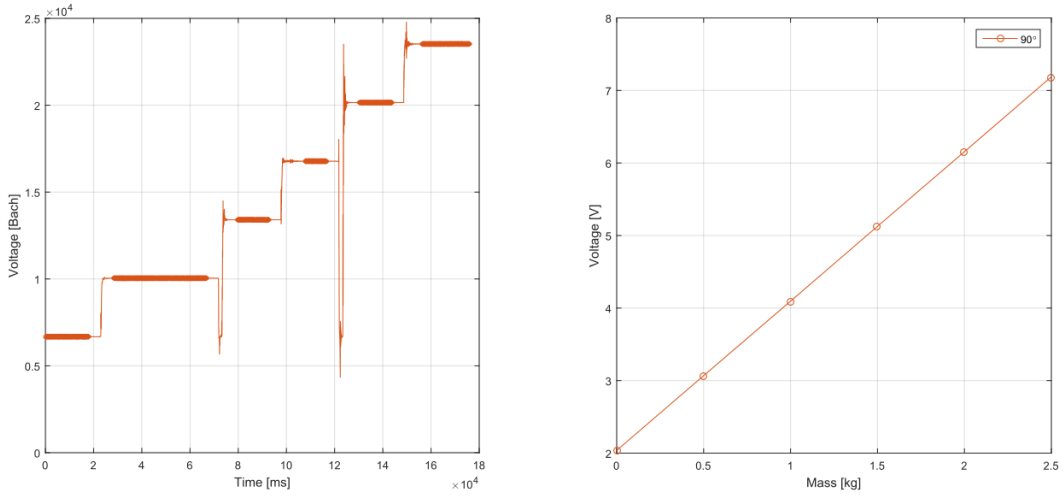

Figure 2.8: Strain gage calibration curve

severe problems of vibrations were encountered, and the nacelle and tower were vibrating so much that bending moments of up to 100 Nm were measured against expected values of about 15 Nm, thus causing yielding ofsome of the strain gages at the tower base.

The reasons of this misbehaviour are several. First, the tower base has been dug in order to increase the strain and therefore to have a greater signal from the strain gages, as shown in Figure 2.9a; this stiffness reduction was probably not well reproduced in the FE model, leading to lower natural frequencies. Moreover, a part of the hub was excavated to allow access to the inner part of the hub, as shown in Figure 2.9b; the holes, however, were not performed in a axisymmetric manner, hence resulting in an unbalanced rotor that could exacerbate the already problematic dynamic behaviour. Finally, the floor of the wind tunnel is made up of wooden panels and beams with very low stiffnesses and the coupling of the tower with this soft support has certainly further decreased the natural frequencies of the tower. The fact that the floor was not homogenous, rather stiffer in some places and softer in other, resulted in different behaviours from the turbines: in the

Tower	Angle	S_{11} [Nm/V]	S_{22} [Nm/V]	M_{01} [Nm]	M_{02} [Nm]
1	0.11 0.15	3.3973	3.3336	0	0
2	0.12 0.10	3.2862	3.4023	0	0
3	0.05 0.07	3.3554	3.2891	0	0
4	0.07 0.03	3.0304	3.0268	0	0
5	0.17 0.01	3.1276	2.8373	−0.0166	0.5163
6	0.06 0.01	3.2814	3.4581	0	−0.0538
7	0.09 0.05	3.1633	3.1879	0.1785	0

Table 2.5: Tower calibration coefficients

same condition, some turbines vibrated too much and some other didn't.

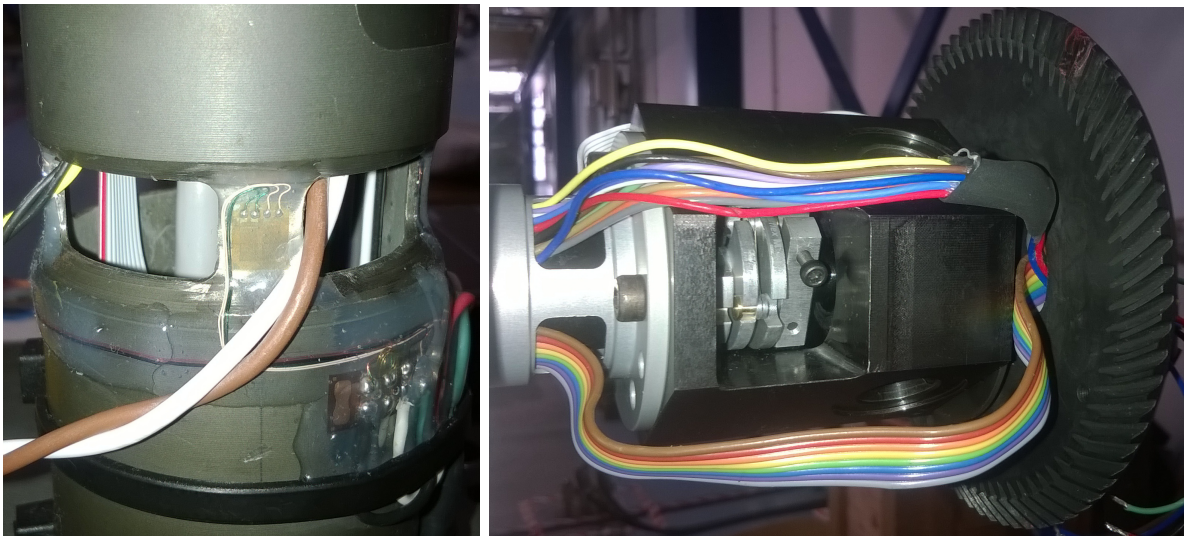

(a) Tower base lightening (b) Hub holes

Figure 2.9: Problematic areas of the model

Therefore, the first step was to identify whether the problem of vibrations was due to mistakes in the manifacturing process, and therefore present only in some wind turbines, or rather a design issue, and thus common to all the models. Moreover, it was also necessary to find a stiff enough support to counterbalance the softness of the wind tunnel floor.

The wind turbine models have been locked on two steel bars, staffed onto a very stiff

floor and than hit with a hammer, thus simulating an impulse excitation; the signal of the strain gages, manipulated through the FFT, allows to verify the values of the natural frequencies. In order to check the accuracy of the measurement, an accelerometer has also been mounted on the tower to identify the natural frequencies; the results are the same as the one obtained from the strain gages. Figure 2.10 shows the result obtained for the first turbine.

The same operation has been repeated for several wind turbines and the results are shown in Table 2.6. Since all the turbines have similar frequencies, which are also much lower than expected, it is clear that the problem was not connected to the manifacturing process.

Tower	Fore-aft [Hz]	Side-side [Hz]
1	14.4	16
2	14.6	16.2
3	14.4	16
5	14.2	15.8
6	14.6	16

Table 2.6: Natural frequencies table

In order to investigate the best support possible, three different kinds were tested. In each one of them a Bosch rail guide was used because, in this way, it is possible to distribute the support among a larger area of the floor and, therefore, reduce the effect of local compliances of the wind tunnel floor. The three configurations, shown in Figure 2.11, differ from each other in the position of the fixing bars and in the fact that, in the last one, no steel bars were used.

Configuration	Fore-aft [Hz]	Side-side [Hz]
1	13	14.6
2	13.4	15.8
3	14.6	15.8

Table 2.7: Natural frequencies table with different supports on stiff floor

It is clear that the removal of the steel bars leads to a much higher fore-aft frequency while leaving unchanged the side-side mode; it is also evident that, as expected, the frequencies of both modes rise by placing the fixing bars closer to the tower base. From the results of Table 2.7 the third configuration appears to be the most suitable and was thus tested on the wind tunnel floor, whose results are shown in Table 2.8. In this conditions, the compliance of the floor and the different fixing method led to a substancial drop of both frequencies, especially the side-side (Conf. 4); to attenuate this effect, two more rails were attached to the Bosch frame (Conf. 5a) leading to a slightly higher side-side frequency. Furthermore, the model was turned by 90 degrees (Conf. 6a), in order to increase the side-side frequency since the fore-aft mode is characterized by a higher aerodinamical damping and thus a lower frequency might still be acceptable. Finally, an alluminium stiffener was fixed to the top part of the tower to try to further increase the stiffness of the turbines. Conf 5b and 6b show a slight increase in both frequencies.

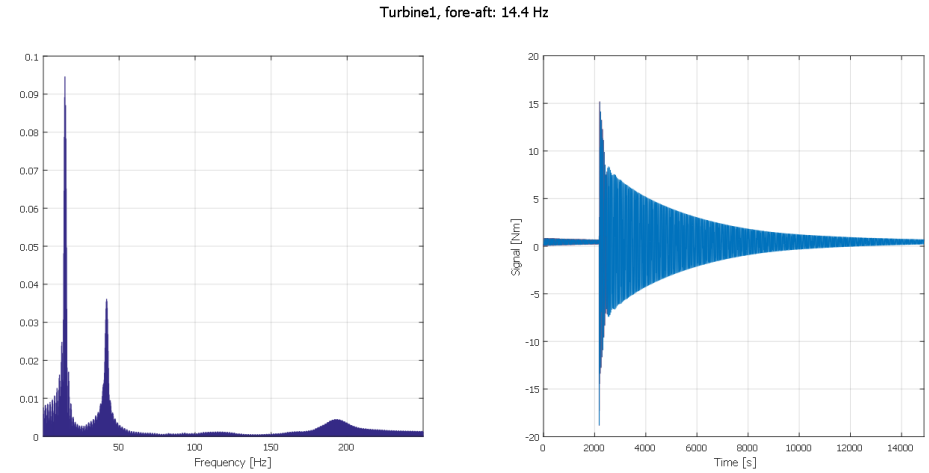

(a) Fore-aft vibration

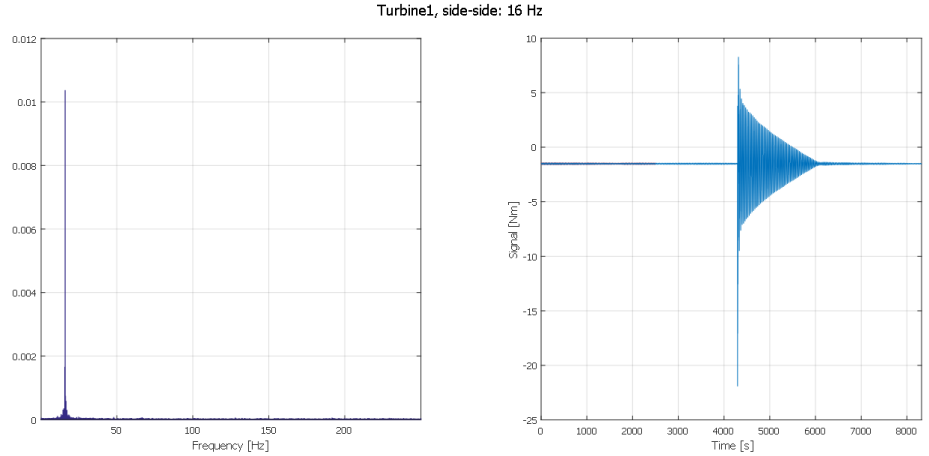

(b) Side-side vibration

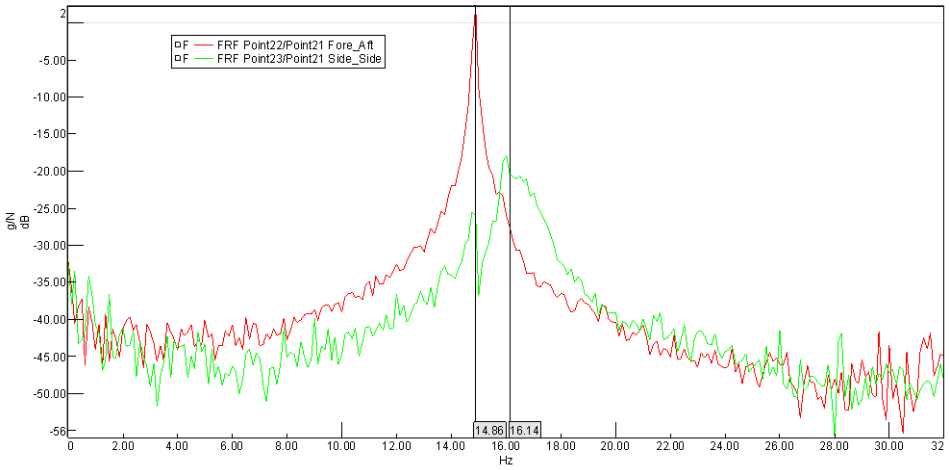

(c) Accelerometer FrF

Figure 2.10: Natural frequencies

In the end, however, none of these configurations were satisfying, since the the natural frequencies of the tower were still too close to that of the loads and the strain gages signal showed high stresses on the tower base. The last effort consisted in the connection of

Configuration	Fore-aft [Hz]	Side-side [Hz]
4	14	13.8
5a	14.2	14.2
6a	15	13.2
5b	15.2	15.2
6b	16.4	14

Table 2.8: Natural frequencies table with different supports on wind tunnel floor

the tower base directly on the steel beams that lie underneath the wooden floor of the wind tunnel; it should be noted, however, that this solution is not the ideal one, because, having the floor only four steel bars, the distance between the two rows of wind turbines is established by this criterion and leads the two rows of turbines to be 50cm closer to the lateral wall of the wind tunnel. This change, although not ideal, is deemed to have a negligible effect on the wind turbine performance and therefore this solution will be adopted in the future wind tunnel tests. The frequencies obtained with this kind of support are shown in Table 2.9; they are all sufficiently far from the load frequency and similar to each other, meaning that all wind turbines have been correctly fixed to the floor.

Tower	Fore-aft [Hz]	Side-side [Hz]
1	16.8	17.4
2	16.8	18
3	16.8	17.2
4	16.6	16.4
5	16.2	17.4
6	6.4	17.6

Table 2.9: Natural frequencies with the tower fixed to the steel beams

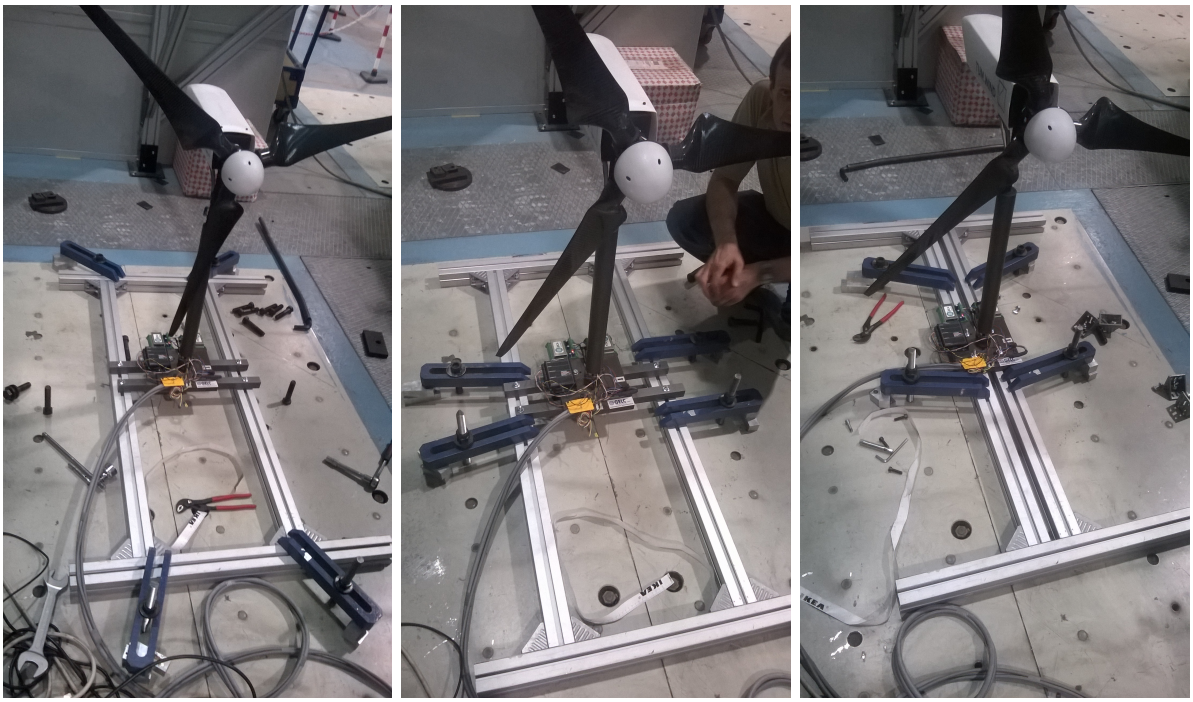

(a) Configuration 1 (b) Configuration 2 (c) Configuration 3

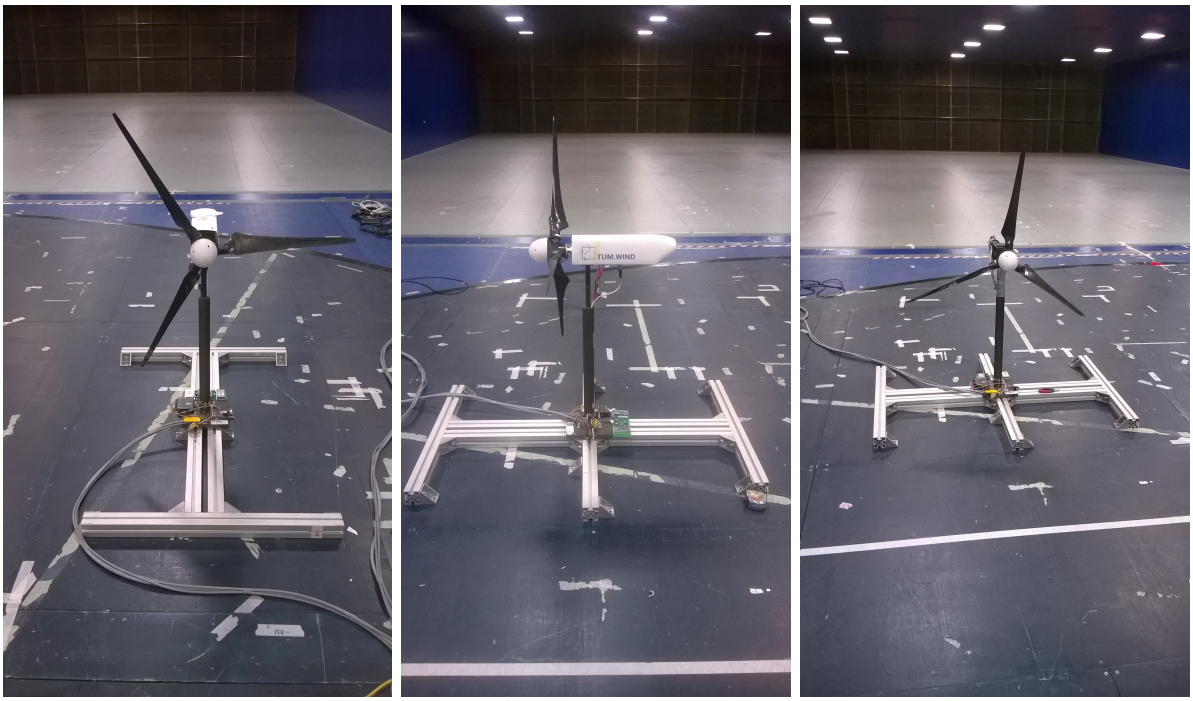

(d) Configuration 4 (e) Configuration 5 (f) Configuration 6

Figure 2.11: Support configurations

2.6 Simulink model

In any experimental test it is always a good practice to develop an analytic model in order to predict the behaviour of the plant prior to the actual test. In our case this modeling phase is particularly important since it fulfills the additional, important, task of tuning the gains of PID controllers that command the generator torque and the blade pitch; hence, an accurate plant model is considered a key aspect of this thesis project. It is important to recall that this is only a preliminary tuning, the final one was done using the physical test bench, which is the closest possible model to the actual behaviour in the wind tunnel. It is important to mention that the model described hereinafter relies in some extend in the data measured using the test bench, in particular regarding the friction torque (see Section 2.3). Therefore, it is not considered a fully analytical model; instead, it is a mixed model that manages to capture the plant behaviour even closer.

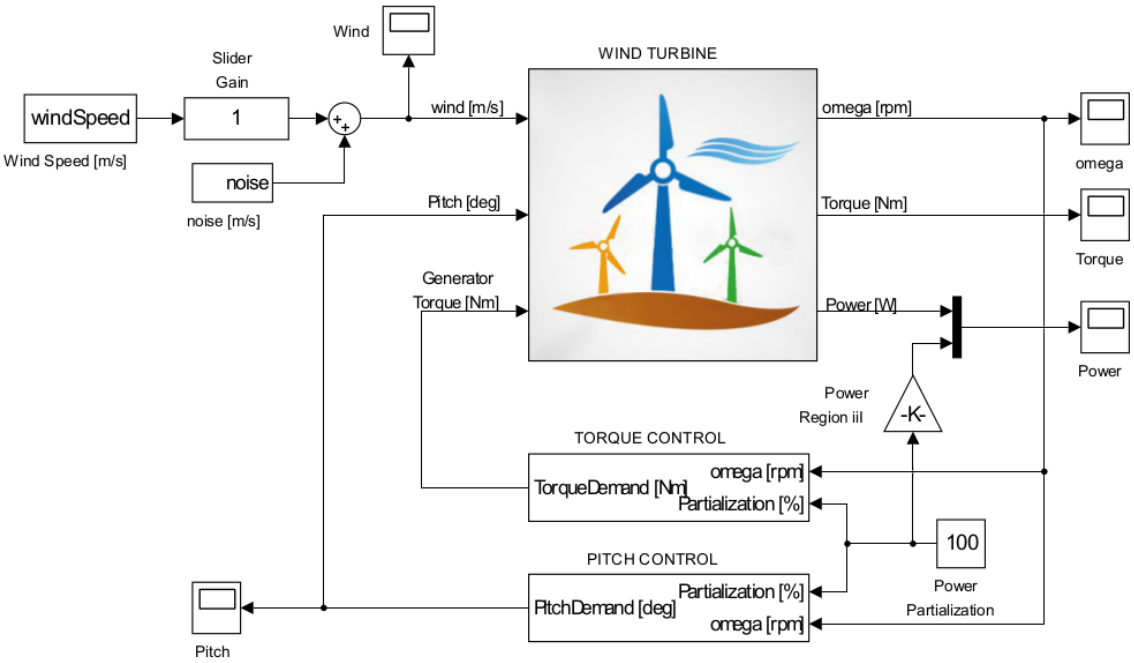

Figure 2.12: Simulink model

The general layout of the model developed in the Simulink environment is shown in Figure 2.12. From the block diagram it is clear that the model is divided in three main blocks: the wind turbine, the torque controller and the pitch controller. It has only two inputs: the wind speed, corrected using the noise measured in previous wind tunnel experiments (Figure 3.3), and the power percentage decided by the user. Which are actually the real inputs for the GUI developed for the wind tunnel testing (Section 3.8). The outputs, on the other hand, are the relevant turbine performance indicators: rotor angular speed, torque, pitch angle and power.

The wind turbine block, which is the central part of the model since it contains the wind turbine dynamic equations, is exploded in Figure 2.13. Its main output parameter is the turbine rotational speed since it is the single quantity used by the controllers to computed the regulation errors. The set of differential equations used to describe the turbine behavior and to integrate the angular speed enclosed in this block are summarized in Eq. 2.3 to 2.5.

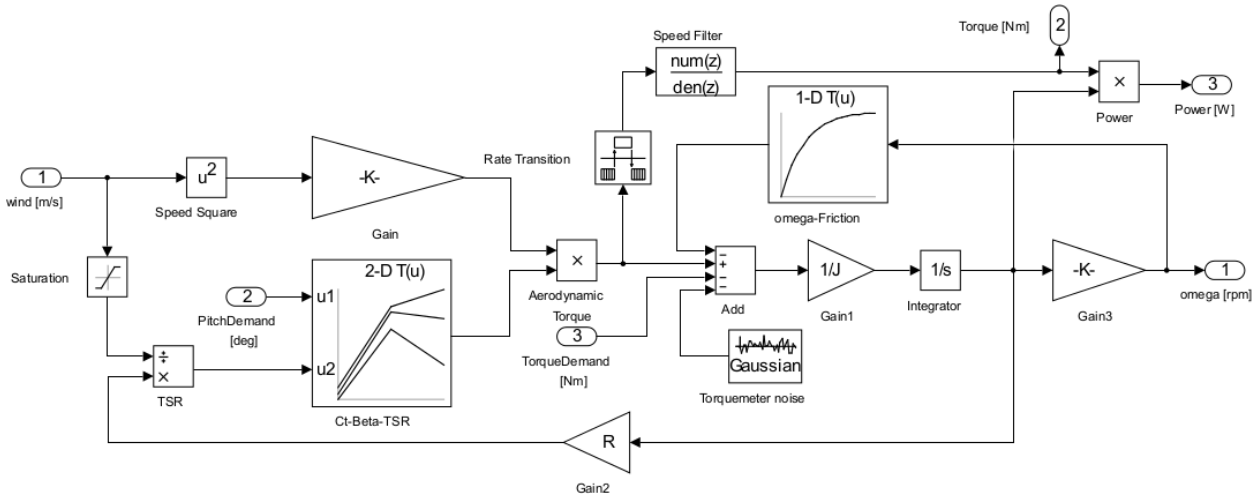

Figure 2.13: Simulink Wind Turbine model

$$J\dot{\omega} = Q_A - Q_F - Q_C - Q_{noise} \tag{2.3}$$

$$Q_A = \frac{\pi}{2}\rho V^2 R^3 C_Q \tag{2.4}$$

$$Q_C = k\omega^2 \tag{2.5}$$

Q_A: Aerodynamic torque.
Q_F: Friction computed using 1-D look-up table. Chapter 2.3.
Q_C: Torque demanded by the controller.
Q_{noise}: Estimated noise of the torquemeter.
C_Q: torque coefficient computed through 2-D look-up table. Chapter 3.2.

The two remaining blocks are exploded in Figures 2.14 and 2.15. Special attention was conferred to these blocks since they must correspond exactly to the code implemented in the real controller in order to be a reliable tuning tool. For instance, Figure 2.14 shows the pitch control, which is mainly a PI regulator based on $\dot{\omega}$ whose gains are scheduled with the blade collective pitch angle. The reference for the controller is function of the power partialization percentage and is specified through a 1-D look-up table, which is important in order to achieve the flexibility necessary to test different power partialization strategies, as is done in the actual controller application. The value specified in the table is the Region III rotation speed that in this case, for example, is assumed to be constant. The same strategy is used to specify the minimum pitch angle used to saturate the pitch demanded by the PI controller. The torque PI controller, shown in Figure 2.15, works in a similar way. It is based on ω and uses look-up tables to specify the reference speed and the upper and lower limits for the torque demand. This control strategy is used only in the Region II 1/2, which is very narrow for our models; nonetheless, it has been implemented because it may be useful in the future. It is worth noting that in both cases a basic PID controller has been chosen even if optimal control strategies could be also implemented. This choice is justified considering that, at this research stage, specifying the weighting indexes for the optimal control has almost the same uncertainty of specifying the PID gains. Moreover, it is important to make the reader aware that the the Simulink model

could be also used as a schematic diagram that summarizes the whole project; thus, it could be helpful to understand the rest of this document; in particular, the application development chapter.

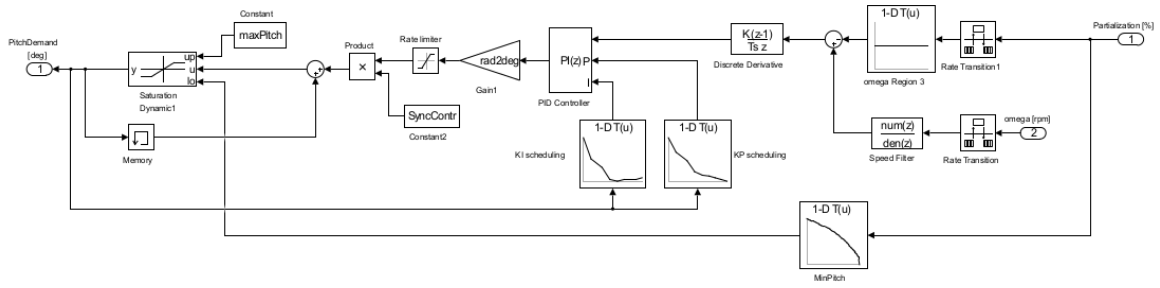

Figure 2.14: Simulink Pitch Control model

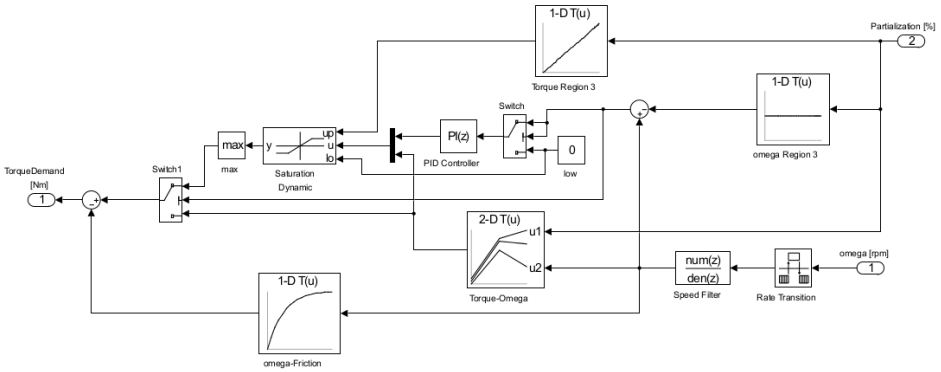

Figure 2.15: Simulink Torque Control model

Finally in order to assert the reliability, at least qualitatively, of the Simulink model, the simulated and measured responses for a wind tunnel power partialization test are compared in Figure 2.16. As expected, the mean speed, torque, pitch and power produced for the steady state response are exactly the same in both cases. The dynamic response, on the other hand, is different from the real one; however, the model manages to capture successfully the amplitude of the oscillatory response. It is worth noting that the values computed using the Simulink model were filtered with the same transfer functions implemented in the control application for the real machine in order to get comparable results.

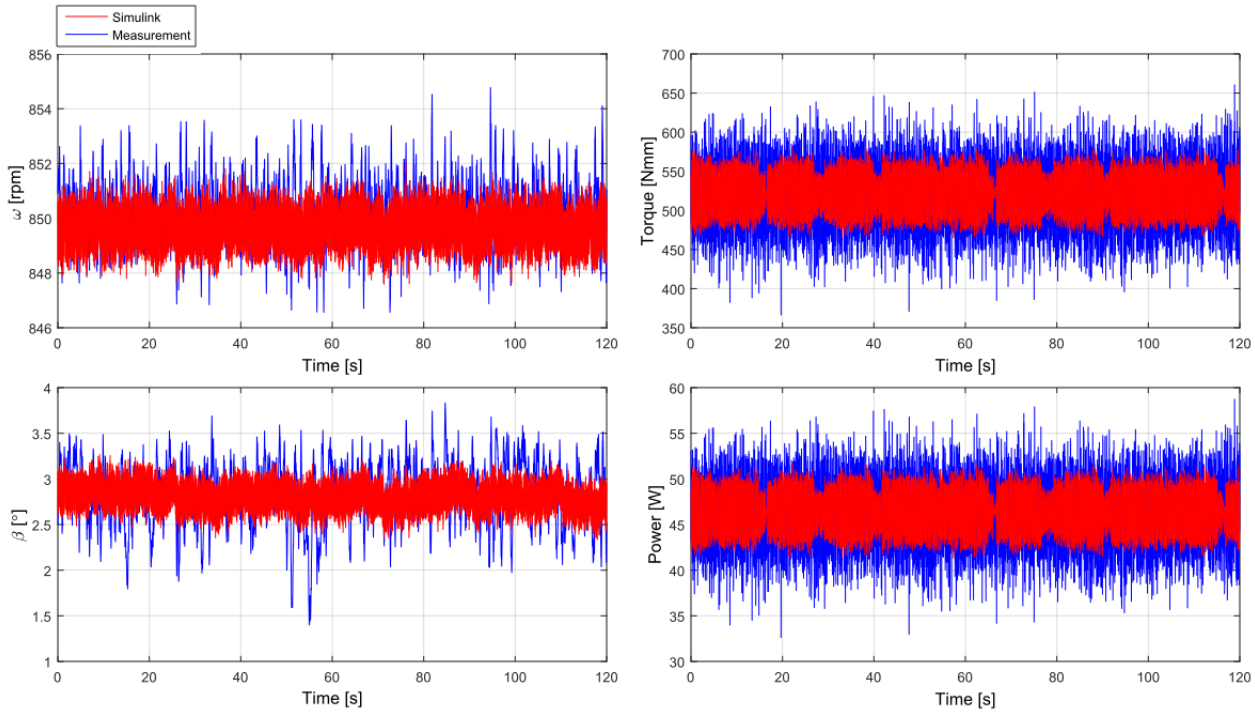

Figure 2.16: Simulink vs Measured data

Chapter 3

Applications development

Although the machine could be operated even without any programming code just by inserting values of current in the corresponding channels, it would be very hard to operate it; it would also be impossible to control it or to simulate the operation of a real wind turbine. To accomplish these purposes, it is necessary to develop applications, which are C language codes written within the Solution Center, the software provided by Bachmann Gmbh., and installed inside the Bachmann hardware. Several applications have been developed, partially from scratch and partially from pre-existing ones, and each one manages a different part of the machine.

Most of the applications communicate with each other through the `svi_GetAddr`, `svi_GetVal` and `svi_SetVal` functions. The first one allows to get the address of a variable, the second to read the value stored at that address, the latter to write a new value. The applications that exchange data through a CAN network represent an exception, since they use other functions such as `mio_GetDrv`, `mio_GetValue` and `mio_SetValue`, which, however, fulfill the same purposes.

3.1 Main

The Main application is the only application that reads values directly from the MIO; in this way, all the conversion of measure units are computed only in this application. In order to have more flexibility, however, the user can still run the other applications without the Main; at the beginning of the code of each application, in fact, the following line

#define runMainApp 1

allows the user to choose whether he wants to use the application together with the Main application or as a stand-alone application. In the former case, the user should set runMainApp equal to 1 and the code will read values from the Main; in the latter, instead, runMainApp should be set equal to 0 and the application will read values directly from the MIO. It should also be remarked that, since the pitch does not communicate through digital/analog inputs/outputs but rather with CAN protocol, the reading of the values related to pitch is demanded to the pitch application, which then writes on the Main application so that all the other apps can read from it. It is also worth noting that the Main application does not read values from other applications, but rather the other applications write on the Main using the `svi_SetVal` function. In this way, it is possible to install the Main alone without incurring in errors.

A second purpose of this application is the removal of offsets in the measurements. This is performed by recording data for 10 seconds, computing the average and substracting it from the measurement. This operation is performed for the encoder angular speed, the strain gages, the generator speed and the torque.

Additionally, the Main application also allows the recording of data. The variables are first stored into a buffer and then written in a binary file. Three different buffers are available: the fast, slow and control buffers. The fast one records time, encoder speed, bending hub and torque measurements at a frequency of 2500 Hz. The slow buffer, instead, records time, power generator speed, current, actual and demand pitch angles, strain gages and Pitot measurements at a frequency of 250 Hz. A third buffer, called control buffer, is available but not currently used. Each buffer also records the ID and the TOP; the first one corresponds to the recording time multiplied by the recording frequency; the latter, instead, allows the user to distinguish between different measurements recorded in the same binary file.

Finally, the Main application computes the angular speed from the encoder azimuth signal placed on the shaft. It is a digital incremental encoder with 2 signals not in phase. Since it is equipped with 2500 counts per round, it has 10000 signals. The actual azimuthal position can therefore be calculated as

$$\theta = (Encoder\_value \,\%\, 10000)\frac{360}{10000} \tag{3.1}$$

Table 3.1 summarizes the variables read in the Main application. The values are not in a physical unit of measure because the Bachmann hardware accepts only voltage; hence, the conversion factors are also shown. The user, however, should be aware that they can change according to the configuration of the EPOS or ESCON control boards.

Variable	AIO288	Conversion
Torque	Mod. 7, Channel 1	$\frac{10}{32768} \cdot \frac{1}{5} \cdot 1000$ [Nmm/Bachmann]
Powergenerator_Speed	Mod. 6, Channel 1	$\frac{10}{32768} \cdot \frac{14000}{4} \cdot \frac{1}{14}$ [rpm/Bachmann]
Powergenerator_Temperature	Mod. 6, Channel 2	$\frac{10}{32768} \cdot \frac{250}{10}$ [Â°C/Bachmann]
Powergenerator_Set_Value	Mod. 6, Channel 9	$\frac{10}{32768} \cdot \frac{4}{10}$ [A/Bachmann]
Powergenerator_Enable	Mod. 6, Channel 10	
Wind_Current	Mod. 7, Channel 9	$\frac{10}{32768} \cdot \frac{4}{10}$ [A/Bachmann]
Wind_Enable	Mod. 7, Channel 10	
Wind_Speed	Mod. 7, Channel 2	$\frac{10}{32768} \cdot \frac{14000}{4} \cdot \frac{1}{14}$ [rpm/Bachmann]

Table 3.1: Main variables

3.2 Wind Generator

The Wind Generator application controls the motor used to simulate the wind; the code reads the values of measured angular speed, measured pitch angle and wind speed from the Main and computes the corresponding current:

`i = WindGenerator(`ω, β`,V)`

The application than reads a table of torque coefficients C_Q as functions of the measured pitch angle β and the tip speed ratio λ; the values of C_Q have been obtained in the design stage and are plotted in Figure 3.1 and 3.2.

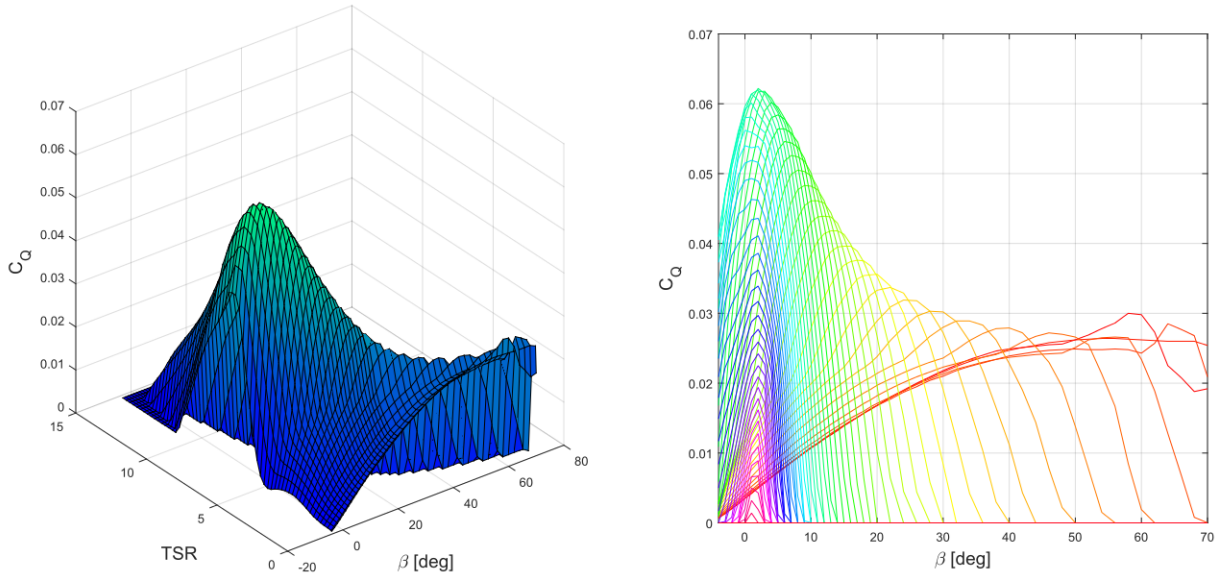

Figure 3.1: Torque coefficient vs β [deg]

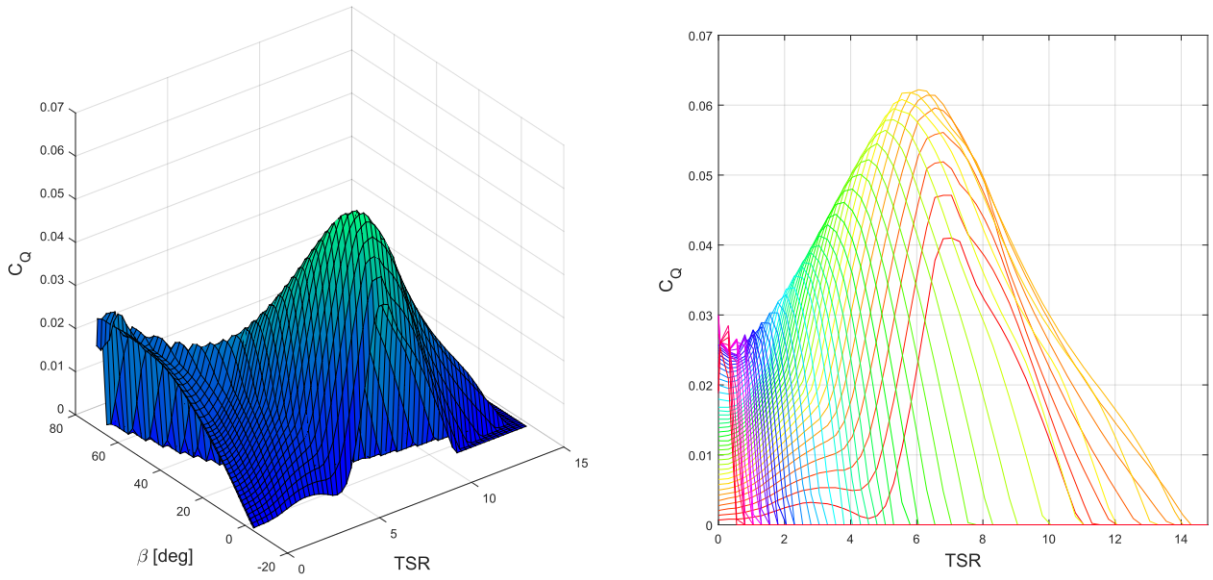

Figure 3.2: Torque coefficient vs TSR

The corresponding aerodynamic torque is

$$Q = K\frac{\pi}{2}\rho V^2 R^3 C_Q(\lambda, \beta) \tag{3.2}$$

where K is a moltiplicative coefficient that accounts for the reduction of aerodynamic torque due to the low Reynolds number and is computed as in Eq. 3.3.

$$K = a\left(\frac{\omega_{ref}}{\omega}\right)^2 + b\left(\frac{\omega_{ref}}{\omega}\right) + c \tag{3.3}$$

$$a = -0.934 \tag{3.4}$$

$$b = 2.1 \tag{3.5}$$

$$c = -0.165 \tag{3.6}$$

The torque is then converted to current by inverting Eq. (2.1)

$$i = \frac{1}{\beta}\left(Q - \alpha\omega - \gamma\right)\left(1 - Brake\right) \tag{3.7}$$

Since the presence of γ leads to a current different from zero even when the speed and torque are null, a brake variable was introduced, so that it is possible to manually set the current to 0 A.

To achieve a more realistic simulation of the wind, noise on the wind speed has also been introduced; a variable that acts as a flag allows the user to choose whether he wants a constant wind speed or a noisy one. The amplitude and shape of the noise have been taken from previous experiments conducted in the wind tunnel at 4 m/s in order to have a reliable trend; Figure 3.3 shows the noise signal that is superimposed to the desired constant wind speed.

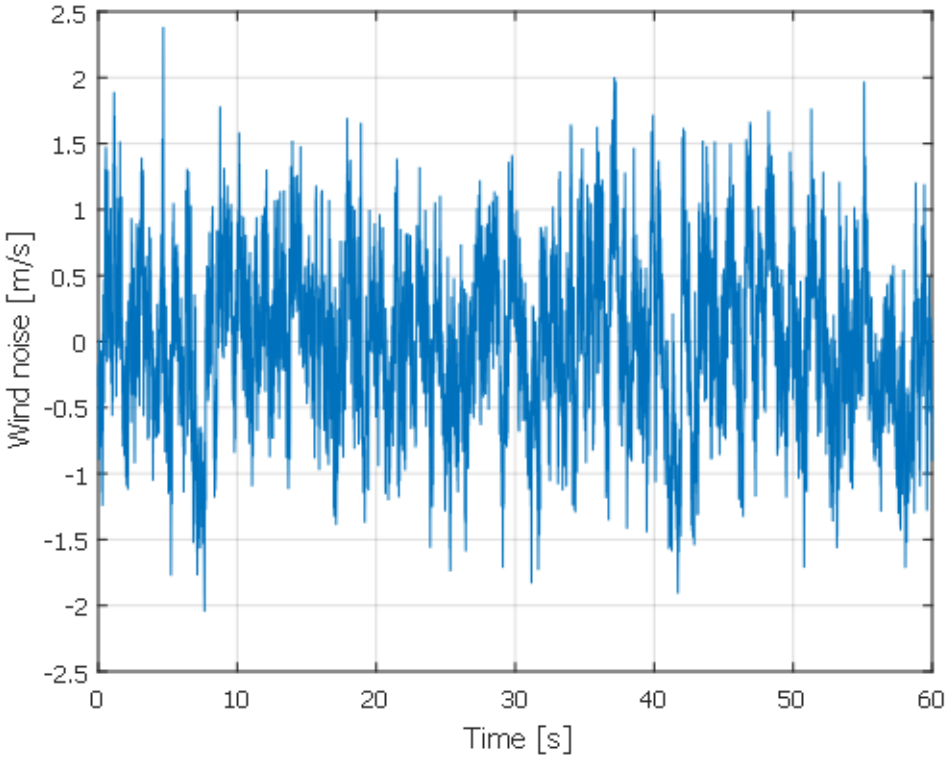

Figure 3.3: Wind speed with noise

3.3 Power Generator

The Power Generator application controls the motor devoted to power production. The application reads the values of angular speed, demanded torque and measured torque as inputs and computes the corresponding current value

$$\texttt{i = PowerGenerator}(\omega, \texttt{Q}_{\texttt{ref}}, \texttt{Q})$$

The variable `Control_Mode` allows the Power Generator application to work according to two different ways: current control, when the variable is set to 2, or speed control, when it set to 3.

3.3.1 Current control

When the current control is selected, the applications works as illustrated in Fig. 3.4

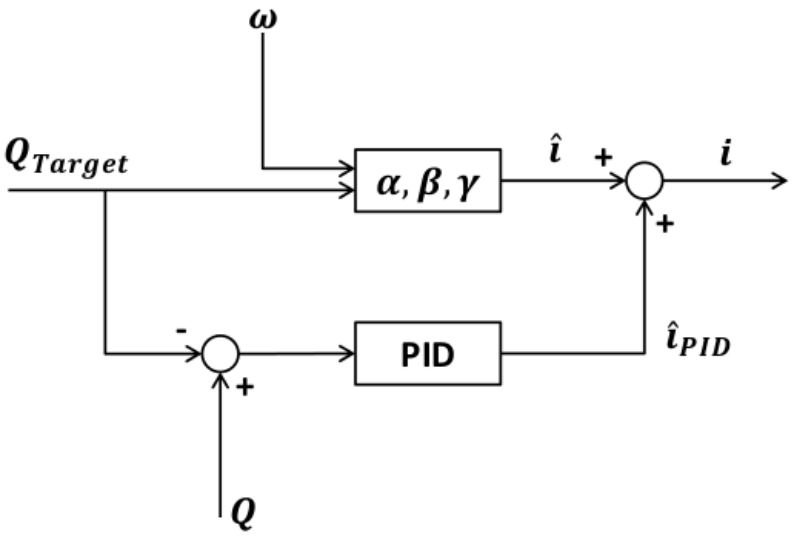

Figure 3.4: Current mode block diagram

Basically, the current $\hat{i}$ is computed according to Eq. 3.9, using the measured rotor speed, the reference torque, which is calculated by the controller application, and the coefficients related to the Power Generator motor. The measured torque, however, could be different from the reference one; for this reason, reference and measured torques are compared and the error is used by a PID controller to provide, as in Eq. 3.10, the current $\hat{i}_{PID}$ that corrects $\hat{i}$. The current value set to the motor is thus

$$i = \hat{i} + \hat{i}_{PID} \tag{3.8}$$

$$\hat{i} = \frac{1}{\beta}(Q_{ref} - \alpha\omega - \gamma)(1 - Brake) \tag{3.9}$$

$$\hat{i}_{PID} = K_P(Q_{ref} - Q) - K_D\dot{Q} + K_I \int (Q_{ref} - Q)dt \tag{3.10}$$

3.3.2 Speed control

When the variable Control_Mode is set equal to 3, the Power Generator works in speed control, which means that employs a PID controller that, acting on the error between the measured angular speed and the desired speed, provides the current value

$$i_{PID} = K_P(\omega_{ref} - \omega) - K_D\dot{\omega} + K_I \int (\omega_{ref} - \omega)dt \tag{3.11}$$

This mode is particulary useful when the controller application is either not installed or not used. In that case, in fact, the reference torque is not available and therefore the previous approach is not exploitable. Moreover, in speed control mode the user can decide the speed of the rotor and therefore easily test different operative conditions.

3.4 Controller

The main purpose of the controller application is to compute the torque and pitch angle that the Power Generator and the pitch motor should apply based on the operative condition of the machine. By plotting torque, speed, power and pitch angle against the wind speed, it is possible to identify different operative conditions, as shown in Figure 3.5:

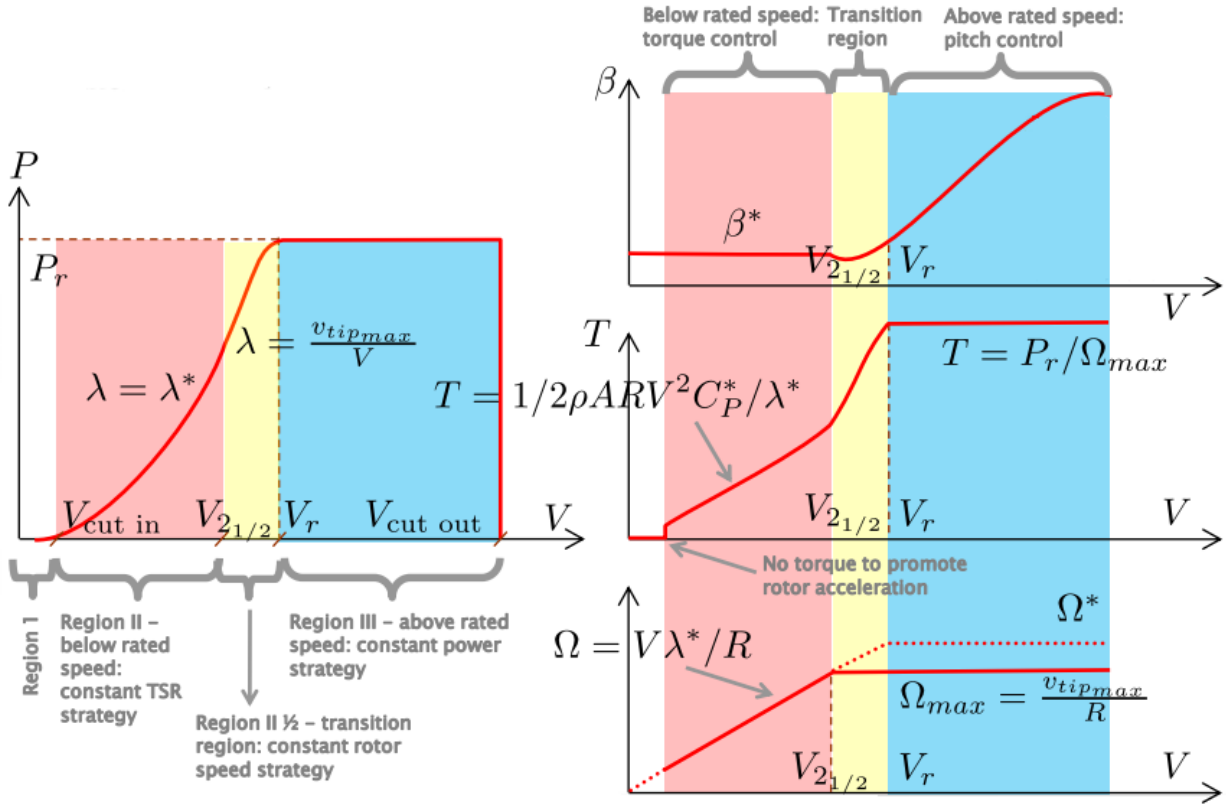

Figure 3.5: Operative conditions of a wind turbine

- **Region I**: when the wind speed is lower than the cut in speed, the wind turbine is not activated; hence the angular speed and the power are both zero.

- **Region II**: when the wind speed is higher than the cut in speed, the machine is activated. Since the wind turbine works at a constant tip-speed-ratio λ^*, the angular speed increases linearly with the wind speed according to Eq. 3.12.

$$\omega = \frac{\lambda^*}{R} V \tag{3.12}$$

The torque, instead, increases quadratically according to Eq. 3.13.

$$Q = \frac{\pi}{2} \rho R^3 V^2 {C_Q}^* \tag{3.13}$$

The power is related to torque and angular speed; however, by substituting Eq. 3.12 into Eq. 3.13, it is possible to obtain a cubic relationship between power and wind speed.

$$P = Q\omega = \frac{\pi}{2} \rho R^2 V^3 {C_P}^* \tag{3.14}$$

In this region, however, the pitch angle is kept to the minimum value.

$$\beta = \beta^* \tag{3.15}$$

- **Region II 1/2**: when the rotor speed reaches the maximum admissible value, the power might not have yet reached the desired value, which means that the torque should further increase. To this purpose, a PID controller acting on the error between the desired and the actual speed is used, whereas the pitch angle is still kept to the minimum admissible value. However, it is worth noting that the current machine presents a very narrow, almost imperceptible, region II 1/2 and therefore the torque PID, although present, is not used.

- **Region III**: at the end of region II 1/2 both power and speed have reached the target value. A further increase of wind speed would thus involve an increase of either torque or power. The solution to this problem is a PID controller acting on the pitch: as the wind speed increases, the pitch angle also increases, keeping constant both the torque and the angular speed.

Hence, it is clear that the controller is a very important application that, by acting on pitch and torque, allows to automatically operate the machine according to the desired values of speed and produced power. Two different controllers have been implemented: the first was written partially at Politecnico di Milano and partially at TUM, whereas the second was written using Simulink by KNU and later converted in a C code.

3.4.1 TUM/POLIMI controller

The TUM/POLIMI controller employs mainly three functions: Controller_App, PoliWindController and ReadData. The first is the main application, whose purpose is the reading and writing of variables from and to the Main application: the values of torque, speed, pitch angle and azimuth position are read and the demanded torque and pitch are written. The second function, PoliWindController, contains the DISCON function, which actually employs the controller. The control action depends on the state of the machine, which is represented by the variable iState:

- **iState = 0: IDLE**
  In this condition the control is not activated. The torque demand is therefore set to 0; as a safety measure, the pitch angle is set to the maximum value.

- **iState = 1: POWER PRODUCTION**
  This case represents the normal operative condition of the scaled wind turbine, which is subjected to the control action in order to automatically produce the desired power. Since two different control types have been implemented (TUM/POLIMI and KNU), the variable data.CTRL allows to choose between them: a value of 100 corresponds to the KNU controller, whereas a value of 0 indicates the PID TUM/POLIMI controller.

  The first task that the controller should perform is the computation of the demanded torque. Since the wind turbine operates at a constant tip speed ratio, the following relationship yields:

$$Q_D = \frac{\pi}{2}\rho R^3 V^2 C_Q = \frac{\pi}{2}\rho R^4 \left(\frac{\omega}{\lambda}\right)^2 C_Q = k\omega^2 \tag{3.16}$$

  Several combination of speed and torque have been used to create a look up table; the code searches the values of speed in the look up table closest to the actual velocity and than interpolates between the corresponding torques to find the demanded torque; the table is also saturated at the maximum admissible torque.

  A second, important, feature of the controller application is the power partialization. Although the scaled wind turbine has been designed to produce 46 W of power, one could be interested in the production of a power lower than 100% of the rated value. This goal is also fulfilled by means of look up tables. It is important to notice that the same overall power partialization can be achieved in different ways; in fact, by defining η the reduction in produced power, it is possible to relate it to speed and torque with Eq. 3.17

$$P_{part} = \eta P = \eta_1 \omega \cdot \eta_2 Q \tag{3.17}$$

  Therefore several combination of η_1 and η_2 are admissible, as long as $\eta_1\eta_2 = \eta$. In this case, it was chosen to mantain constant the angular speed of the rotor and thus to partialize power by reducing only the torque, as in Eq. 3.18 and 3.19.

$$\eta_1 = 1 \tag{3.18}$$

$$\eta_2 = \eta \tag{3.19}$$

  Figure 3.6 shows the values of torque depending on the partialization percentage that are currently used in the TUM/POLIMI controller.

  Finally, the control application employs a PID controller for the computation of the demanded pitch. First, the demanded pitch rate is computed according to Eq. 3.20.

$$\dot{\beta}_D = K_P(\dot{\omega}_{ref} - \dot{\omega}) - K_D\ddot{\omega} + K_I(\omega_{ref} - \omega) \tag{3.20}$$

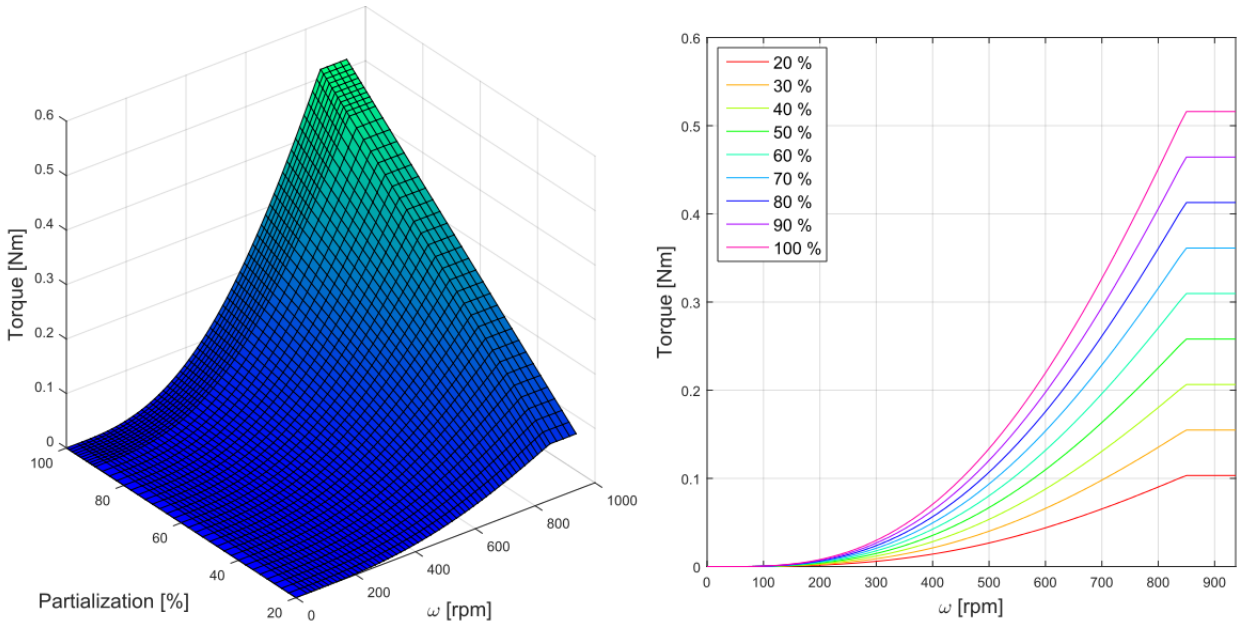

Figure 3.6: Power partialization with TUM/POLIMI controller

The demanded pitch angle is therefore equal to

$$\beta = \beta_{old} + \dot{\beta}_D \Delta t \tag{3.21}$$

Both the pitch angle and and the pitch rate are limited between the maximum and the minimum admissible values.

- **iState = 2: SHUT DOWN**
  In this condition the pitch angle is set to the shut down value. The torque is then calculated with a look-up table based on the speed until the angular speed becomes lower than a certain, prescribed, value; when it happens, the torque demand is automatically set to zero.

- **iState = 10: START UP**
  When the the user chooses the automatic control mode, the machine is by default in start up. If the rotor speed is less than a prescribed value, defined in the data.StartSpeed variable and equal to 220 rpm, the control computes the tip speed ratio λ based on the wind speed and rotor speed measurements and calculates the demanded pitch angle, as function of λ, through a look-up table; this angle is than limited between a maximum and minimum values computed based on the maximum admissible pitch rate. On the other side, the demanded torque is equal to zero. As soon as the rotor speed exceeds the limit value the demanded torque and pitch are set equal to the measured ones and the iState variable is set equal to 1. Moreover, a low pass IIR filter on the pitch angle was implemented because, during the start up stage, the pitch should stay still at a fixed value (50 deg); due to the noise, however, the pitch motor tried to apply small but fast variation of the pitch angle; a filter with a very low cut off frequency (5 Hz) solved this problem. Eq.

3.22 shows the discrete transfer function used for the pitch filter.

$$H_{pitch}(z) = \frac{0.000013z^4 + 0.000053z^3 + 0.000080z^2 + 0.000053z + 0.000013}{z^4 - 3.671729z^3 + 5.067998z^2 - 3.115967z + 0.719910} \quad (3.22)$$

It is worth noting that such a low cut off frequency will definitly slow down the response of the system; in the start up stage, however, this is a negligible issue.

if $\omega >$ data.StartSpeed

Q = MeasuredTorque;

β = MeasuredPitch;

data.iState = 1;

else

Q = 0;

$\beta_{start,i} = \beta(\lambda)$

β = LIMIT($\beta_{start,i}$,$\beta_{start,i-1} - \dot{\beta}t$,$\beta_{start,i-1} + \dot{\beta}t$);

3.4.2 KNU controller

The KNU controller was developed, using Simulink, by the Kyungpook National University (KNU). It had, however, to be converted to a C code and then integrated into the suite of applications that govern the operation of the machine.

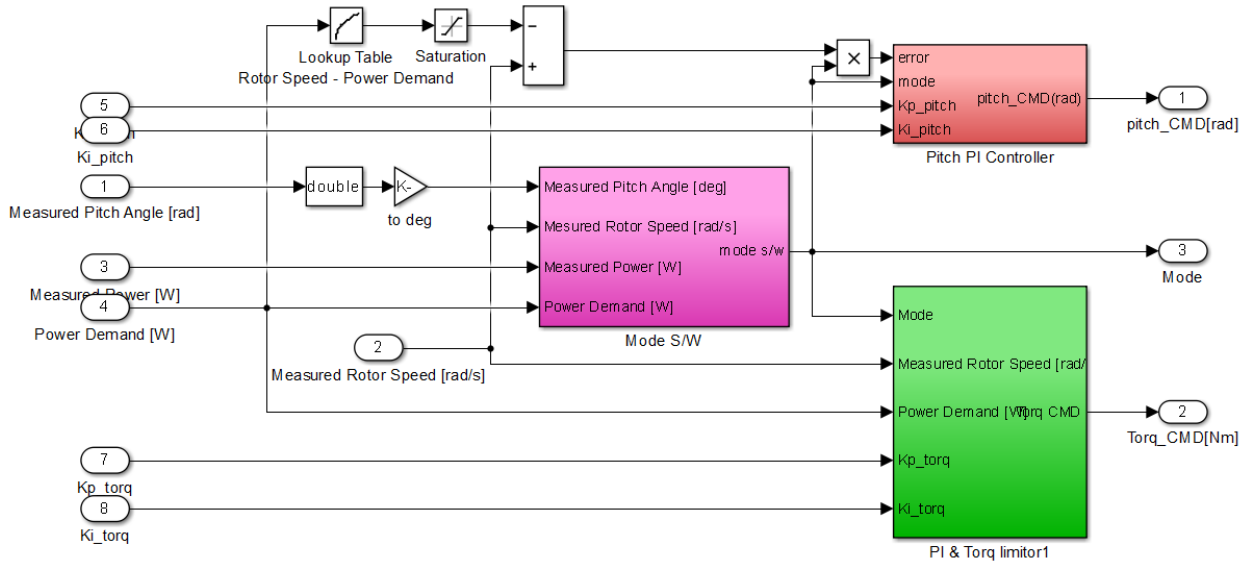

Figure 3.7: KNU control model

The control is realized, similar to the TUM/POLIMI one, with two PID controllers on torque and pitch. A switch allows to decide whther the machine is operating in Region II or Region III, based on the values of pitch angle, rotor speed and power.

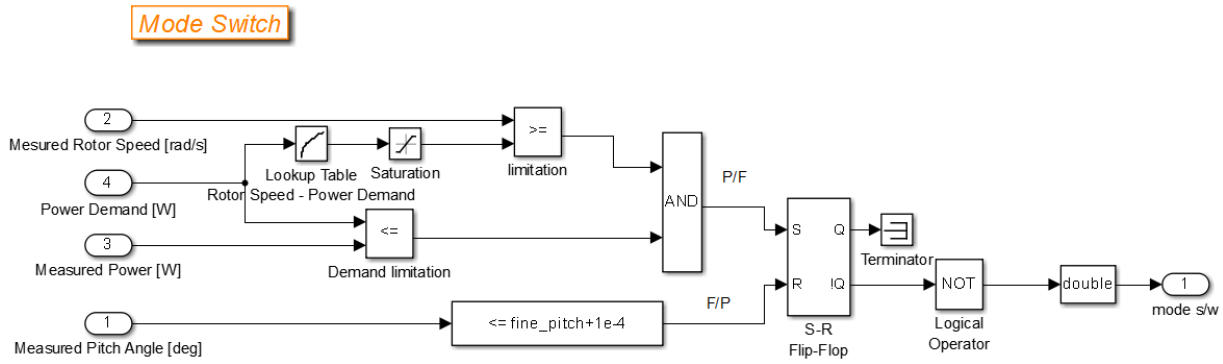

Figure 3.8: KNU control model: switch

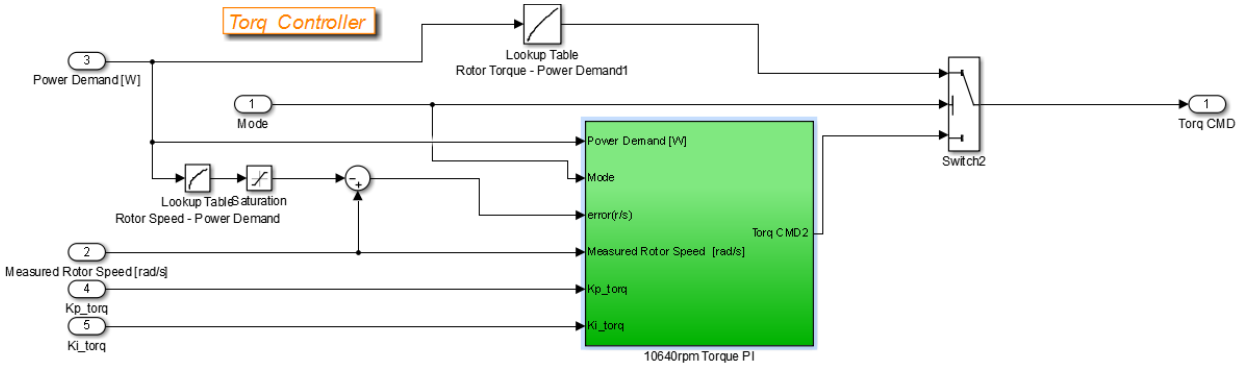

Figure 3.9: KNU control model: torque controller

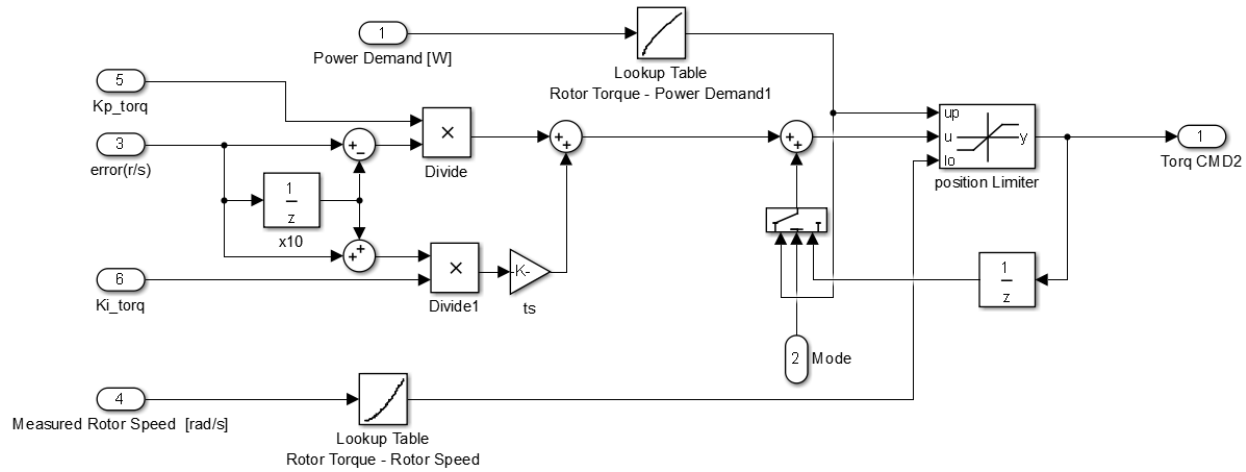

Figure 3.10: KNU control model: torque PI

It is worth noting that the power partialization strategy adopted in the KNU code is slightly different from that used in the TUM/POLIMI controller. In this case, in fact, it was chosen to give the same scaling coefficient to the velocity ω that appearas twice in the formula of the power:

$$P = T\omega = k\omega^2\omega \tag{3.23}$$

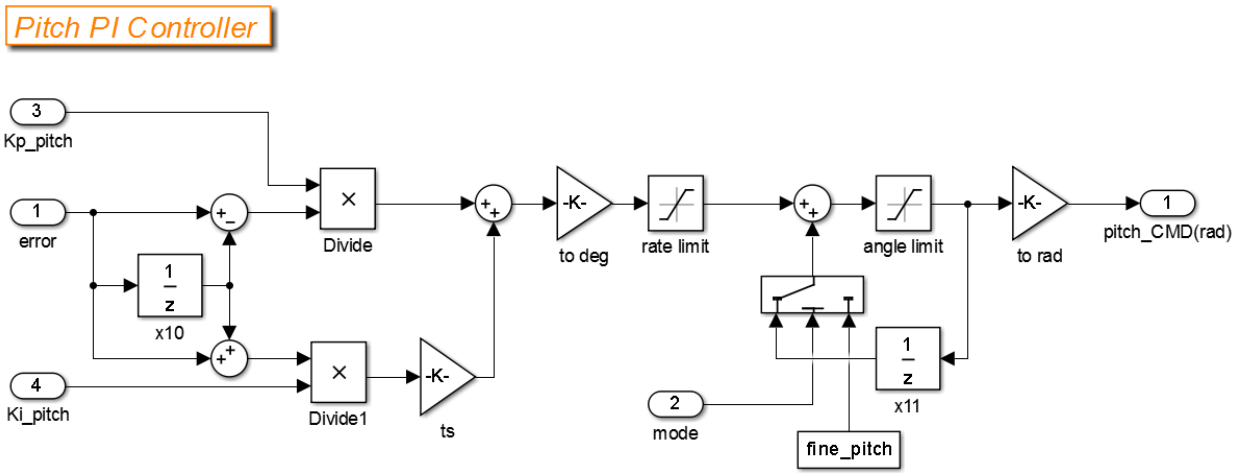

Figure 3.11: KNU control model: pitch PI

Therefore, the following combination of coefficients was chosen:

$$\eta_1 = \eta^{2/3} \tag{3.24}$$

$$\eta_2 = \eta^{1/3} \tag{3.25}$$

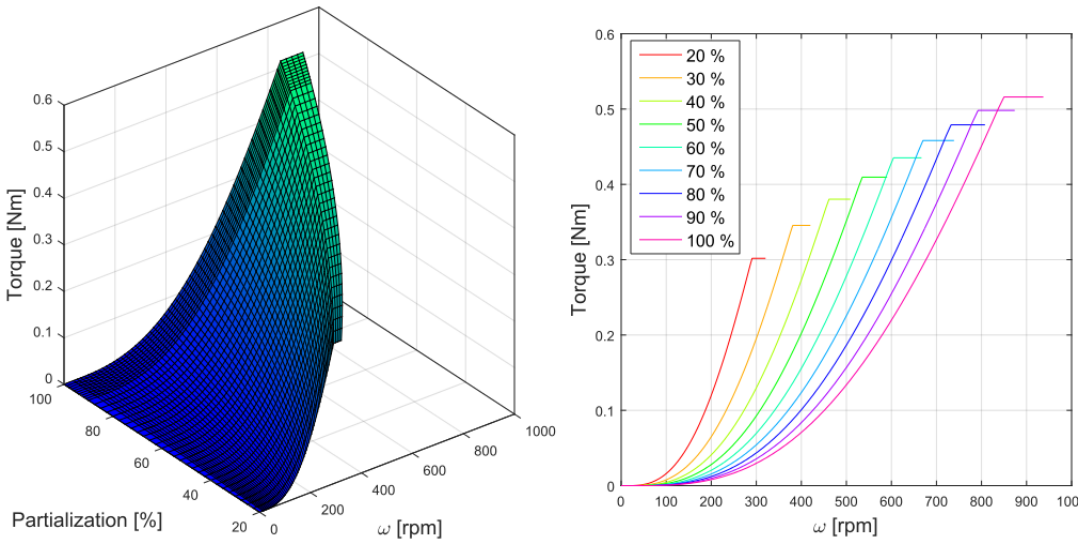

Figure 3.12: Power partialization with KNU controller

3.4.3 Speed and torque filter design

Since the controller application computes the demands based on the values of speed and torque, it is important to limit the effect of noise on these two variables; therefore, two different IIR low-pass digital filters have been designed. A representative signal for both torque and speed was recorded and converted into the frequency domain using the Fast Fourier Transform and the results are shown in Fig. 3.13 and Fig. 3.14 for torque and speed respectively.

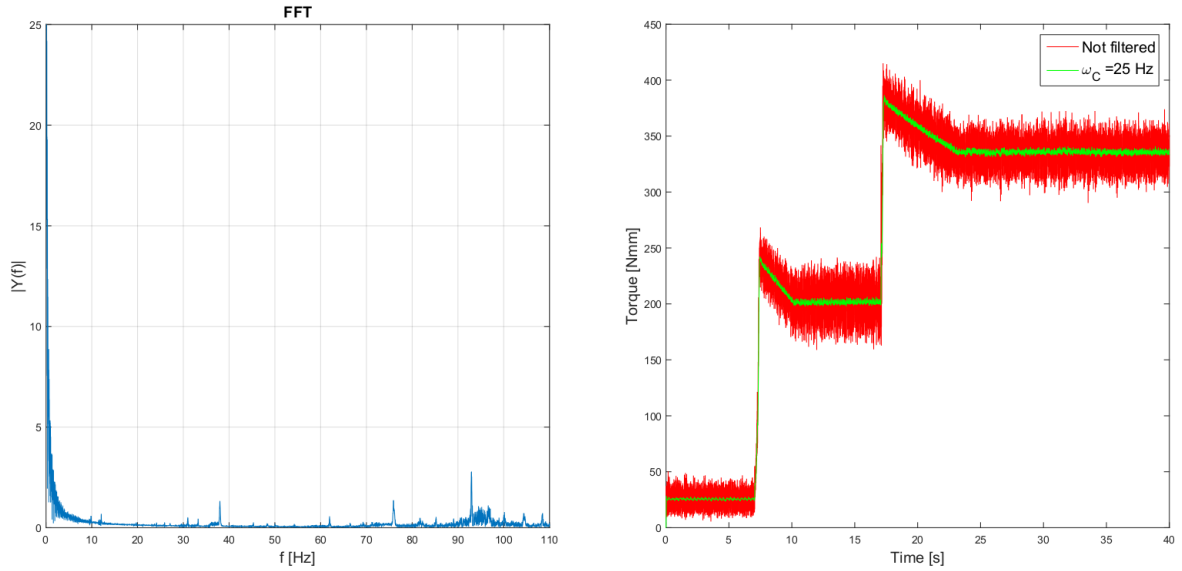

Figure 3.13: Torque FFT and signal

It is clear that the speed signal is quite unaffected by noise; nonetheless it is wise to include a filter, so that any unexpected fast variation of the signal would be filtered out. However, since no particulary filtering capabilities are required, the filter should be designed so that its response is as fast as possible; the cut off frequency was thus chosen as high as possible (100 Hz). The torque signal, however, is slightly more complicated. As always, the design of a filter is a compromise between its filtering capabilities and its response speed. In this case, a 4^{th} order filter with a cut off frequency of 25 Hz was deemed suitable. Eq. 3.26 and 3.27 show the transfer functions of the torque and speed filters.

$$H_{torque}(z) = \frac{0.004824z^4 + 0.0193z^3 + 0.02895z^2 + 0.0193z + 0.004824}{z^4 - 2.37z^3 + 2.314z^2 - 1.055z + 0.1874} \quad (3.26)$$

$$H_{speed}(z) = \frac{0.4328z^4 + 1.731z^3 + 2.597z^2 + 1.731z + 0.4328}{z^4 + 2.37z^3 + 2.314z^2 + 1.055z + 0.1874} \quad (3.27)$$

3.5 Pitch

The pitch application communicates with the EPOS control board in order to set the pitch demand to the pitch motor and to read the measured pitch angle and the communication

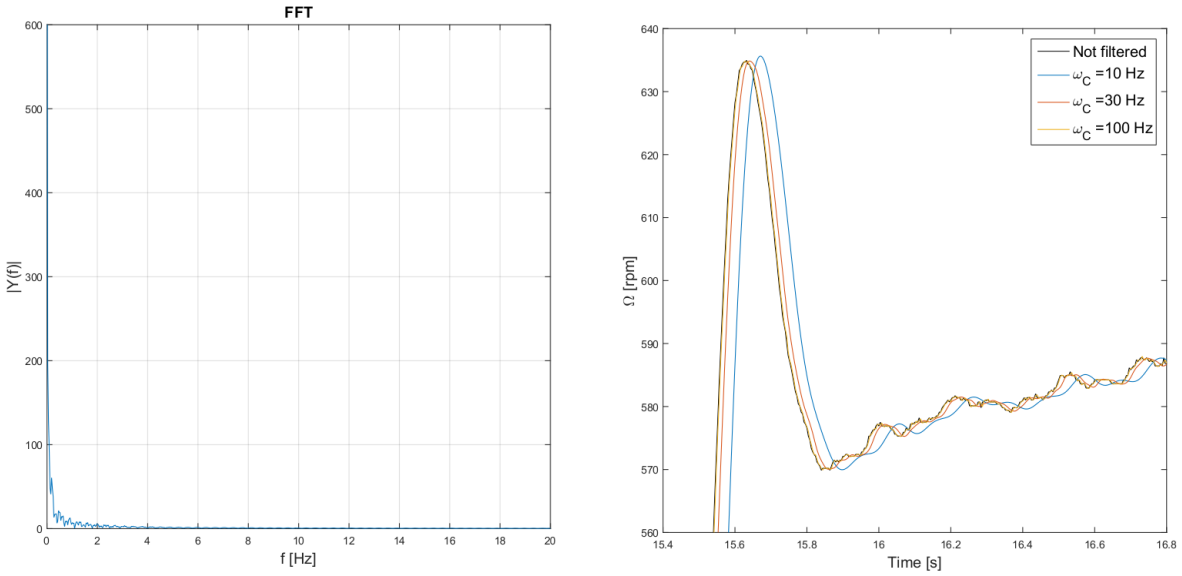

Figure 3.14: Speed FFT and signal

is performed according to the CAN-Open protocol. In order to have access to the pitch motor variables, the PDO connections have to be configured. There are two kind of PDOs, receiver and transmitter, and each one of them can contain variables up to 8 bytes. Table 3.2 shows how the PDOs should be configured.

PDO Number	Variables
RxPDO1	Controlword Modes of Operation Target Position
RxPDO2	Position Mode Setting Value
TxPDO1	Statusword Modes of Operation Display Position Actual Value
TxPDO2	Current Demand Value Current Actual Value Continuous Current Limit
TxPDO3	Analog Input 1 Analog Input 2

Table 3.2: PDO configuration

Once the PDOs are configured, the variables written within will be assigned to certain channels, ranging from 1 to the number of variables. It is important to check which channel corresponds to which variable because this information has to be provided to the pitch application, in the ProcImg_Init function, in order to write or read the correct values.

Although the main goal of the pitch application is to communicate measured and demanded pitch angle, it also performs other important tasks necessary to ensure the functionality of the motor and the correct measurements of pitch angles. To accomplish these purposes, the pitch application is developed as a state machine through a switch statement on the variable Flag_state_machine. This means that, according to the values of this variable, different operations will be performed and, when a certain criterium is satisfied, the variable will be incremented by 1, thus leading to a new state.

- **case 0**: this state corresponds to the first condition encountered as soon as the pitch application starts running. The only operation performed in this state is the definition of the mode of operation. As explained in [11], several operating modes are possible, such as position, velocity, current and homing mode; although the position mode represents an obvious choice due to the fact that the pitch motor is used to control the pitch angle, two different kinds are possible: Profile Position Mode and Position Mode. The first possibility can be chosen by setting the variable Modes_of_Operation equal to 1; the target position is given to a trajectory generator, which creates a demand value to reach the target values according to the two different motion profile types shown in Figure 3.15: a linear ramp and a ramp multiplied by a squared sinus. In order to use this mode, it is important to set in the EPOS software the desired values of maximum profile velocity and max acceleration; moreover, it is necessary to include in the PDOs the variables Controlword and Target position to command the motor.

  In Position mode, instead, no trajectory is generated and the motor goes from the actual to the target position in the fastest way possible. To choose this mode, the Modes_of_Operation variable should be set equal to -1 and the variable Position Mode Setting Value should be included in the PDO.

  In this first stage, the chosen mode is Profile Position Mode, since it is only an initial stage where a smooth trajectory is more important than a fast response. Once the mode is set, the Flag_state_machine is increased by 1.

- **case 1**: after setting the operating mode to 1, the motor is commanded to switch on and enable voltage through the Controlword variable. This is an important variable used to command the motor while in Profile Position mode: it is made up of 16 bits, each one of them with a different meaning. In this case, only the first two bits are set to 1, allowing the motor to switch on and enable voltage. Table 3.16 summarizes the meaning of each bit of the variable controlword; some bits (4-5-6-8-15) can have a different meaning according to the chosen operating mode.

- **case 2**: in this stage it is checked whether the motor actually switched on or not. This check is performed by comparing the Statusword, which represent the actual condition of the motor, to the Controlword, which instead is the desired, or target, condition. In particular, the bits number 1,4 and 9 should be equal to 1; Table 3.17 summarizes their meaning.

- **case 3, 4, 5, 6**: in these stages the calibration procedure of the pitch angle is performed by using a hall sensor. This kind of sensor is mounted directly on the blade and emits a different voltage depending on the achieved pitch angle. In particular, when the pitch angle is close to the zero degrees value, the output value of the hall sensor, defined as the ratio between the actual voltage (analog input 1) and

Acceleration	Velocity	Position
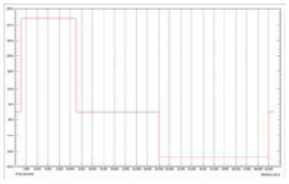	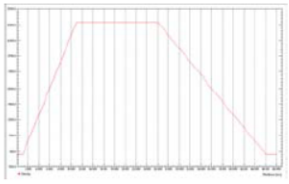	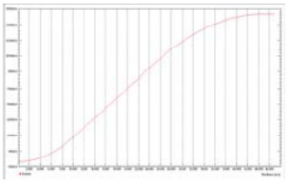
A_{max} = Profile acceleration A_{min} = Profile deceleration	V_{max} = Profile velocity	Absolute Movement P_{end} = Target position Relative Movement P_{end} = Position demand value + Target position

(a) Linear ramp profile

Acceleration	Velocity	Position
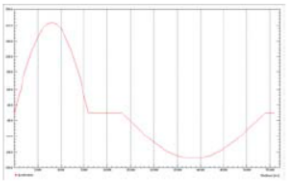	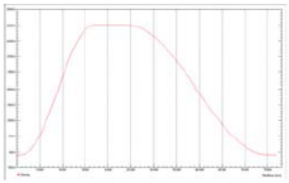	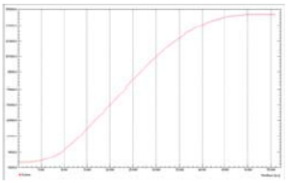
A_{max} = Profile acceleration A_{min} = Profile deceleration	V_{max} = Profile velocity	Absolute Movement P_{end} = Target position Relative Movement P_{end} = Position demand value + Target position

(b) $\sin^2$ ramp profile

Figure 3.15: Different motion profile types

Bit	Description	PPM
15	Operating mode-specific	Endless movement
14 11	reserved	
10, 9	reserved	
8	Operating mode-specific	Halt
7	Fault reset	
6	Operating mode-specific	Abs / rel
5	Operating mode-specific	Change set immediately
4	Operating mode-specific	New setpoint
3	Enable operation	
2	Quickstop	
1	Enable voltage	
0	Switch on	

Figure 3.16: Controlword bits

a reference voltage (analog input 2), is equal to 0.5. Since the blades are equipped with a spring, they are initially pushed to pitch angles close to the maximum value; the pitch angle is therefore progressively decreased until the pitch is close to the

Bit	Description	PPM
15	Position referenced to home position	
14	Refresh cycle of power stage	
13	Operating mode-specific	Following error
12	Operating mode-specific	Setpoint ack
11	Internal limit active	
10	Operating mode-specific	Target reached
9	Remote (➔NMT Slave – State on page 7-90)	
8	Offset current measured	
7	Warning	
6	Switch on disable	
5	Quickstop	
4	Voltage enabled (power stage on)	
3	Fault	
2	Operation enable	
1	Switched on	
0	Ready to switch on	

Figure 3.17: Statusword bits

zero value. It is worth noting that the output of the hall sensor, defined as the ratio between the actual voltage and a reference voltage, has an almost perfectly linear relationship with the pitch at low angles and assumes values between 0.4 and 0.55. In particular, when the hall sensor is correctly mounted on the blade, the value of 0.5 is unique and is exactly in the middle of the linear region; as soon as this value is passed, therefore, the pitch calibration procedure stops and, since discrete samples are taken, a linear interpolation is performed to find the pitch angle that corresponds to an output of 0.5. During the assembling process, however, some hall sensors were not correctly mounted and showed a slightly different behaviour, as described in Figure 3.18.

By looking at the output value of 0.5, it is clear that it is no more unique since it is achieved also at high pitch angles; one possible solution would have been the change of the target output value from 0.5 to the first unique value. This, however, would have involved either a different procedure between the correctly mounted hall sensors and the wrong ones or a target output value that, for some hall sensors, was very close to the boundaries of the linear region. To avoid this two conditions, the stop criterion has been modified according to Eq. 3.28

$$\frac{Analog\_input\_1}{Analog\_input\_2} \cdot sign(Threshold) > Threshold \tag{3.28}$$

The threshold value is read from an external file and corresponds to 0.5 for a

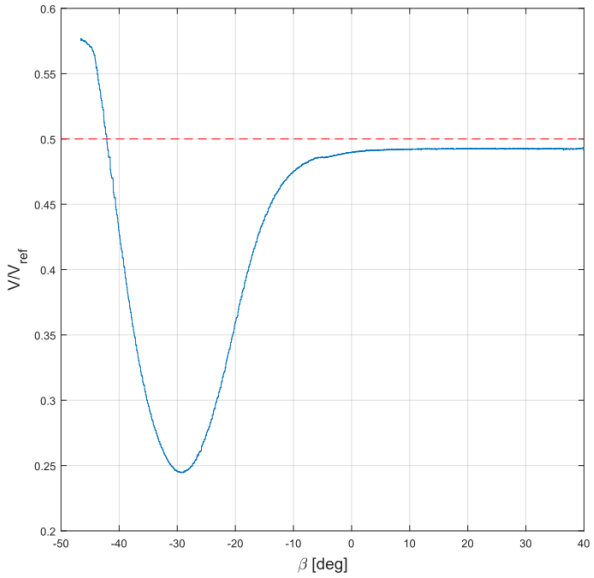

(a) Correct assembly

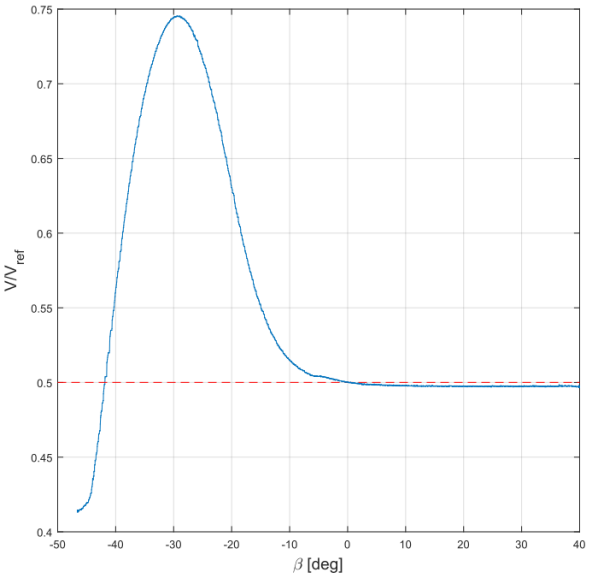

(b) Wrong assembly

Figure 3.18: Hall sensor voltage - pitch angle relationship

correctly mounted hall sensor and to -0.47 for a wrong hall sensor, since 0.47 was a unique value for all the tested hall sensors.

At this point of the procedure, each blade has reached a reference position which can be univocally reached each time the procedure is repeated. The next step is to relate the hall sensor output value of 0.5 to a physical pitch angle. To this purpose, each blade has been tested at different pitch angles, measured with an inclinometer, and the corresponding hall sensor value has been recorded. From Figure 3.19 it is clear that the blades do not have the same pitch angle; this is due to the fact that they are assembled on a bevel gear using four screws. Due to a communication error between the designer and the company that manufactured the bevel gears, however,

the holes for the screws do not have the same azimuthal position in all the bevel gears, leading to different pitch angles for each blades. This results in a maximum error in the pitch angle of half a tooth of the bevel gear, which corresponds to 5 degrees. Due to lack of time, it was not possible to manufacture new bevel gears and, to reduce the differences between the blades, the most similar ones were assembled together. The angle corresponding to the value of 2.5 V is then substracted to the current pitch angle in order to reach a pitch of 0 degrees and is shown in Table 3.3, together with the maximum difference in pitch angle between the three blades that belong to the same rotor.

Rotor	Hall sensor	Angle [deg]	$\Delta\beta_{max}$ [deg]
1	7	5.9039	1.81
	4	5.6245	1.79
2	18	5.8129	1.79
3	11	1.34	0.21
	22	10.6478	-
4	24	6.0249	1.27
5	21	-4.8933	1.13
	15	-1.6418	1.13
6	13	-2.0173	0.9

Table 3.3: Hall sensor

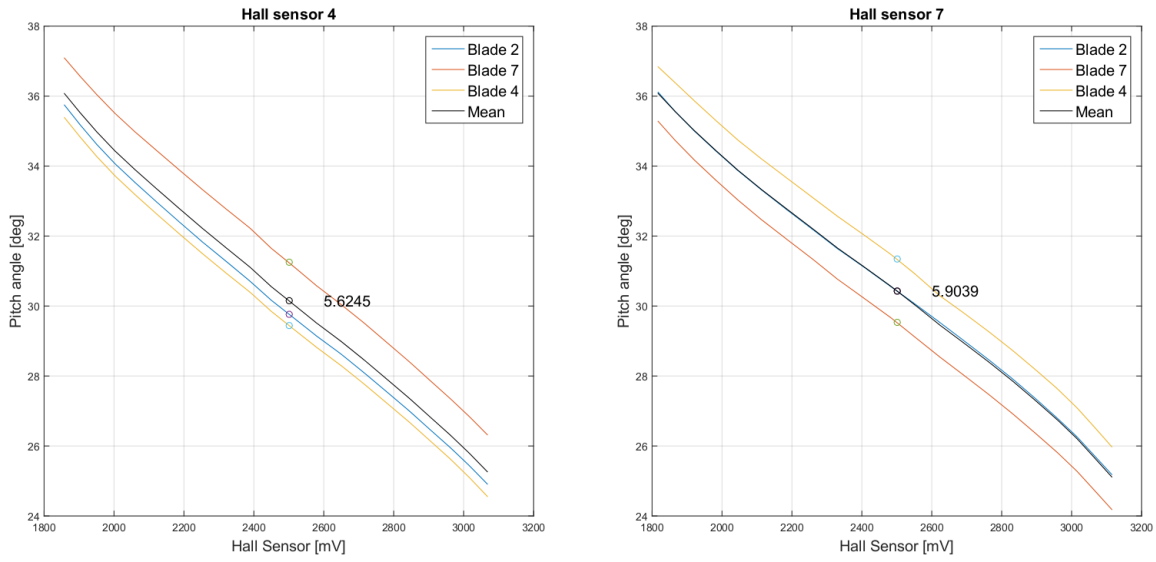

(a) (b)

Figure 3.19: Hall sensor voltage - pitch angle relationship

- **case 7**: in this stage the motor is stopped using the Controlword variable at the current position.

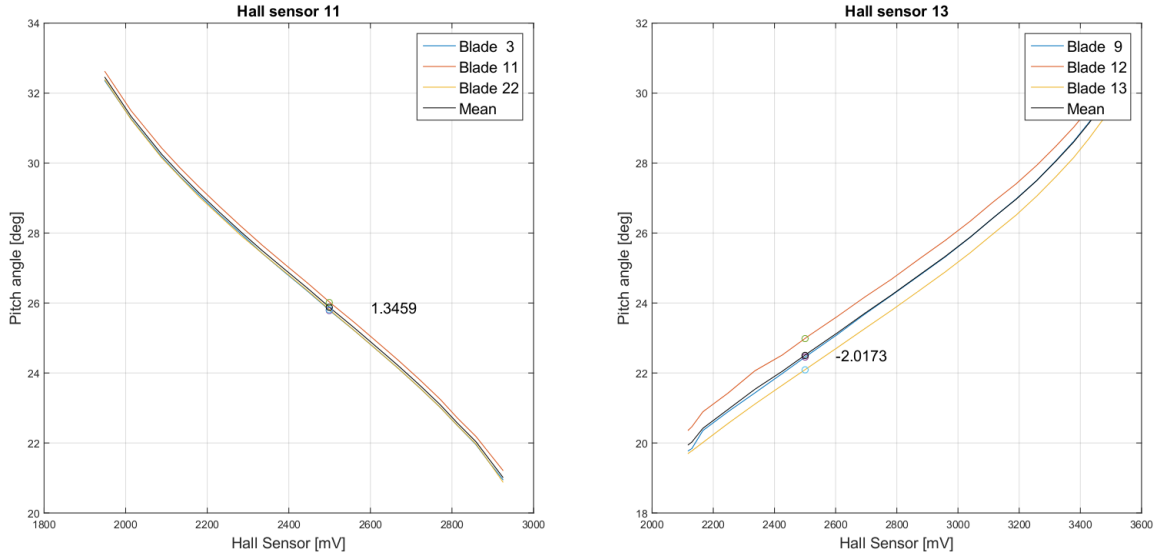

(a) (b)

Figure 3.20: Hall sensor voltage - pitch angle relationship

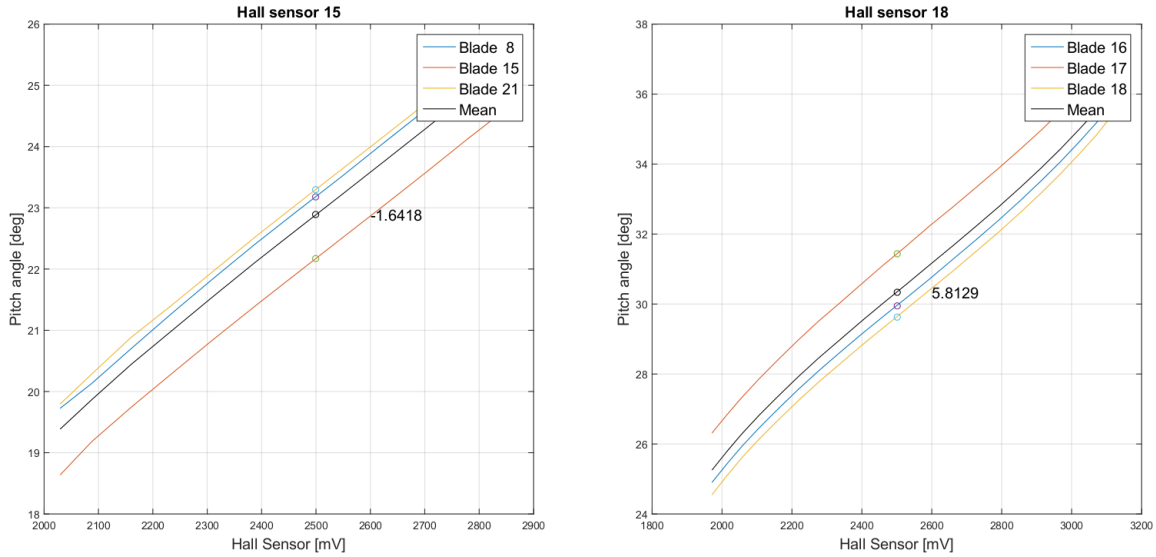

(a) (b)

Figure 3.21: Hall sensor voltage - pitch angle relationship

- **case 8, 9 ,10**: the operating mode is changed to 6, which means homing mode; it is a particular mode that allows to reset the zero of the motor to the current position.

- **case 11**: the mode of operation is changed again to either Profile Position Mode or Position Mode; the choice depends on the user's will, even though, sometimes, the Profile Position Mode has proved to be too slow to follow the demand. The calibration procedure ends at this stage and the pitch demand is set to 0.

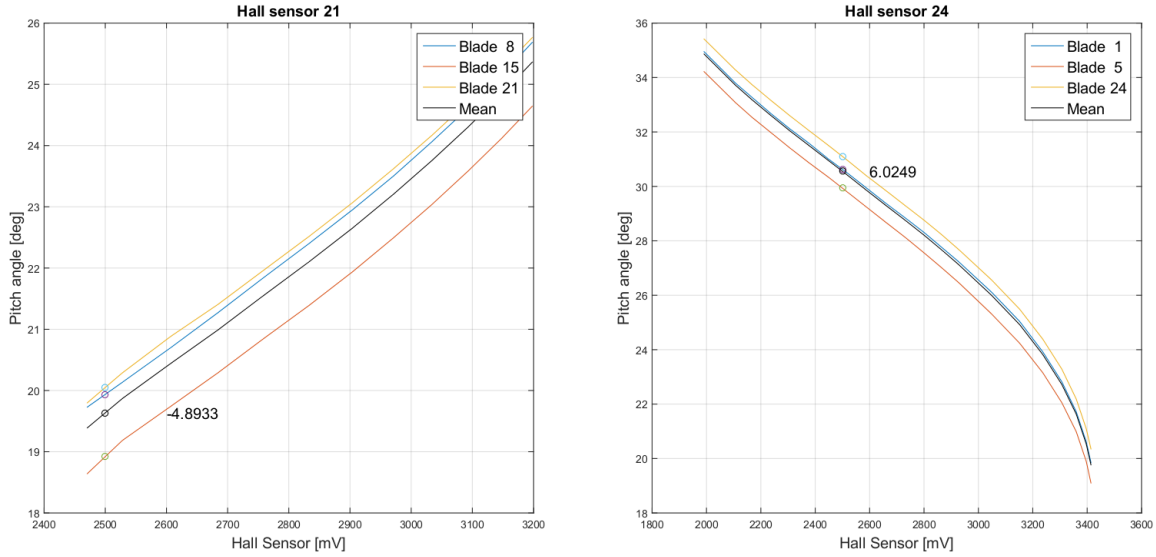

(a) (b)

Figure 3.22: Hall sensor voltage - pitch angle relationship

- **case 12**: first a check on the actual operating mode is performed and finally the motor is prepared to be moved. This stage is kept thorughout the whole operating condition of the wind turbine unless the calibration procedure is restarted.

3.6 State Machine

The state machine application governs the overall behaviour of the wind turbine model by defining 5 different operating states: Idle, Calibration, Parking, Manual and Auto.

- **Idle**: this represents the initial stage of the machine, in which both the pitch motor and the power generator are deactivated. From this stage it is possible to move only to Calibration.

- **Calibration**: in this stage several steps that allow to check the full functionality of sensors and actuators are carried out. First, the generator calibration is performed by enabling it, switching to speed control and making it rotate at low speed: this allows to check whether the motor works or not. Second, the pitch calibration procedure is performed, as described in Section 3.5. Once the calibration procedure is completed, it is possible to remove the offset and either proceed to Parking or go back to Idle.

- **Parking**: while in Parking the generator speed is set to 0 rpm and the pitch angle to 20 degrees. This is an intermediate state that allows to stop the machine in a safe position without the necessity to repeat the calibration procedure, which can take several minutes; while in Parking, it is possible to remove the offsets and move on to any other state.

- **Manual**: in this condition the generator is commanded in speed control and the user can impose certain values of speed and pitch angle. The state machine, there-

fore, writes these values on the Pitch and Power Generator applications. From this stage it is only possible to go back to Parking.

- **Auto**: when the machine is set in automatic mode, the user cannot decide on its own the speed and pitch angle because the control application computes them. It is however possible to decide the power demand, the control type (TUM/POLIMI or KNU) and to stop or start the control application.

3.7 Supercontroller

The supercontroller application is just a "dummy" application used to comunicate with the wind farm control device and shows the values of power for three turbines together with some variables necessary to start the recording of data in the wind farm control algorithm. It is installed only on the first turbine of each wind farm row.

3.8 Wind Turbine interface

In order to decrease the work load of the operator, an interface for each wind turbine has been developed. One one hand, the interface should allow total control over the machine without the necessity to access the SolutionCenter software and also grant the possibility to see graphs of the most important variables. On the other hand, however, it should be as small and compact as possible to be able to run 6 interfaces on two monitors.

At the top of the interface, three boxes contain all the commands necesary to interact with the machine. The left boxes, for instance, allow to choose between the 5 states of the state machine. The central box, instead, contains only the information related to the specific operating mode in order to preserve space; in idle, the user can only perform the offset removal; in calibration, two green or red lights indicate the successfulness of the generator and pitch calibration procedures, a button allows to remove the offset, whereas a textbox shows the value of the hall sensor output; in Parking, the offset removal is again the only available choice. In Manual, the user can decide the values of speed and pitch angle by directly inserting a value in the corresponding textbox; when the speed is higher than 500 rpm, however, the pitch angle can only be modified through the + and - buttons, which change the value by 1 degree. In Auto, finally, the operator can start or stop the control application, change control type and reload it; a textbox allows to change the power partialization, whereas a button permits to open a second window where the values of pitch and torque gains can be modified. The right box, finaly, allows to record data: the user can insert the file number, the TOP number and the time to record; by pressing the button record, the data start being recorded and the grey bar on the right side starts filling in order to show the progress of the recording.

Four variables were deemed important enough to have a dedicated plot: angular speed, pitch angle, power and bending moment from the two strain gages. For the pitch angle and the power, both the measured and demanded values are shown. Two other graphs showing the torque, filtered and not filtered, and the bending hub can be opened upon necessity in another window. Each graph has the possibility to be started and stopped, to record the results in a .csv file as well as the most basic tools to change the visualization, such as zoom in/out, lateral/longitudinal and autofit. Finally, at the top of each graph, a text box permits to see the current value of the plotted variable.

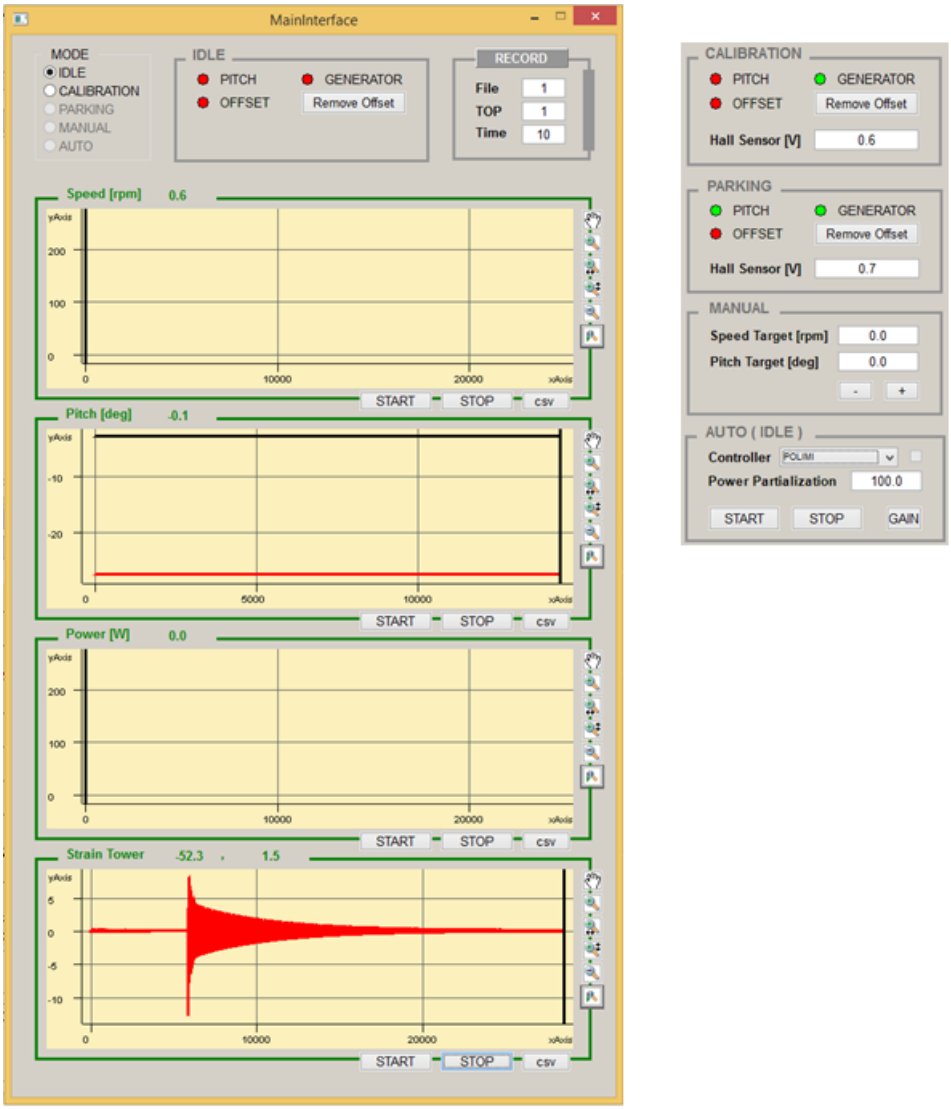

Figure 3.23: Wind Turbine Interface

3.9 Wind Farm interface

The Wind Farm interface permits to quickly change the values related to the Supercontroller application. It also shows the plots of power and speed, which can be displayed for each turbines separately or for all of them on the same graph.

3.10 Wind Tunnel interface

The wind tunnel interface allows to insert the air density and to see the wind speed measured by the Pitot sensor mounted in the wind tunnel. The value of wind speed can either be inserted manually by the user, in case no Pitot is connected, or be read from the sensor by inserting the correct sensitivity coefficient.

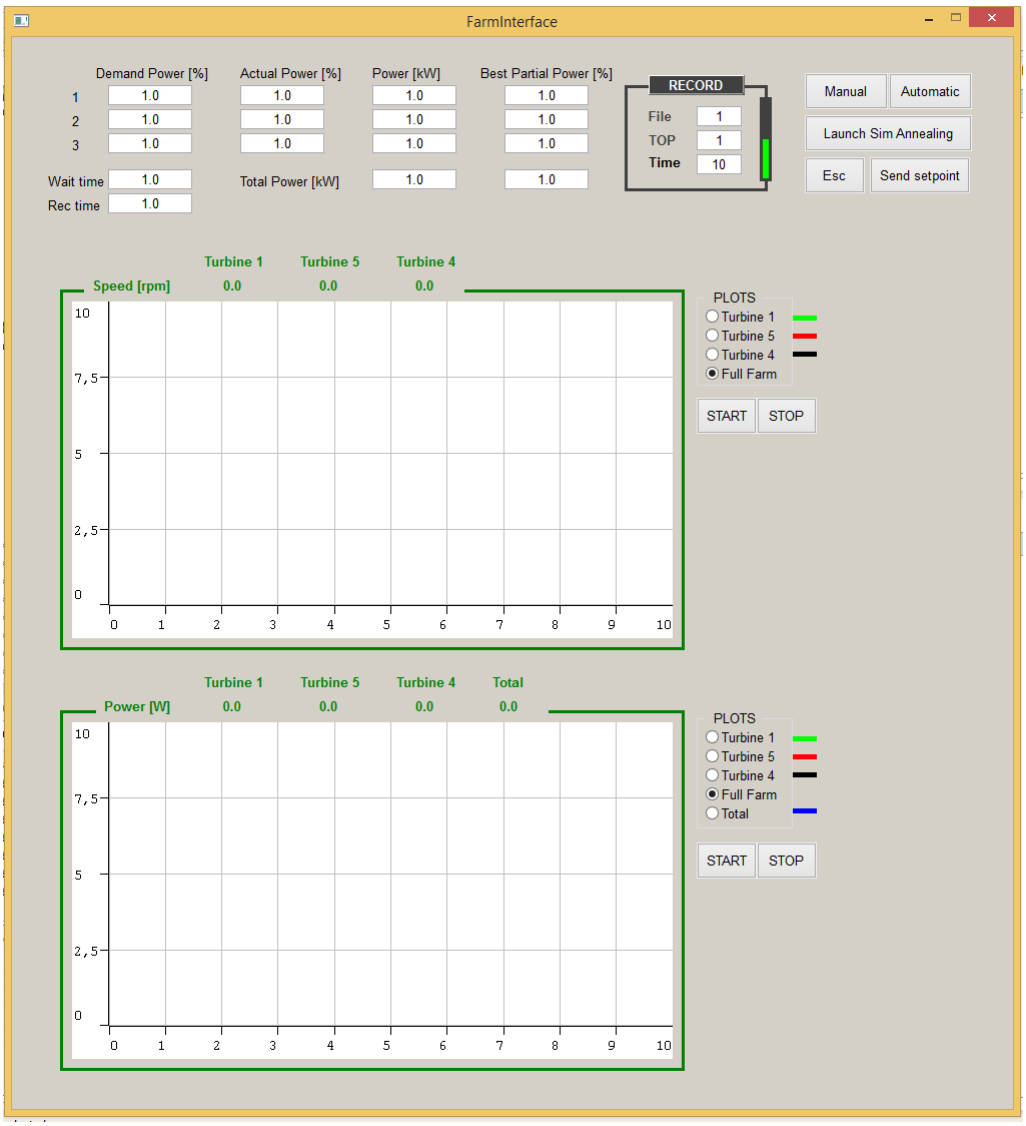

Figure 3.24: Wind Farm Interface

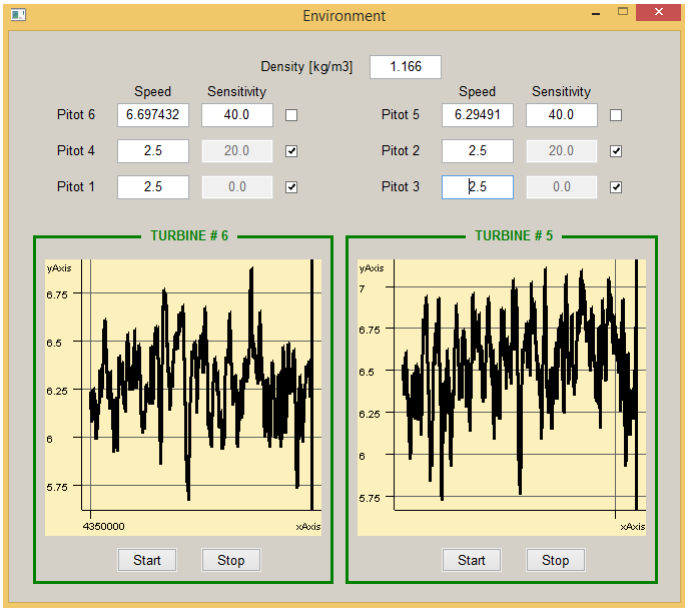

Figure 3.25: Wind Tunnel Interface

Chapter 4

Experimental tests

4.1 Pre-Test comparison

Before the beginning of the tests, both control algorithms have been confronted with the expected performance of the wind turbine, obtained from a Simulink model, in order to check the reliability of the wind tunnel experiments.

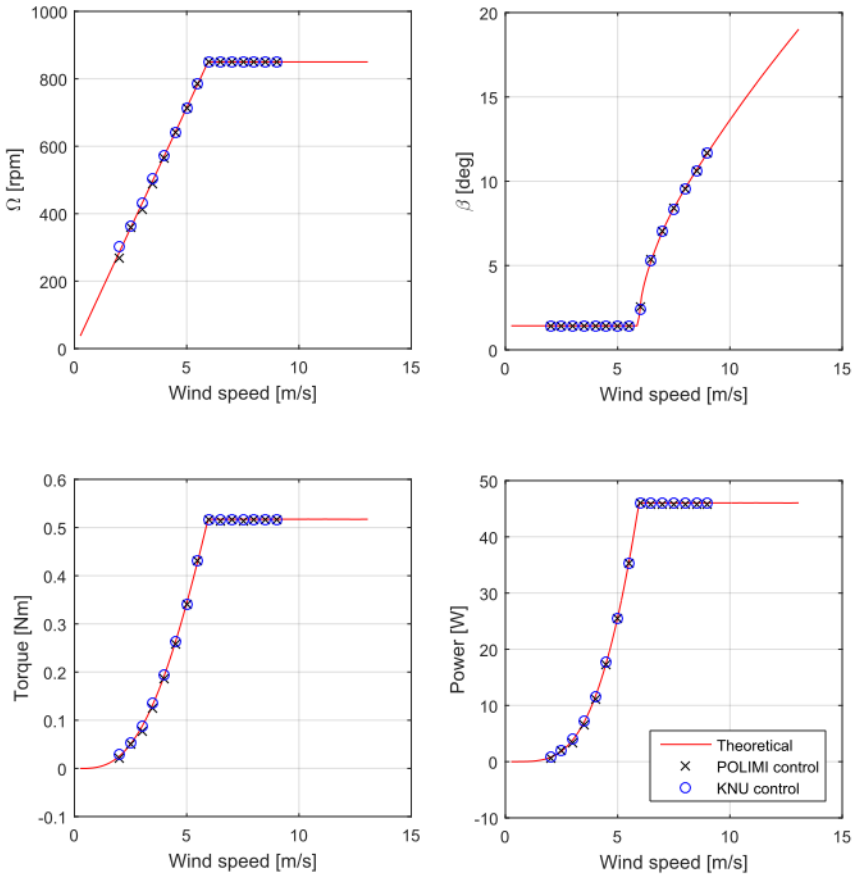

Figure 4.1: Comparison between the Simulink model and the TUM/POLIMI and KNU control algorithms

Figure 4.1 shows the results related to angular speed, torque, pitch angle and produced power; it is evident that they are quite satisfactory for both control algorithms, since the

results are very similar to what expected. Figure 4.2 shows the percentual error with respect to the Simulink model. The KNU algorithm performs slightly better than the TUM/POLIMI controller, especially at low speeds. This, however, is not surprising since it is a more detailed and complex algorithm that employs few more features, such as a torque PID. Moreover, this algorithm shows a smooth, monotonic convergence to the theoretical values with respect to the wind speed, whereas the TUM/POLIMI control has an oscillating behaviour.

It is also worth noting that the error is generally more relevant at low velocities and decreases at higher speeds; on one hand, this behaviour is not particularly suprising since the wind turbine is designed to operate at higher angular speeds (850 rpm); on the other hand, however, this behaviour is not desired either. In the wind tunnel, in fact, two columns of three wind turbines each will be tested, and the further away the wind turbine is, the slower it will rotate due to the presence of the wake of the turbines placed ahead. Nevertheless, the expected angular speed of the slowest turbine is about 400 rpm, which would result in an acceptable percentual error of 0.99%. Finally, it should be noted that the error on the pitch has a different behaviour with respect to the other errors, showing a sudden increase at 6 m/s. However, this is not surprising either since the pitch control starts activating at this wind speed.

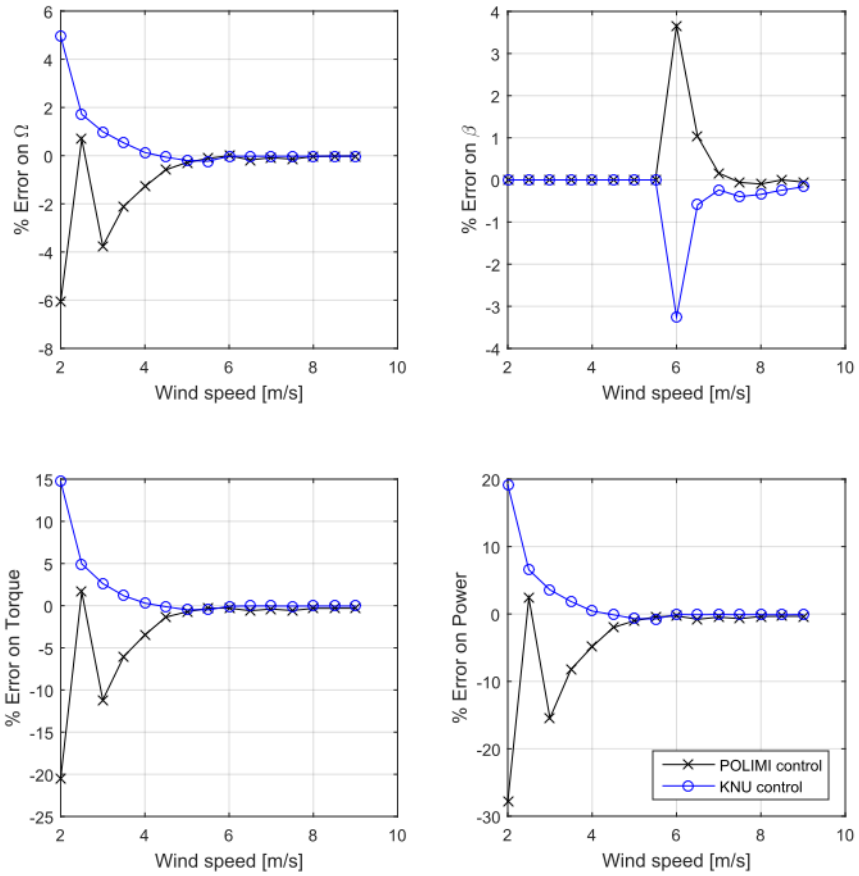

Figure 4.2: Comparison between the Simulink model and the TUM/POLIMI and KNU control algorithms

4.2 Drag measurement

In order to have a more accurate measure of the thrust, the drag of the nacelle without the blades has been computed. The results achieved for wind speeds between 4 and 8 m/s, plotted in Figure 4.3, show a typical quadratic trend for the drag force. Figure 4.3 also show the drag coefficient multiplied by the surface, since it was not possible to compute the drag coefficient alone due to the difficulty of exactly calculating the surface S.

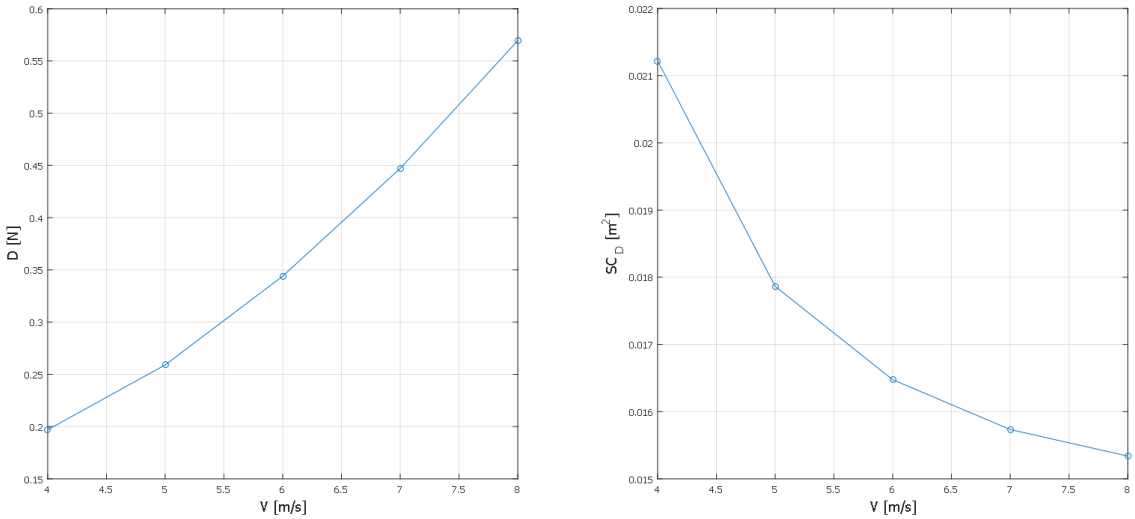

Figure 4.3: Drag measurement

4.3 Wake characterization

In order to get an insight into the flow field behavior downstream of the first wind turbine, a wake characterization test has been performed for two different wind speeds, one above and one below the rated conditions. The experiment setup is really simple; a Pitot tube was placed upstream of the model (-1.5D), in order to check the asymptotic speed, and a traversing system was placed behind it, varying its longitudinal position from 1.4D to 9D during the test. The latter is equipped with a couple of three-directional constant temperature anemometry devices (CTA) and it is in charge or recording the velocity measurements in the wake cross-section. Moreover, considering the scope of the test, triangular-shaped spires were installed at the test section inlet in order to properly simulate the atmospheric boundary layer (ABL). The experiment arrangement together with the reference system considered are shown in Figure 4.4.

The wind speeds chosen for the experiments were 5 m/s and 7 m/s, conditions placed in Region II and Region III of the control trajectory shown in Figure 4.1, respectively corresponding to the Trim conditions summarized in Table 4.1.

Both vertical and horizontal traversing measurements were performed in this set of conditions; the former, however, was done only in front on the rotor hub because its aim is only to verify the actual ABL conditions in the wind tunnel. The outcomes of the test

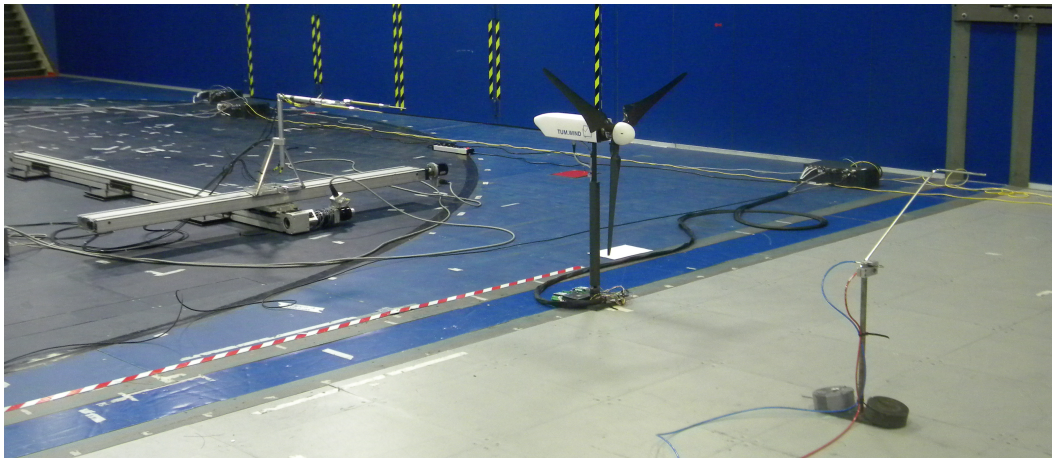

Figure 4.4: Wake measurement setup

Wind speed [m/s]	ω [rpm]	β [deg]
5	720	1.4
7	850	6.8

Table 4.1: Wake test parameters

are the speed components of the flow field (u(t),v(t),w(t)) at all the measured stations; for each one, the average speed values and the intensity of turbulence can be computed. The results are presented and discussed in the following subsections.

4.3.1 Wake Wind Field (Region II)

Figure 4.5 shows the longitudinal, lateral and vertical wake velocity distributions at different downstream stations. The horizontal axis represents the non-dimensional longitudinal position (x/D) and the non-dimensional velocity normalized with respect to the undisturbed wind; the equivalence of each division of scale in dimensionless speed is indicated at the top of each plot. The vertical axis represents the non-dimensional lateral position (y/D). Additionally, in order to assess the wake expansion, the longitudinal speed corresponding to the 95% of the free stream velocity has been identified in each wake section segment; connecting these points a qualitative indication of the wake diameter was obtained (dashed-lines).

As expected, Figure 4.7, shows a decrease in the wake longitudinal speed caused by the turbine power extraction that expands with the increase of longitudinal position. A vertical counterclockwise speed in the near wake is also observed, which is coherent with the clockwise rotation of the turbine with respect to its body reference frame. Furthermore, in the longitudinal near wake, it is possible to note the presence of a small characteristic peak caused by the nacelle section that, by not generating power, slows down the flow in a lesser extent. It is interesting to note that, for a rotor in axisymmetric flow conditions, this minor peak should be perfectly centered, situation that is not verified in our case.

A possible explanation to this behavior is a slight asymmetry generated by the boundary layer at the wind tunnel lateral wall which induces a small lateral velocity that deviates the main stream, a phenomenon commonly known as viscous displacement effect. In

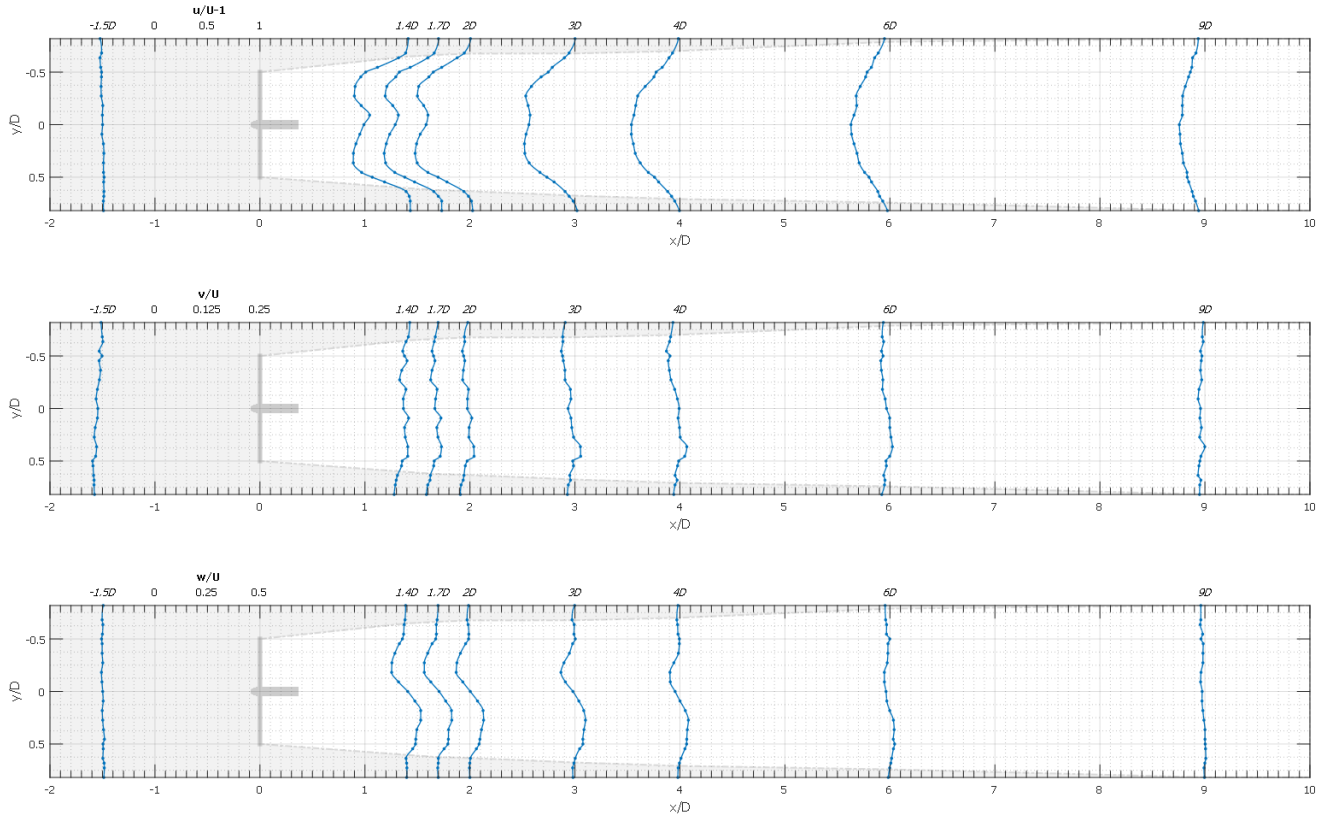

Figure 4.5: Wake speed, 5 m/s

fact, from the lateral velocity measurements, it is possible to appreciate this effect since a soft negative slope that goes toward zero at the wind tunnel center can be identified in both the main stream and the near wake. In the far wake, on the contrary, the wake recovery mixing dilutes the peak and slope, as well as the transversal swirl velocities. The locus at which the recovery starts to be dominant can be recognized from Figure 4.8, in which the wake longitudinal speeds in two different positions are superimposed. The wake mixing with the mainstream starts between the 2D and the 3D stations, modifying the wake diameter expansion rate.

The intensity of turbulence, shown in Figure 4.11, in which the axis definition is analogous to the ones of the previous figure, gives also an insight in the wake behaviour; for instance, the peaks corresponding to the tip vortex are found in the wake boundaries of the near wake, which then spread across the whole wake as it moves downstream. It is worth noting that, in the far wake, the magnitude of the turbulence intensities in the three directions are commensurable, indicating a high flow recovery.

The same considerations explained earlier remain valid for the flow conditions in Region III; however, three key differences should be noted. First, this operation condition exhibits almost no center peak, associated with the interference with the nacelle; second, the turbulence intensities were reduced roughly by half compared to the previous case; third, the wake diameter expansion diminishes. All these deviations are generated by the decrease in the turbine axial induction; in order words, since the model is operating with a strong partialization, it disturbs the main flow to a lower extent.

Viewed from the wind farm control perspective two contrasting effects are encountered

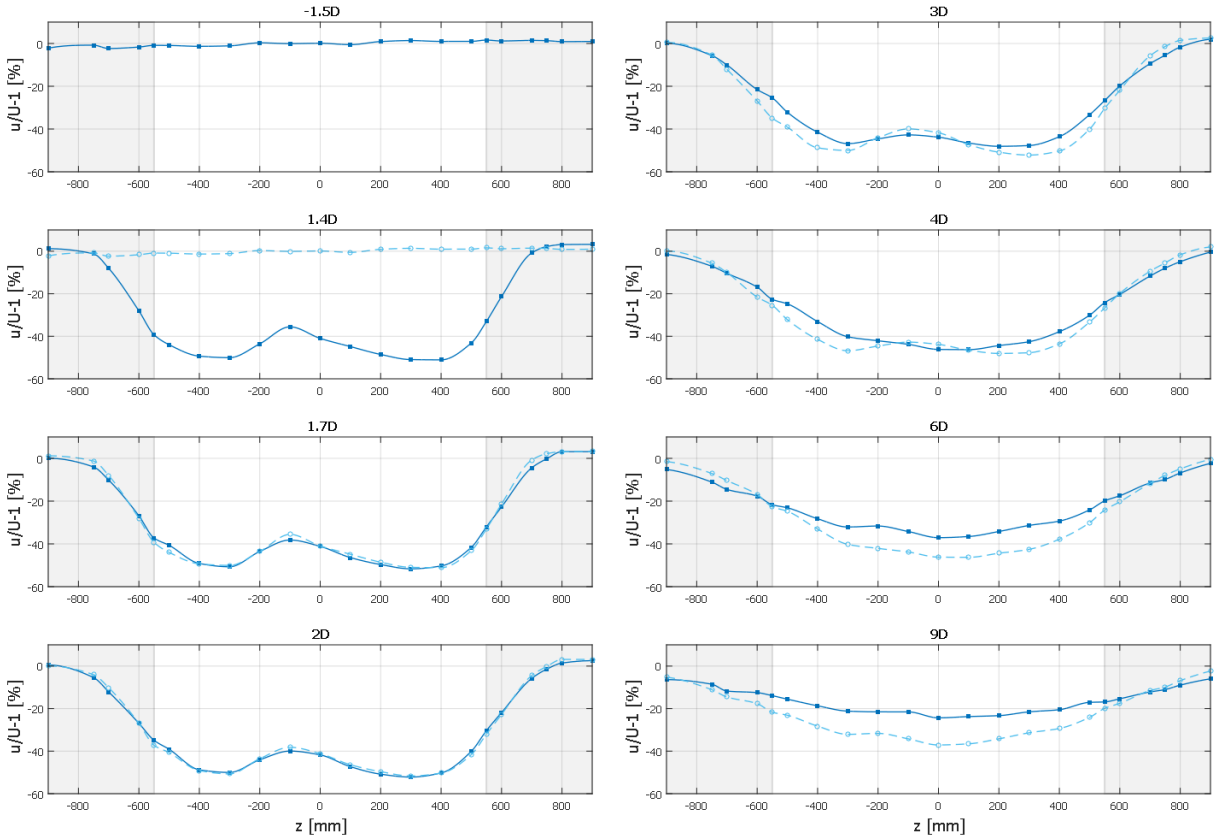

Figure 4.6: Wake longitudinal speed, 5 m/s

upon a power partialization. On one hand the wake diameter is reduced; therefore, the downstream turbine feels an increased wind speed. On the other hand, the turbulence intensity decrease mitigates the wake speed recovery. The power generated by the second turbine is therefore a function of these two parameters. The real profit of the power partialization, in case it exists, is a tradeoff between the power lost by the first turbine and these two phenomena. Performing a further comparison between these situations is not possible because they are in two different wake regimes, which are driven by different mechanisms; in particular, turbulent wake state for region II and windmill brake state for region III, respectively as shown in [19]. In order to do so and get a deeper insight into the expected performance of the power partialization strategies, in future it is recommended to perform wake characterization keeping the wind speed constant while varying the partialization percentage, which is a current research trend since the theory in this matter is still weak.

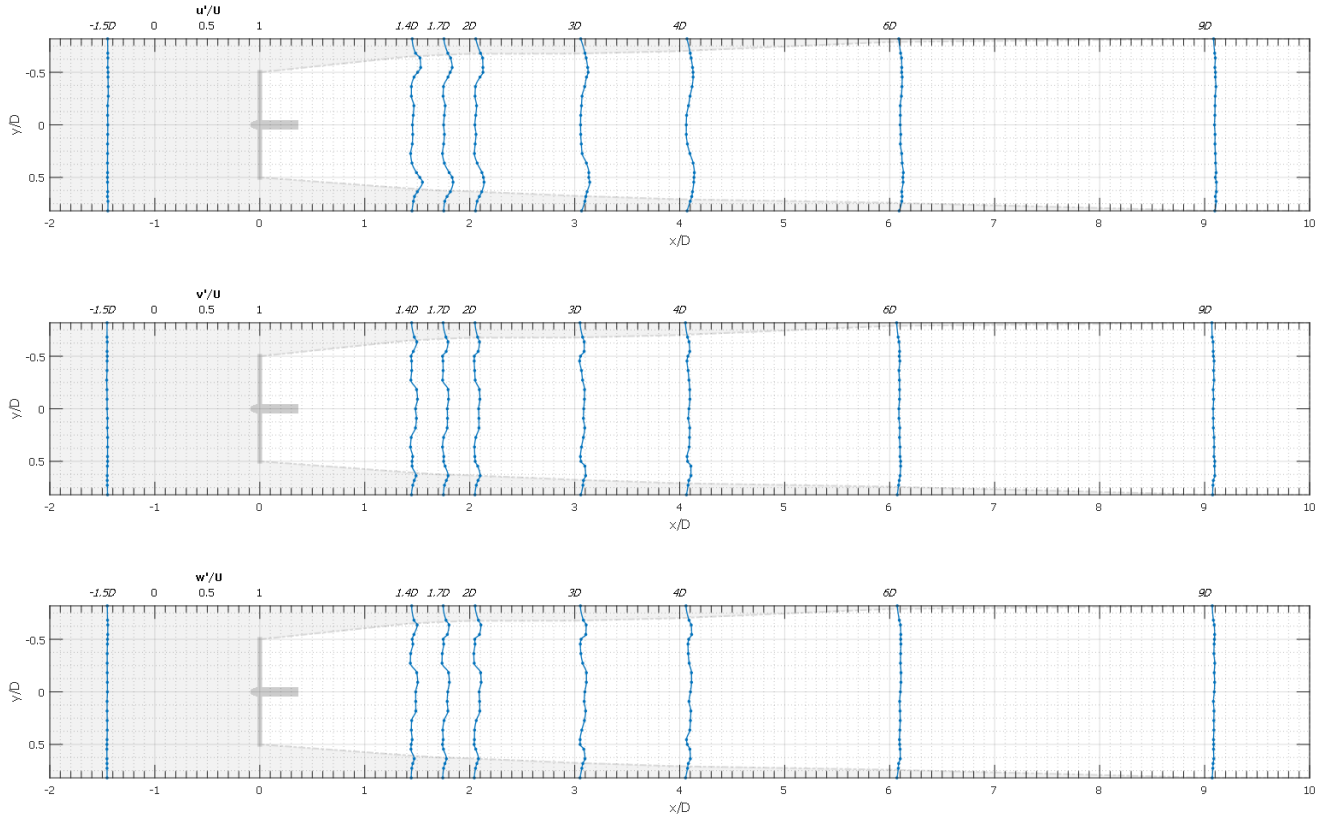

Figure 4.7: Wake turbolence intensity, 5 m/s

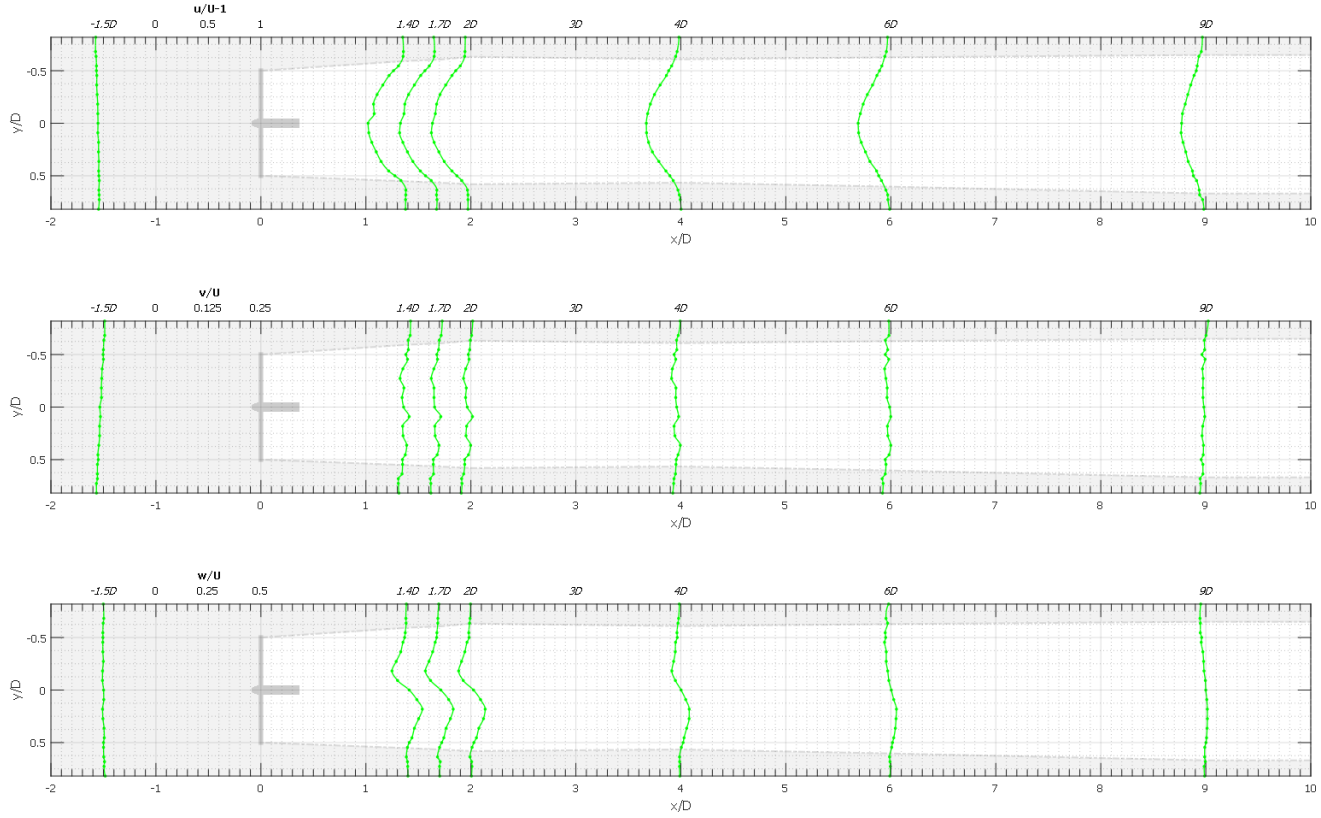

Figure 4.8: Wake speed, 7 m/s

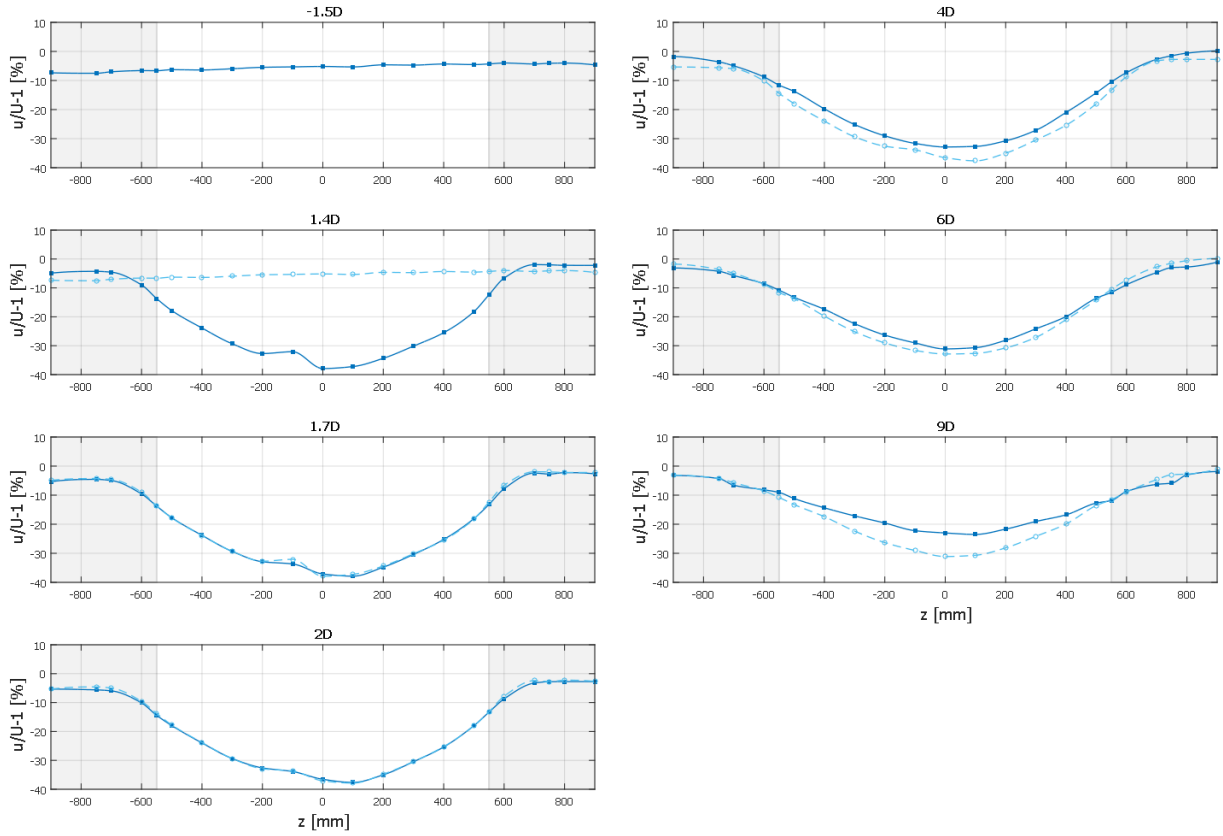

Figure 4.9: Wake longitudinal speed, 7 m/s

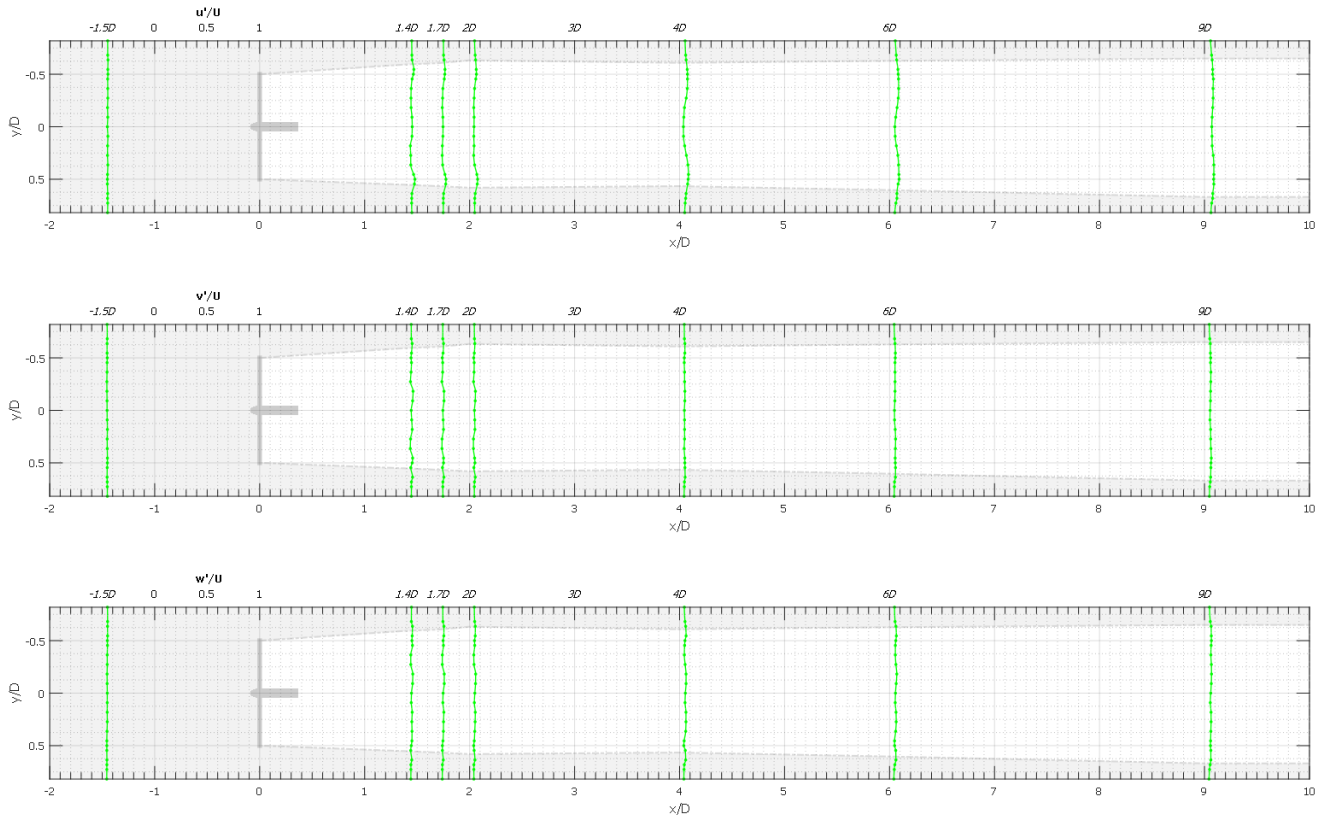

Figure 4.10: Wake turbolence intensity, 7 m/s

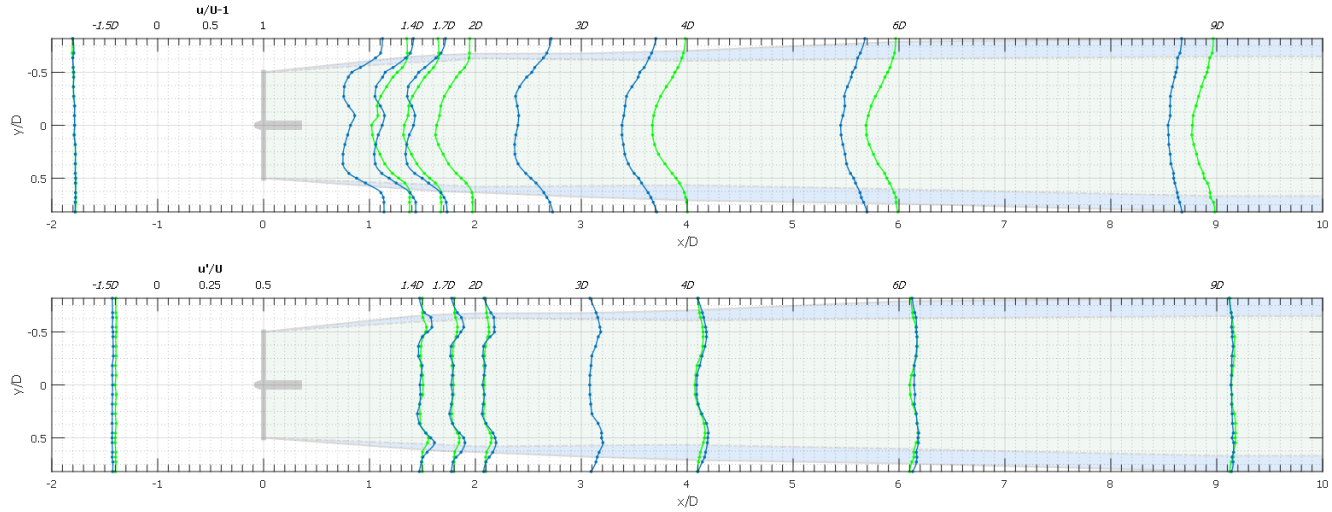

Figure 4.11: Wake speed and turbolence intensity, 5 and 7 m/s

4.4 Partialization measurement

The partialization measurement were performed on two columns of three wind turbines each, shown in Figure 4.12. The machines on the left column have a distance of 4D between them, whereas those on the right side have a distance of 6D.

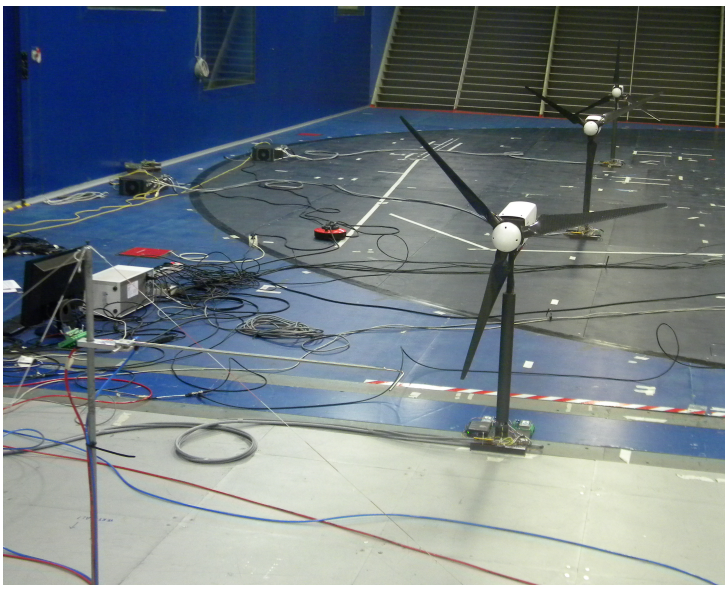

(a) 4D distance

(b) 6D distance

Figure 4.12: Partialization setup

Figure 4.13 summarize the results of the partialization test performed with the full wind farm; i.e, with a row of three turbines. The x-axis represents the partialization power percentage (η), which can be referred to the 1^{st} or 2^{nd} turbine according to the case. The y-axis represents the power produced by each turbine normalized with respect to the principal turbine maximum power production capacity; i.e, the power generated before a member of the farm was de-rated. It is worth noting that the partialization

sweep was limited to 90%, because this is the region where a global improvement in the power generation is expected when using this type of control strategies. Moreover, the experiments were conducted in Region II of the control envelope in order to propitiate the wind farm control capabilities.

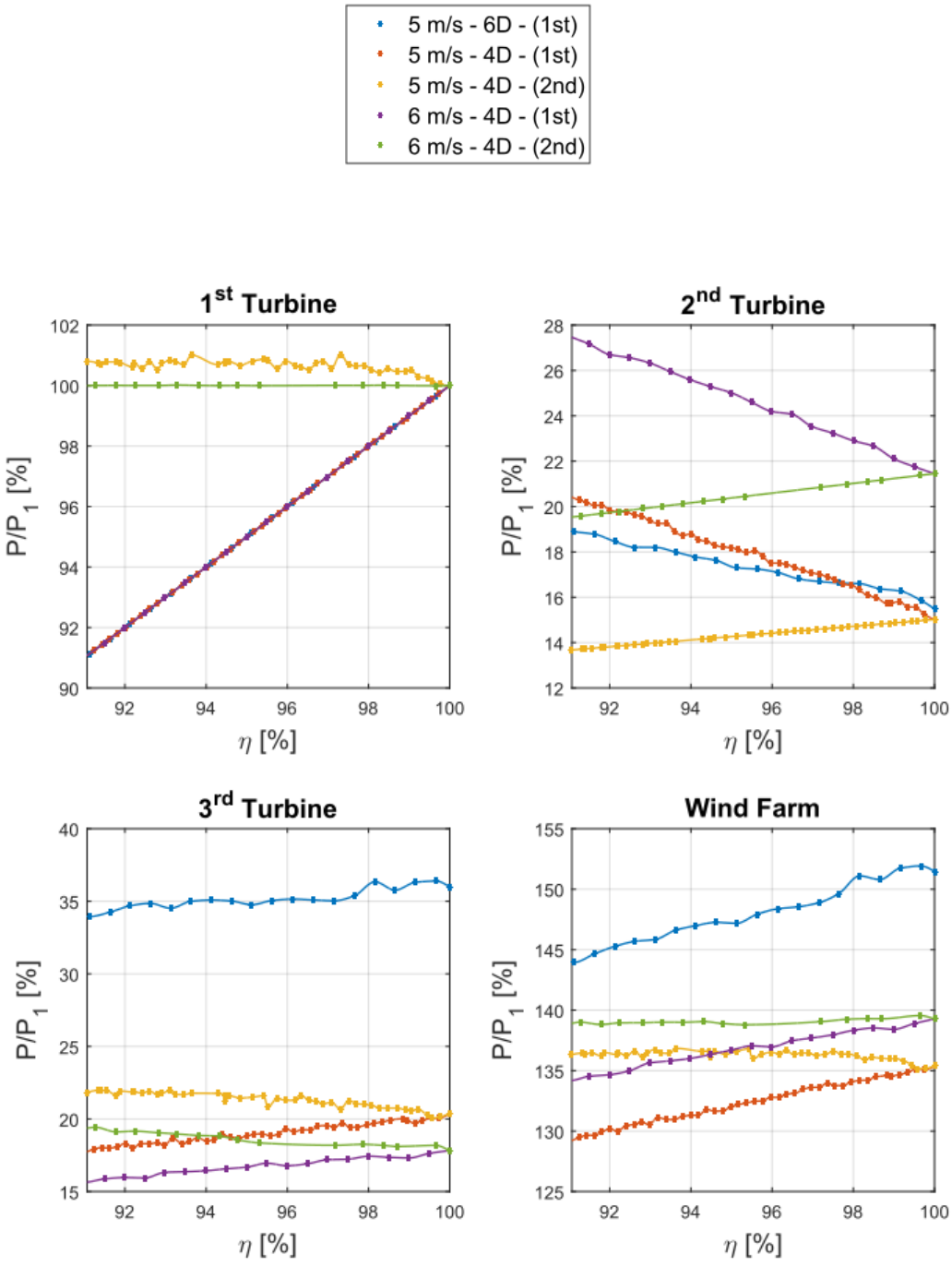

Figure 4.13: Partialization

Unfortunately, from the figure 4.13 it is absolutely clear that the power partialization does not generate a significant improvement of the wind farm performance, at least in the conditions tested in the present experiments. In fact, the maximum total power increase corresponds barely to 0.5%, which is negligible compared to the results foreseen

by the preliminary studies conducted at TUM wind energy institute (∼4%). Even worse, it is hard to distinguish whether this improvement is real or merely casual, since the uncertainties related to the models itself are of this order of magnitude. However, some other interesting conclusions can emerge from this test. The first thing that could be noticed is that, in the flow conditions characteristic of Region II (5 m/s), the performance of the 2^{nd} turbine is lower than the 3^{rd} one, which is quite an unexpected result. This strange behaviour suggests a strong wake recovery behind the 2^{nd} machine that is further exacerbated by increasing the distance between the models to 6D. It is worth noting that the same improvement is not verified in the second model, an unconsistency that will be further investigated in the following test campaign. The expected behaviour is obtained introducing the partialization of the main turbine, since it enhances the power production of the 2^{nd} turbine at the expense of the other two models, or by increasing the wind speed up to Region III (above 5.8 m/s). In both cases, in fact, there is a power excess that is exploited by the 2^{nd} model; thus, at a certain partialization percentage, the same power output is obtained from the last two models, and by further increasing the partialization, the 2^{nd} turbine actually starts producing more than the 3^{rd}. Moreover, it is worth noting that the partialization of the second turbine leads to a small increase of the last machine, even though it is not high enough to generate an overall wind farm power increment.

Since the wake speed defect was deemed guilty of the unsuccess of the power partialization, a further analysis on the wind speed perceived by the downstream turbine was performed. Figure 4.15 shows the measured power and the wind speed, computed from the measured angular speed and considering that the downstream machine is operating at constant TSR (Region II). Additionally, the tests were performed with only two turbines, in order to check whether the third could have a detrimental effect.

In case of a couple of turbines a simple mathematical approximation can be performed to compute the minimum wind speed (m.p.s., minimum profit speed) that the second turbines must encounter in order to have an overall power increase after partializing the first machine. This value can be computed as in Eq. 4.2.

$$\Delta P_2 = \Delta P_1 = P_1(1-\eta) = 1/2\rho\pi R^2 C_P(V'^3 - V^3) = K\left(V'^3 - V^3\right) \tag{4.1}$$

$$V' = \left(\frac{P_1(1-\eta)}{K} + V^3\right) \tag{4.2}$$

ΔP_1: power decrease of the first wind turbine due to power .
ΔP_2: minimum necessary power increase of the second wind turbine.
η: power partialization percentage.
V': wind speed perceived by the second turbine before partialization of the first.
V': wind speed perceived by the second turbine upon partialization of the first.

From Figure 4.15 it is clear that, even though the demanded wind speed increase is small, the actual one is lower.

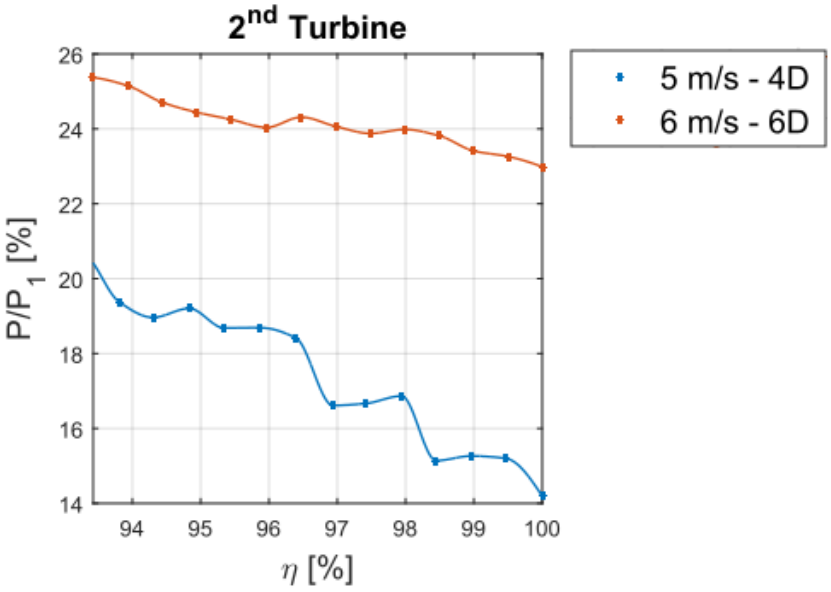

Figure 4.14: Partialization

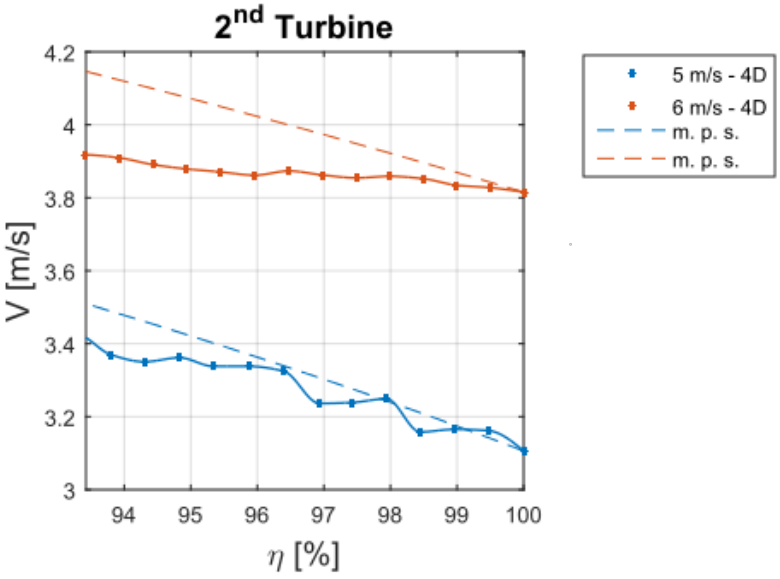

Figure 4.15: Partialization

4.5 Performance measurement

The purpose of this set of tests is to characterize the performance of the wind turbine models in terms of torque coefficient C_Q, power coefficient C_P, and thrust coefficient C_T. In particular, the main goal of this test is to assert if there is an impact of the downstream models onto the main one. The performance study is completed with a comparison with the aerodynamic coefficients computed in the preliminary design stage with the measured experimental results. The only particularity in the setup of this test, that should be kept in mind, is the difference in the operational mode used for the main and secondary turbines. The 1^{st} model is controlled in manual mode, since the automatic mode operates at a fixed TSR and pitch angles and we want to reach different combinations of these parameters, while the downstream models operate in automatic mode. The latter models, being always in Region II, keep a constant pitch angle of 1.44 degrees and adjust the generator torque according to the wind speed. It is important to mention that we focus our discussion on the C_P considering that it is the most representative aerodynamic coefficient for the wind turbines analysis, since it is fully correlated with their ultimate task, the power production. However, all the considerations are still valid for the thrust and torque coefficients being all of them consequence of the blade airfoil aerodynamic behaviour.

It is worth noting that, according to the considerations exposed in the Section 2.3, the torque and power coefficients were computed accounting for the friction losses, which are different for every model. Following this approach it was possible to make a single test and extend the results to all the machines. In the same way, the thrust measurements were depurated from the aerodynamic drag created by the nacelle and the tower base components (as explained in Section 4.2), allowing a direct comparison with the analytic data. The aerodynamic coefficients were therefore computed based on the measured data (Pitot plus model sensors) and corrected with the results obtained in previous tests, as shown in Equations 4.3 to 4.5

$$C_P = \frac{(Q+F)\omega}{\frac{\pi}{2}\rho R^2 V^3} \tag{4.3}$$

$$C_Q = \frac{Q+F}{\frac{\pi}{2}\rho R^3 V^2} \tag{4.4}$$

$$C_T = \frac{T_{FA}-D}{\frac{\pi}{2}\rho R^2 V^2} \tag{4.5}$$

Q: Torque measured by the Torquemeter $[Nm]$.

T_{FA}: fore-aft thrust measured by the tower strain gages $[N]$ (see Section 2.4).

ω: speed measured by the Turbine encoder $[rad/s]$.

V: Wind speed measure using a Pitot tube 3D downstream of the model $[m/s]$.

ρ: Density computed from the wind tunnel temperature, barometric pressure and humidity sensors $[kg/m^3]$.

F: friction torque, measured in Section 2.3.

D: Model passive drag, measured in Section 4.2.

4.5.1 Power coefficient

Figure 4.16 and Figure 4.17 show the power coefficients obtained in the performance test. Since the C_P is function of both the TSR and the pitch angle, it is plotted against both variables to give the reader a complete understanding of the experimental results. It is worth noting that in this analysis the blade pitch angle and the TSR are always referred to the 1^{st} turbine even if, in reality, all the models operate in totally different conditions (ω, V, β). Furthermore, in order to easily check if there is an increase or decrease with respect to the preceding conditions a dashed line with the results of the previous TSR or pitch step has been added to each graph.

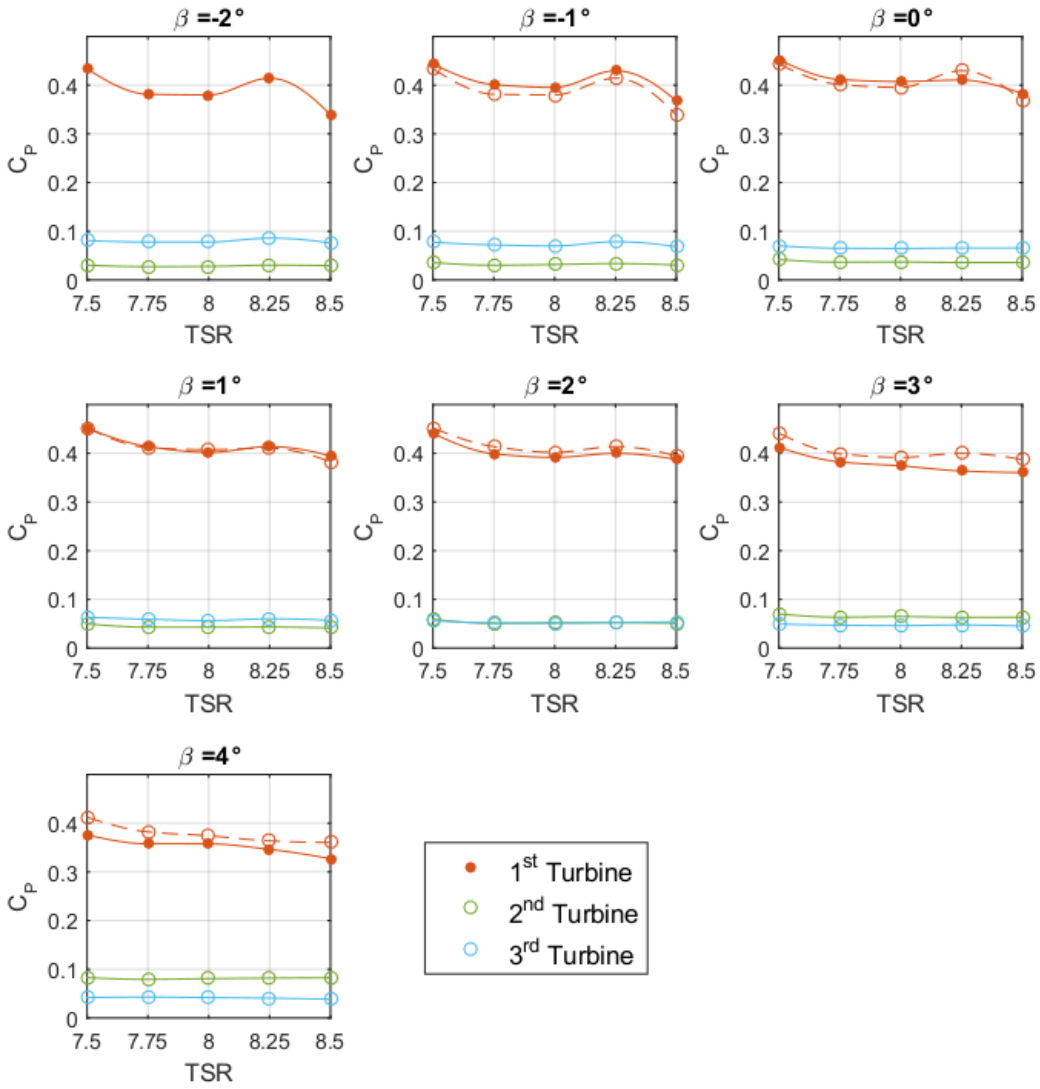

Figure 4.16: C_P vs TSR (3 Turbines)

The performance results resemble what was observed in the power partialization tests; in particular, it is clear that the power coefficients of the second and third wind turbines switch places in the power production ranking according to the pitch angle of the main one. Behavior that is even better captured by Figure 4.17, in which a characteristic "scissor" trend describes the C_P of the second and third machines. For instance, at the minimum pitch angle the third turbine presents a C_P roughly 65% higher than the

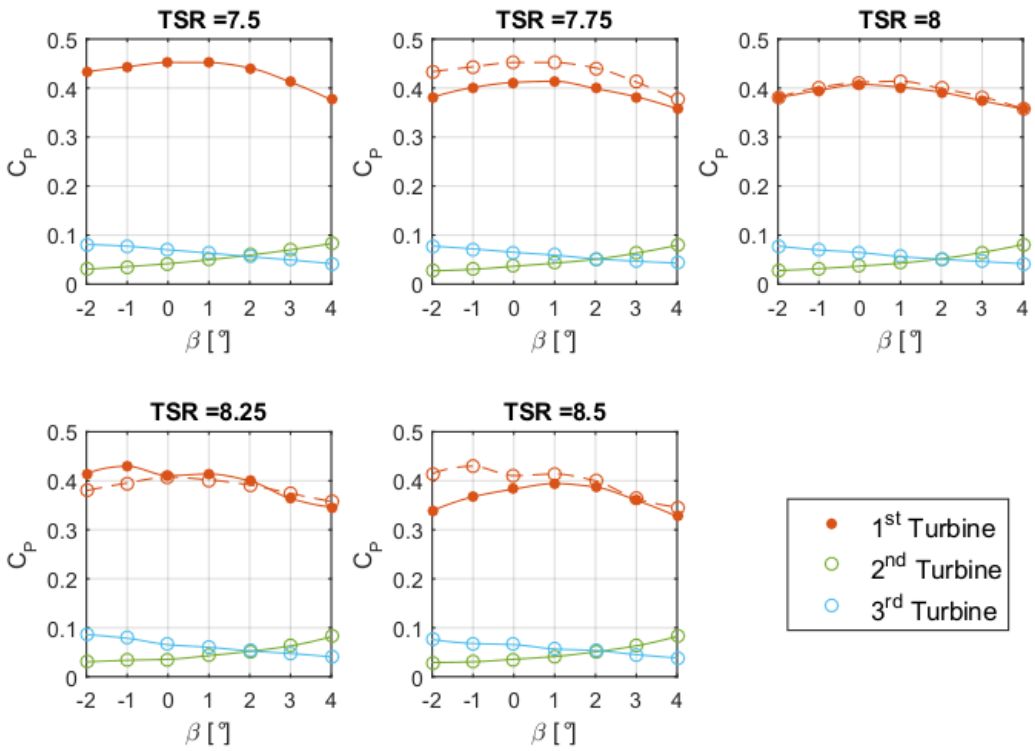

Figure 4.17: C_P vs β (3 Turbines)

second one; however, as the pitch increases the difference between the downstream models is reduced gradually. In fact, at 2 degrees the two turbines achieve the same C_P and from this point on the trend is reversed in favor of the 2^{nd} model. It is also possible to note that, for these two latter models, the dependence of C_P from the TSR is really weak since the the C_P lines in Figure 4.16 are almost horizontal. Therefore, it is reasonable to conclude that the partialization of the 1^{st} turbine modifies the wake recovery between the two downstream models; notwithstanding which kind of partialization strategy is used, whether it is one that keeps the rotational speed constant and with it the TSR or one that does not (as explained in Chapter 3.4). This phenomena will be object of detailed studies in future tests.

As already mentioned, the main purpose of these sets of experiments was to verify whether there is an influence of the downstream turbines on the upstream ones. Figures 4.18 and 4.19 are useful to valutate this effect, since the C_P of the 1^{st} model is plotted for two different cases, a stand-alone machine and a full row of models, together with the analytic values computed using the Blade Element Momentum Theory (BEM) tuned using experimental data from previous tests. Making a comparison with the analytic data it can be seen that the overall trend of the C_P agrees with the computations only in the case of β (Figure 4.19), where a remarkable match exists in most of the cases, even if all the blades are mounted at different pitch angles and therefore the equivalent pitch angle of the models could be slightly different from what was used to compute the theoretic values. On the contrary, it is noted a poor match when the curves are function of the TSR, which presents also a really irregular behaviour. This suggests that the test is really sensitive to the wind speed variations and that they should be controlled in a more accurate way in future testing. Moreover, it is worth noting that the achieved performance

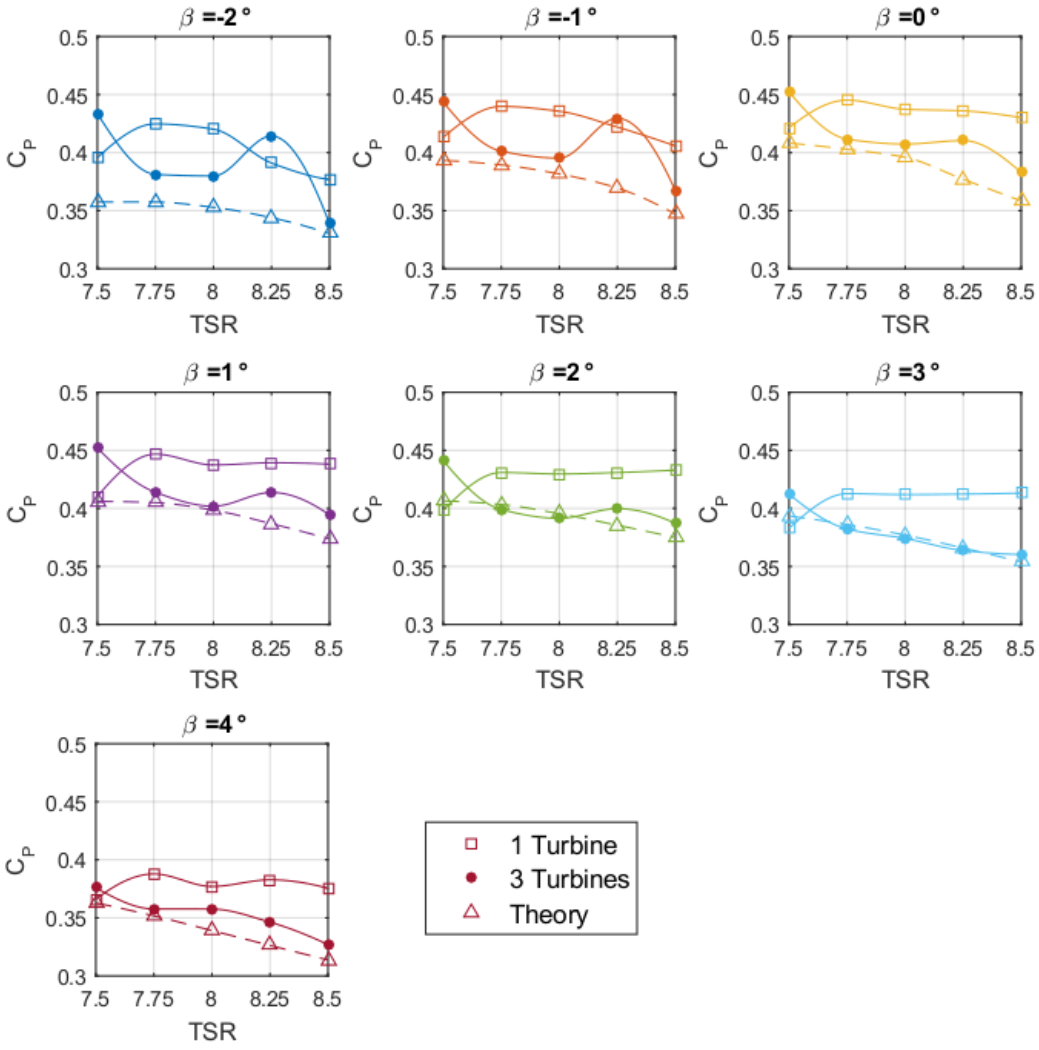

Figure 4.18: C_P vs TSR (comparison)

are, in general, better than the values obtained with the tuned BEM theory. This fact could indicate a positive wind speed shift that moves the curves to the left, towards their maximum. Again, a review of the precision of the wind speed control procedure and even of the speed measurement device position, since it is the only element that changes between the BEM tuning conditions (-1.5D) and the present test (-3D), is recommended. Finally, from the test it is clear that the downstream turbines do have an impact upon the upstream one. In fact, from Figure 4.19 it is evident that, in general, the presence of the 2^{nd} and 3^{rd} turbines produces a diminution of the power coefficient of the 1^{st} machine, diminution that corresponds roughly to 10% of the stand-alone case. It is important to mention that this reduction of the power coefficient, only by chance, moves the full row case closer to the analytic curve.

4.5.2 Torque coefficient

The behavior of the torque coefficient C_Q viewed from the wind farm perspective, i.e the general trend of each member of the row, is exactly the same one explained previously

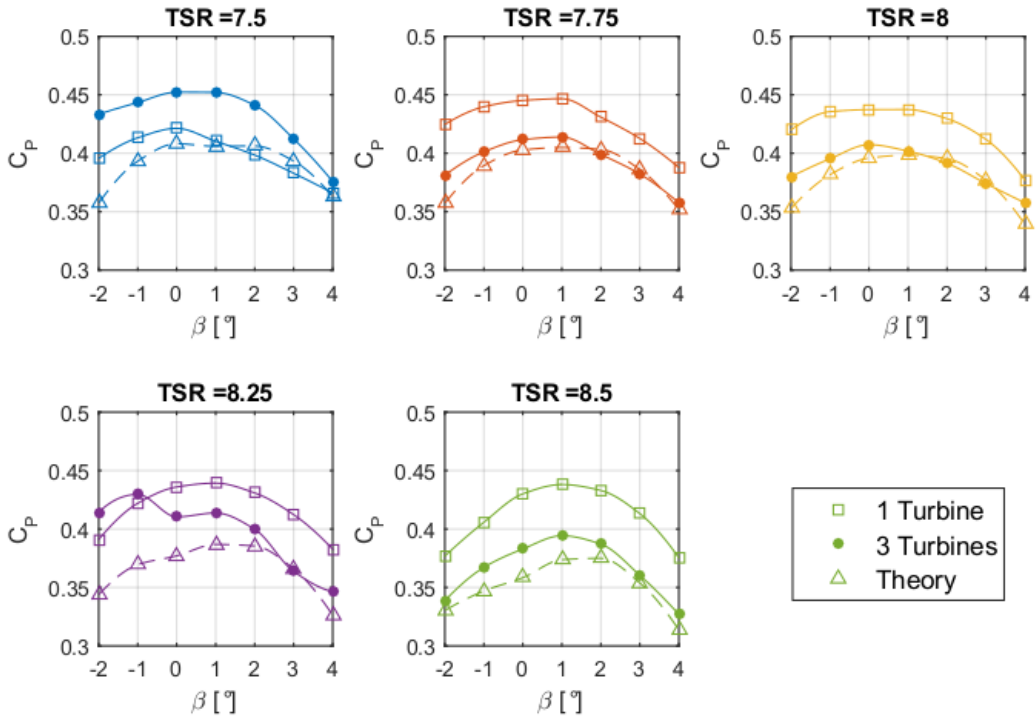

Figure 4.19: C_P vs β (comparison)

for the power coefficient (Figures 4.16 and 4.17). Therefore, this typology of curves are not included in this section since they do not provide any additional information. On the other hand, the comparison between the stand-alone case, the full row and the BEM model is shown in Figures 4.20 and 4.21. Once again, it can be seen that, in general, a single turbine has a better performance than a row of three turbines and that the analytic results underestimate the actual performance of the machine. As mentioned in the previous section, the mismatch with the theoretical data could be explained by a deficiency of the measured wind speed with respect to the actual wind speed experienced by the model. It is interesting to note that a change of one decimal in the measured wind speed modifies dramatically the outcome of the comparison between the analytic and measured data. For instance, considering a minor TSR shift of 0.15 in the BEM model computations, the analytic curves turn out to be optimistic, foreseeing a better performance than the measured ones. Therefore, it is reasonable to think that the minor wind tunnel interference effects, such as the blockage effect, could be responsible for this mismatch and should be controlled accordingly in the future. These kinds of issues were not encountered in previous test campaigns because the models were always tested at the center of the wind tunnel section where these phenomena are negligible.

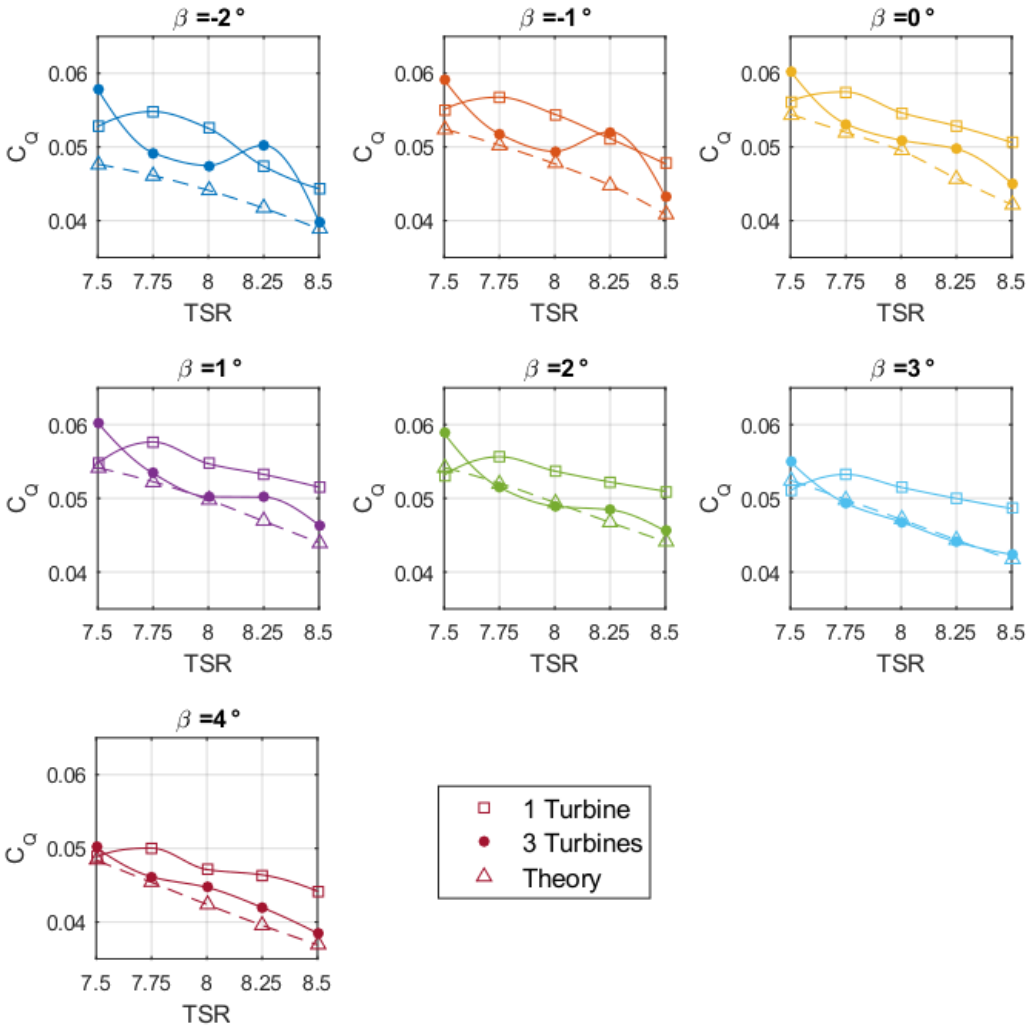

Figure 4.20: C_Q vs TSR (comparison)

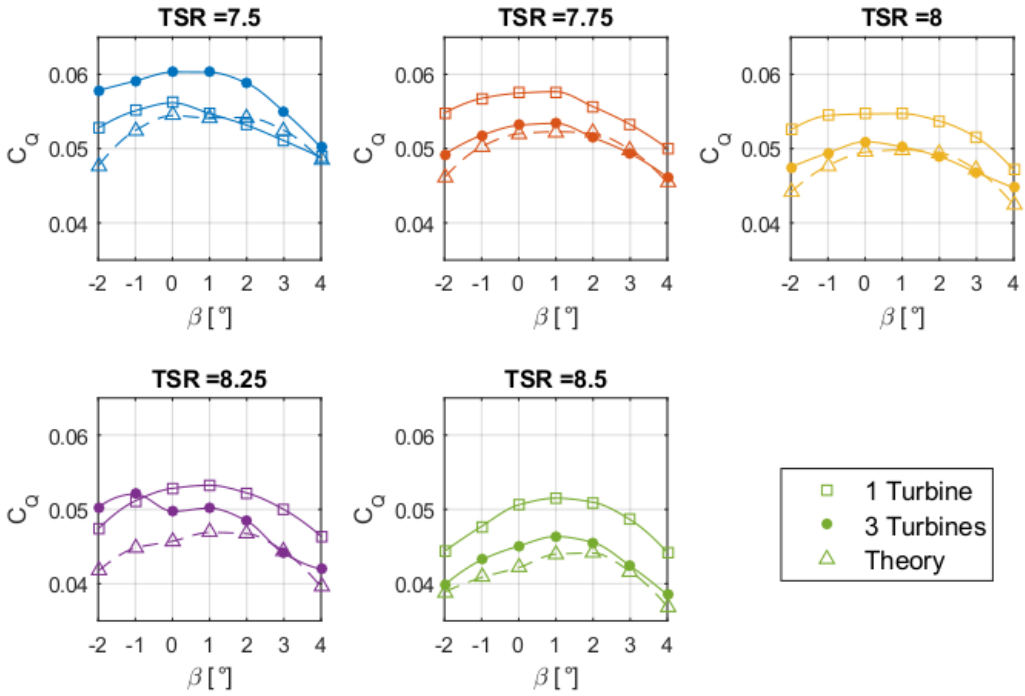

Figure 4.21: C_Q vs β (comparison)

4.5.3 Thrust coefficient

The comparison plots between the stand-alone, full row and BEM analytic results in function of both the TSR and the pitch angle are shown in Figures 4.22 and 4.23, respectively. Once again the behavior of the two downstream turbines is omitted since all its relevant features are the same explained in the subsection devoted to the power coefficient. From Figures 4.22 and 4.23 it is evident that the thrust coefficient has a weak dependence on the TSR and that, on the contrary, the pitch angle largely modifies the C_T behavior, in agreement with the analytic model. Furthermore, it is noted a reduction in the negative effect generated by the introduction of the downstream turbines which produces a decrease in the C_T of roughly 4%, compared with the diminution of 10% caused in the C_P; thus, it is possible to conclude that the C_T is affected in a lower extent by the wake behaviour. Finally, since the C_T has a lower sensitivity to the TSR changes, it is also noted an improvement in the agreement with the analytic data even if the discrepancies between the measured and the actual speed in front of the main turbine are still an issue. This, in fact, highlights the mismatch caused by the differences in the pitch angles of the three blades, which are now the principal source of error. For instance, a good match exists only in the neighbors of the zero pitch angle, up to ± 2 degrees, which gets worse as we move far from this zone. Therefore, in the design of the next generation of scaled models, systems that avoid any possibility of blade misplacement should be engineered.

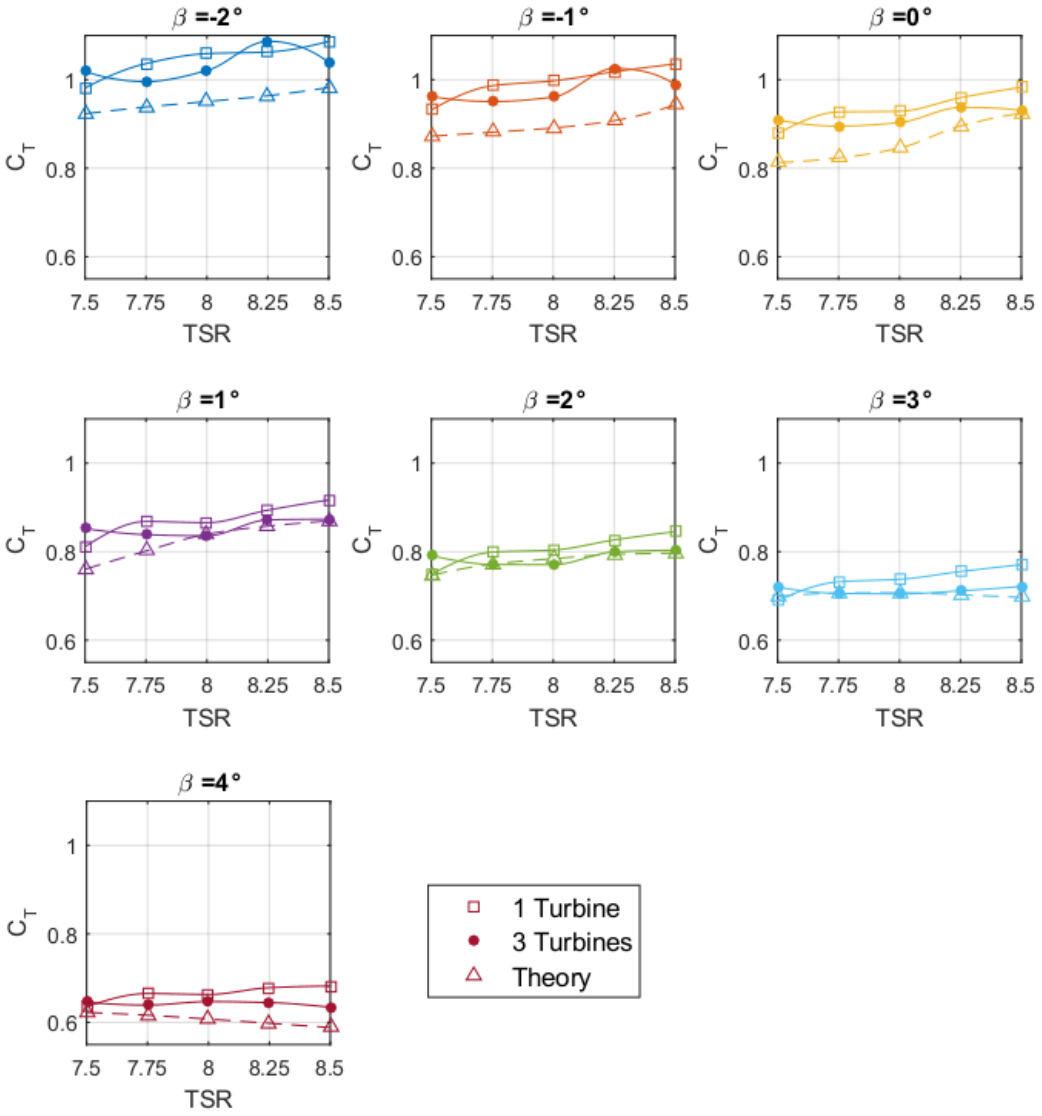

Figure 4.22: C_T vs TSR (comparison)

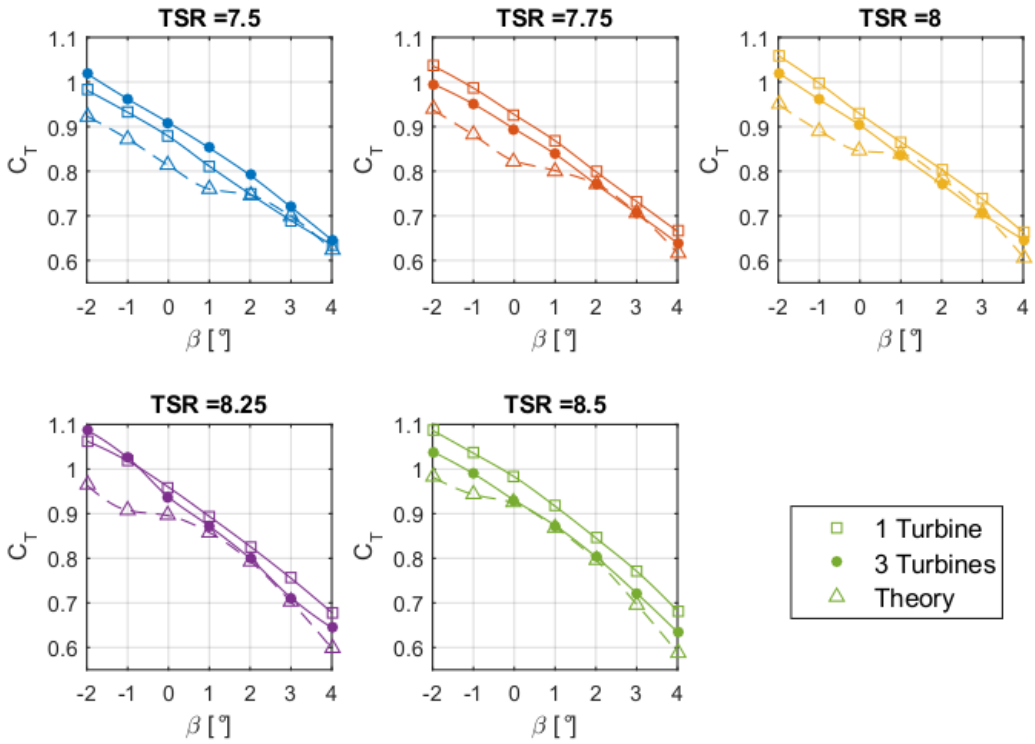

Figure 4.23: C_T vs β (comparison)

Chapter 5

Conclusions and future developments

The present work was carried out at TUM Wind Energy Department within the context of a close collaboration between universities and industrial partners.

The main goal of this thesis was the assembly of six working scaled models of wind turbines to be tested in the wind tunnel for experiments related to the development of wind farm control algorithms. The models were fully instrumented with sensors, measuring the torque, the blade pitch angle, the rotor speed and the tower base bending moments. Additionally, a real-time control logic was implemented using the Bachmann CPU, which is the same hardware that governs the operation of real wind turbines. The models are provided with two control algorithms, one developed at TUM, the other at KNU, that allow them to work in an automatic mode, meaning that they regulate their rotor speed, generator torque and blade pitch angle based on the sensors measurements and look-up tables in order to operate at the optimal design conditions. All the sensors have been calibrated, the control algorithms tested on the test bench and verified with respect to the expected behaviour. A Simulink model was also developed to help with the development of the control algorithm, to have a basis to compare the behaviour of the real machine and study the influence of certain parameters, such as the noise on measurements. The main goal of this thesis can therefore be considered as fully accomplished, since the six wind turbines were perfectly operating in the wind tunnel experiments with both control algorithms and were able to record the data related to their operation conditions to allow the post processing of the results.

A secondary goal of this thesis was the conduction of preliminary wind tunnel tests on the wind farm and the analysis of the results. The experiments were performed, even though some issues were encountered during the tests sessions; in particular, some vibration problems limited the amount of tests that could be performed. It is important to notice, however, that these problems were caused by a poor design of the wind turbines tower, which was not part of this thesis but was developed by other people. As part of this thesis, however, a research on possible modifications of the tower connection to the floor to solve these vibration problems was conducted, and a definitive solution was found. The solution has been also tested in the following test campaign and proved to solve all the issues, thus allowing the operating of the machine at rated rotor speed without worries about the stresses acting on the tower base.

The experimental tests consisted in the measurement of the aerodynamic performance of the wind turbine, expressed as power, torque and thrust coefficients and the nacelle

drag, the turbine wake characterization, performed through hot-wire measurements, and some partialization tests.

The wake measurements showed a wake structure similar to what was expected, with a wake diameter that increases moving downstream from the turbine and a vertical, counterclockwise, speed in the near wake, perfectly coherent with the clockwise rotation of the rotor. Moreover, a typical peak of velocity appeared near the center of the wake, caused by the presence of the tower and nacelle, components that do not extract energy from the wind; this peak, however, was not perfectly centered, as was expected. This can be explained by the fact that, being the turbine not in the center of the wind tunnel, the fluid is subjected to the effect of the boundary layer of the side wall, which caused a small lateral component of wind speed that slightly shifted the peak. This hypothesis was later confermed by the measurements of the lateral wind speed.

The partialization tests were performed with wind turbines at two different distances, 4D and 6D, with the goal of discovering whether a reduction of the power produced by the first turbine of a row could improve the wake, and therefore the performance of the downstream turbines, so much as to generate an increase of the overall wind farm power; it is important to notice, however, that this assumption, up to now, has never been experimentally demonstrated. The tests, however, were inconclusive, since a significant increase in power was not encountered. Moreover, the tests showed that, by having three turbines in a row, the third turbines has better performance than the second one; by partializing the first turbine, however, it is possible to revert this phenomenon. This behaviour, clearly strange and unexpected, should be further investigated in future tests, also to find out if it could be caused by the wind tunnel closed environment.

The performance tests were conducted first with a single turbine, in order to measure its aerodynamic characteristics, and then with three turbines in a row, in order to assess the effects that the two downstream turbines have on the upstream one. The results obtained with a full row confirmed the partialization tests results, showing that the power coefficient of the second turbine is, at low pitch angles, lower than that of the third one and that by increasing the pitch angle, or in other words partializing the first turbine, this behaviour is reverted. Moreover, a comparison between the two tested cases shows that the two downstream machines cause a decrease of the power coefficient of the upstream one of about 10% and of the thrust coefficient of about 4%. Finally, a comparison between the theoretical values and the measured ones showed a good, although not as good as expected, match; it also suggested, however, a strong sensitivity to the wind speed, which should be measured more carefully in the next tests.

5.1 Future developments

The present work is set within the context of a three years long contract and will be further improved by the addiction of other three wind turbines, thus creating a wind farm of nine models. The other three models, moreover, will be equipped with a yaw motor, thus allowing to perform several more tests. For instance, it will be possible to evaluate the effect of a yaw angle on the wind turbine performance and to tests new control strategies that account also for an active control on the yaw.

During the development of this thesis, several minor issues were encountered and are here briefly summarized in order to suggest possible improvements for the next tests or even the next generation of scaled models. First, the pitch angle was proved to be

different for each blade due to the wrong placement of the holes on the bevel gears, which leads to different rotors for each turbines; it is therefore suggested to manufacture new bevel gears in order to have six, and later nine, similar rotors. Another possible solution or improvement related to the pitch angle is the introduction of an individual blade pitch control; although it would cause an increase in the complexity of the nacelle structure, it would also compensate for possible misalignement of the blades and thus guarantee that all rotors have the same pitch angle. A second, possible, improvement is related to the torque measurement, which is of extraordinary importance since it is closely related to the power; currently, a torquemeter measures the generator torque, which differs from the aerodynamic torque acting on the rotor because of the friction. In other words, to correctly estimate the torque and power coefficients it is of the utmost importance to correctly measure the friction torque as function of rotor speed. This, however, has proved to be more difficult since it is influenced by a great number of parameters. First, the temperature of the mechanical components changes the friction and, therefore, its value depends on how much time the machine has been operating and on the environment temperature. Second, the bearings wear out with time, significantly changing the friction. Finally, the amount of grease or oil used for the bearings and the time passed since the last application also have an appreciable effect. It is thus clear that a measurement of the torque that does not involve the computation of the friction would really simplify the measurements; this could be possible by using a torque measuring system directly mounted on the hub shaft near the rotor, so that the measured torque is not the generator but directly the aerodynamic one.

Furthermore, the experimental results showed some aspects worthy of further investigation in future test campaigns. The wake characterization, for instance, was performed at two different wind speeds that correspond to Region II and Region III; since the operating condition is very different, it is not so easy to compare the results. A more significant comparison could be performed when the wind speed is constant and the power percentage is changed. In this way, in fact, it would be possible to analyze how the wake improves when the upstream turbine extracts less power; the wake improvement, as previously said, is a critical factor for the partialization strategy, since it is the main element that cause an increase of the downstream turbines performance, as should therefore be carefully characterized.

The experimental tests also suggested a strong sensitivity of the turbine performance to the wind speed, which should thus be measured more carefully and in more places; if possible, also more close to the turbine in order to assess the real wind speed that the turbine experiences.

Appendix A

Installation procedure

A.1 ESCON 50/5 configuration

To correctly configure the ESCON control boards, connect the USB cable to the board and configure the parameters as shown in Figure A.1.

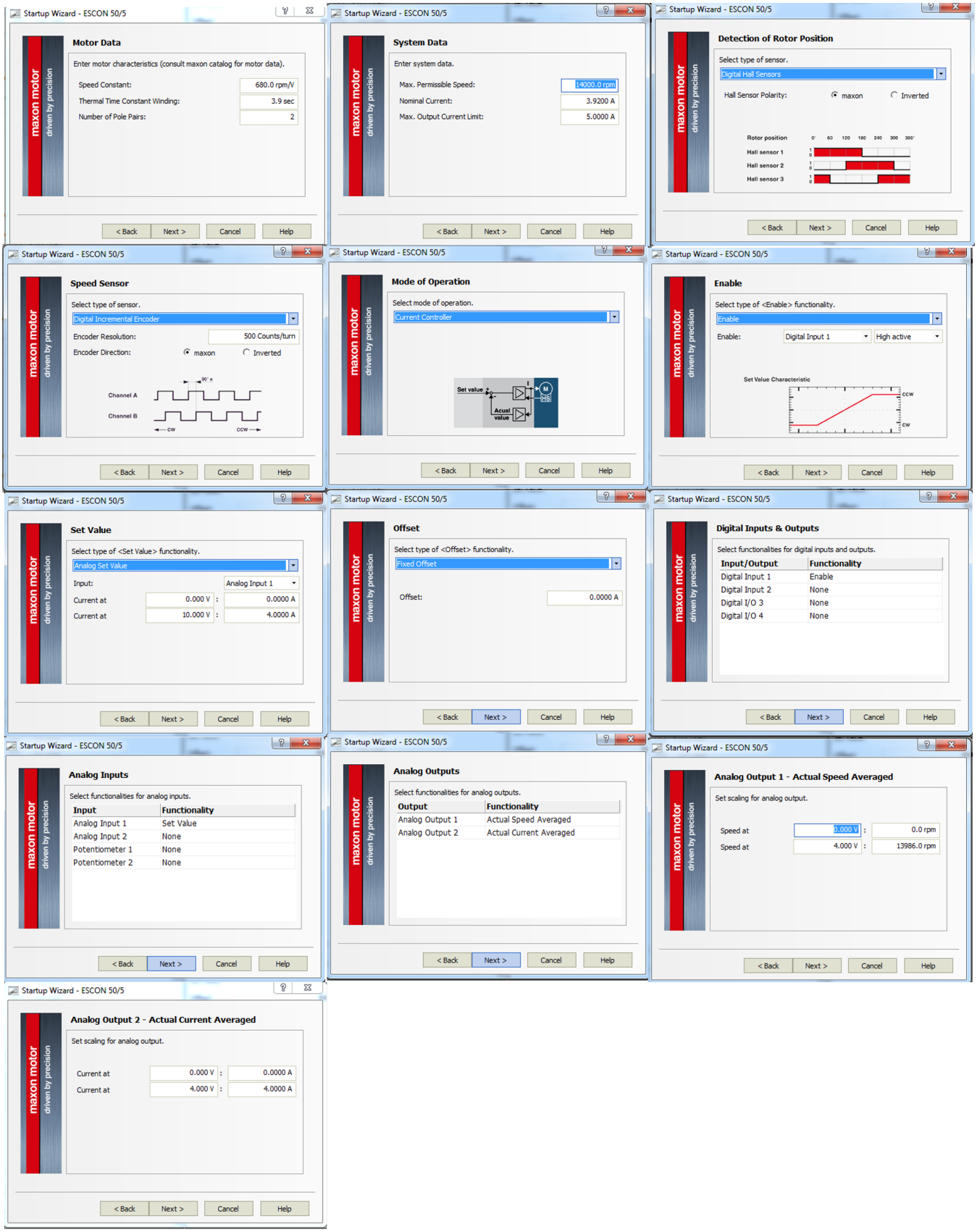

Figure A.1: ESCON configuration

Bibliography

[1] J. F. Ainslie. "Calculating the flowfield in the wake of wind turbines". In: *Journal of Wind Engineering and Industrial Aerodynamics* (1988).

[2] J. Annoni et al. "Evaluating wake models for wind farm control". In: *American Control Conference (ACC), 2014*. IEEE. 2014, pp. 2517–2523.

[3] M. J. Behmer. "Preliminary design of a scaled wind turbine for wind tunnel testing". Bachelor Thesis. Technische Universität München, 2014.

[4] F. Bianchi. *Wind Turbine Control Systems*. Springer, 2007.

[5] C. Bottasso. *Lecture Notes on Wind Turbine control*.

[6] F. Campagnolo. "Wind tunnel testing of scaled wind turbine models: aerodynamics and beyon". PhD Thesis. Politecnico di Milano, 2013.

[7] *CANopen Communication/Function Manual*. Faulhaber.

[8] P. Seiler E. Bitar. "Coordinated control of a wind turbine array for power maximization". In: *American Control Conference* (2013).

[9] *EC-4pole 22 Datasheet*. Maxon Motors.

[10] *EPOS2 24/2 Communication Guide*. Maxon Motors.

[11] *EPOS2 24/2 Firmware Specification*. Maxon Motors.

[12] *EPOS2 24/2 Hardware Reference*. Maxon Motors.

[13] *ESCON Hardware Reference*. Maxon Motors.

[14] E. Hau. *Wind Turbines*. Springer, 2013.

[15] P. Seiler M. Guala J. Annoni K. Howard. "An experimental investigation of the effect of individual turbine control on wind farm dynamics". In: *Wind energy* ().

[16] S. Van der Pijl J. Schepers. "Improved modelling of wake aerodynamics and assessment of new farm control strategies". In: *Journal of Physics* (2007).

[17] N. O. Jensen. "A note on wind generator interaction". In: *Tech. Rep. Riso* (1983).

[18] K. E. Johnson and G. Fritsch. "Assessment of extremum seeking control for wind farm energy production". In: *Wind Engineering* (2012).

[19] W. Johnson. *Rotorcraft Aeromechanics*. Cambridge University Press, 2013.

[20] N. Thomas K. E. Johnson. "Wind farm control: Addressing the aerodynamic interaction among wind turbines". In: *American Control Conference* (2009).

[21] J. Leishmann. *Principles of Helicopter Aerodynamics*. Cambridge University Press, 2006.

[22] F. M. López. "Development and preliminary testing of a wind tuneel-wind turbine model conceived for wind farm control testing". Bachelor Thesis. Technische Universität München, 2014.

[23] S. Lee M. Churchfield. *NWTC design codes-SOWFA*. `http://wind.nrel.gov/designcodes/simulators/SOWFA`. 2009.

[24] L. Maffenini. "Sviluppo di un sistema di controllo real-time per un modello di aerogeneratore in gallera del vento". Master Thesis. Politecnico di Milano, 2010.

[25] A. Mauri. "Development and preliminary testing of a wind tuneel-wind turbine model conceived for wind farm control testing". Master Thesis. Politecnico di Milano, 2014.

[26] J. W. van Wingerden P. M. O. Gebraad F. C. van Dam. "A modelfree distributed approach for wind plant control". In: *American Control Conference* (2013).

[27] D. Spera. *Wind Turbine Technology*. ASME Press, 2009.

[28] N. Jenkins E. Bossanyi T. Burton D. Sharpe. *Wind Energy Handbook*. John Wiley and Sons, 2001.

[29] N. Troiano. "Development of a wind farm controller and wind farm control algorithm for wind tunnel testing". Master Thesis. Politecnico di Milano, 2013.

[30] L. Vermeer. *Wind turbine wake aerodynamics*. Tech. rep. Delft University of technology, 2003.

[31] M. J. Werle. "Wind Turbine Wall-Blockage Performance Corrections". In: *Journal of Propulsion and Power* 26.6 (2010).

[32] S. K. Wessel. "Power optimization of wind farms by curtailment of upwind turbines". Master Thesis. Technical University of Denmark, 2015.

[33] F. Sotiropoulos X. Yang. "On the predictive capabilities of LES-actuator disk model in simulating turbulence past wind turbines and farms". In: *American Control Conference* (2013).